Published for SISSA by Springer

Received: *February 2, 2023*
Accepted: *June 9, 2023*
Published: *July 11, 2023*

Inclusive-photon production and its dependence on photon isolation in pp collisions at $\sqrt{s} = 13$ TeV using 139 fb^{-1} of ATLAS data

The ATLAS collaboration

E-mail: atlas.publications@cern.ch

Abstract: Measurements of differential cross sections are presented for inclusive isolated-photon production in pp collisions at a centre-of-mass energy of 13 TeV provided by the LHC and using 139 fb^{-1} of data recorded by the ATLAS experiment. The cross sections are measured as functions of the photon transverse energy in different regions of photon pseudorapidity. The photons are required to be isolated by means of a fixed-cone method with two different cone radii. The dependence of the inclusive-photon production on the photon isolation is investigated by measuring the fiducial cross sections as functions of the isolation-cone radius and the ratios of the differential cross sections with different radii in different regions of photon pseudorapidity. The results presented in this paper constitute an improvement with respect to those published by ATLAS earlier: the measurements are provided for different isolation radii and with a more granular segmentation in photon pseudorapidity that can be exploited in improving the determination of the proton parton distribution functions. These improvements provide a more in-depth test of the theoretical predictions. Next-to-leading-order QCD predictions from JETPHOX and SHERPA and next-to-next-to-leading-order QCD predictions from NNLOJET are compared to the measurements, using several parameterisations of the proton parton distribution functions. The measured cross sections are well described by the fixed-order QCD predictions within the experimental and theoretical uncertainties in most of the investigated phase-space region.

Keywords: Hadron-Hadron Scattering

ArXiv ePrint: 2302.00510

https://doi.org/10.1007/JHEP07(2023)086

JHEP07(2023)086

Contents

1 Introduction **1**

2 ATLAS detector **2**

3 Data sample and Monte Carlo simulations **3**

4 Event and photon selection **5**

5 Background evaluation and signal extraction **7**
- 5.1 Multi-jet background 8
- 5.2 Background from electrons faking photons 12
- 5.3 Signal yields 12

6 Cross section measurement **14**
- 6.1 Unfolding procedure for the measurement of the differential cross sections 14

7 Systematic uncertainties **15**
- 7.1 Signal modelling 15
- 7.2 Background subtraction 16
  - 7.2.1 Choice of background control regions 16
  - 7.2.2 Identification and isolation correlation in the background 16
  - 7.2.3 Background from electrons faking photons 17
- 7.3 Photon reconstruction 17
  - 7.3.1 Photon-reconstruction efficiency 17
  - 7.3.2 Photon-identification efficiency 17
  - 7.3.3 $E_{\mathrm{T}}^{\mathrm{iso}}$ modelling 17
- 7.4 Unfolding procedure 17
  - 7.4.1 Parton-shower and hadronisation model dependence 17
  - 7.4.2 Unfolding closure 18
  - 7.4.3 MC statistical uncertainties 18
- 7.5 Running conditions 18
  - 7.5.1 Pile-up 18
  - 7.5.2 Trigger efficiency 18
  - 7.5.3 Measurement of the integrated luminosity 18
- 7.6 Photon calibration: energy scale and resolution 18
- 7.7 Total systematic uncertainty 19

8 Theoretical predictions **22**
- 8.1 Hadronisation and underlying-event corrections to the fixed-order pQCD calculations 26
- 8.2 Theoretical uncertainties 26

9 Results **32**
9.1 Differential cross sections as functions of E_T^γ in different η^γ regions 32
9.2 R dependence of the fiducial cross section for inclusive isolated-photon production 37
9.3 Ratio of the differential cross sections with different isolation-cone radii 41

10 Summary and conclusions **45**

The ATLAS collaboration **51**

JHEP07(2023)086

1 Introduction

The production of prompt photons[1] at high transverse momentum (p_T) in proton-proton collisions, $pp \to \gamma + X$, provides a testing ground of perturbative QCD (pQCD) in a cleaner environment compared to jet production, since it is less affected by hadronisation effects. At leading order (LO) in pQCD, two processes contribute to prompt-photon production: the direct process, in which the photon originates directly from the hard interaction, and the fragmentation process, in which the photon is produced when a high p_T parton fragments [1, 2]. In hadron colliders, photons are produced copiously in decays of neutral hadrons; thus, isolation requirements are necessary to separate prompt-photon production, whose dynamics is governed by pQCD, from those photons arising from hadron decays. The inclusive production of isolated photons in pp collisions has been studied previously by ATLAS [3–8] and CMS [9–11] at centre-of-mass energies ($\sqrt{s}$) of 7, 8 and 13 TeV.

This paper presents measurements of inclusive isolated-photon production in pp collisions at $\sqrt{s} = 13$ TeV with the ATLAS detector at the LHC using an integrated luminosity of 139 fb^{-1} collected between 2015 and 2018. Differential cross sections as functions of the photon transverse energy,[2] E_T^γ, are measured in different regions of the photon pseudorapidity, η^γ, for $E_T^\gamma > 250$ GeV and $|\eta^\gamma| < 2.37$. The photon is required to be isolated at particle level by demanding that the transverse energy of the stable particles within a cone of radius $R = 0.4$ or $R = 0.2$ around the photon direction, $E_T^{\rm iso}$, is smaller than a certain value; this isolation method is called 'fixed-cone' and $E_T^{\rm iso} < E_{T,\rm cut}^{\rm iso} \equiv 4.2 \cdot 10^{-3} \cdot E_T^\gamma + 4.8$ GeV is chosen in this analysis for the isolation requirement.

Next-to-leading-order (NLO) and next-to-next-to-leading-order (NNLO) pQCD predictions are compared to the measurements. The dominant production mechanism in pp collisions at the LHC proceeds via the $qg \to q\gamma$ process; in this way, measurements of

[1] Photons that are not secondaries from hadron decays are considered as prompt.

[2] ATLAS uses a right-handed coordinate system with its origin at the nominal interaction point (IP) in the centre of the detector and the z-axis along the beam pipe. The x-axis points from the IP to the centre of the LHC ring, and the y-axis points upwards. Cylindrical coordinates (r, ϕ) are used in the transverse plane, ϕ being the azimuthal angle around the z-axis. The transverse energy is defined as $E_T = E \sin\theta$, where E is the energy and θ is the polar angle. The pseudorapidity is defined as $\eta = -\ln\tan(\theta/2)$ and the angular distance is measured in units of $\Delta R \equiv \sqrt{(\Delta\eta)^2 + (\Delta\phi)^2}$.

prompt-photon production are sensitive to the gluon density in the proton [12–14] and can be used as input to global QCD fits to help to constrain the proton parton distribution functions (PDF). Recent studies [15] have shown that the inclusion of prompt-photon measurements [6] from ATLAS provides a reduction in the gluon density uncertainties.

The results presented in this paper extend in several aspects those at 8 and 13 TeV reported in previous publications [6–8]. The measurements use a finer granularity in η^{γ} and so they provide more data points as input to the QCD fits. The measurements benefit from a reduction of the experimental systematic uncertainty, especially that in the photon identification efficiency, as well as from an approximately four-fold increase in the integrated luminosity. The dependence of the fiducial cross section on the isolation-cone radius R is also investigated as well as the ratios of the differential cross sections for $R = 0.2$ and $R = 0.4$ as functions of E_{T}^{γ} and η^{γ}. These measurements test the R dependence of the inclusive isolated-photon cross section. At LO pQCD, there is no dependence of the cross section on R and so the first non-trivial theoretical contribution arises at higher orders in pQCD [16]. Therefore, these measurements provide a test of pQCD at high orders. From the theoretical point of view, isolation helps to suppress the fragmentation contribution. The fragmentation component is available in the calculations from Jetphox 1.3.1_2 [17, 18] and Nnlojet [19]. In the calculations from Sherpa 2.2.2 [20], an isolation requirement is essential to avoid divergencies in the matrix elements when the photon is collinear with a parton. This is achieved by using the method based on the Frixione criterion [21] or the hybrid method [16], which combines the Frixione criterion and the fixed-cone method. The measurements presented in this paper are performed using the fixed-cone criterion since, due to the finite size of the detector elements, a discrete version of the Frixione criterion leads to large experimental uncertainties. The R dependence of the measured cross sections allows a test of the different theoretical approaches to the photon-isolation modelling.

The paper is organised as follows: the ATLAS detector is described in section 2. The details of the data samples and the Monte Carlo simulations as well as the event and photon selection are included in sections 3 and 4, respectively. The background evaluation and signal extraction are explained in section 5: the main background to isolated-photon events arises from jets misidentified as photons, which includes non-prompt photons, and is subtracted using a data-driven technique. The strategy for the cross section measurements is summarised in section 6. Section 7 is devoted to the description of the experimental uncertainties. Theoretical predictions and their uncertainties are discussed in section 8. The results are reported in section 9. A summary is given in section 10.

2 ATLAS detector

The ATLAS detector [22–24] is a multipurpose detector with a forward-backward symmetric cylindrical geometry. It consists of an inner tracking detector surrounded by a thin superconducting solenoid, electromagnetic and hadronic calorimeters, and a muon spectrometer incorporating three large superconducting toroid magnets. The inner-detector system is immersed in a 2 T axial magnetic field and provides charged-particle tracking in the range $|\eta| < 2.5$. The high-granularity silicon pixel detector is closest to the interac-

JHEP07(2023)086

tion region and provides four measurements per track. The pixel detector is followed by the silicon microstrip tracker, which typically provides four three-dimensional space point measurements per track. These silicon detectors are complemented by the transition radiation tracker, which enables radially extended track reconstruction up to $|\eta| = 2$. The calorimeter system covers the range $|\eta| < 4.9$. Within the region $|\eta| < 3.2$, electromagnetic (EM) calorimetry is provided by barrel and endcap high-granularity lead/liquid-argon (LAr) calorimeters, with an additional thin LAr presampler covering $|\eta| < 1.8$ to correct for energy loss in material upstream of the calorimeters; for $|\eta| < 2.5$, the EM calorimeter is divided into three layers in depth. Hadronic calorimetry is provided by a steel/scintillator-tile calorimeter, segmented into three barrel structures within $|\eta| < 1.7$, and two copper/LAr hadronic endcap calorimeters, which cover the region $1.5 < |\eta| < 3.2$. The solid-angle coverage is completed out to $|\eta| = 4.9$ with forward copper/LAr and tungsten/LAr calorimeter modules, which are optimised for EM and hadronic measurements, respectively. Events are selected using a first-level trigger implemented in custom electronics, which reduces the maximum bunch crossing rate of 40 MHz to a design value of 100 kHz using a subset of detector information. Software algorithms with access to the full detector information are then used in the high-level trigger to yield a recorded event rate of about 1 kHz [25].

An extensive software suite [26] is used in the reconstruction and analysis of real and simulated data, in detector operations, and in the trigger and data acquisition systems of the experiment.

3 Data sample and Monte Carlo simulations

Data sample. The data used in this analysis were collected with the ATLAS detector during the proton-proton collision running periods from 2015 to 2018, when the LHC operated at a centre-of-mass energy of $\sqrt{s} = 13$ TeV. The integrated luminosity of this data set, in which events are required to pass data quality requirements [27], is $139.0 \pm 2.4\,\text{fb}^{-1}$ [28]. Events in which the calorimeters or the inner detector were not fully operational or showed data quality problems are excluded.

Simulated event samples. Samples of simulated events were produced using Monte Carlo (MC) techniques to study the characteristics of the signal events. The MC samples are also used to determine the ingredients necessary to obtain the measured cross sections. In addition, MC samples are used to estimate non-perturbative corrections to the fixed-order pQCD calculations.

The MC programs Pythia 8.186 [29] and Sherpa 2.1.1 [30] were used to generate the simulated signal events. In both generators, the partonic processes are simulated using LO matrix elements, with the inclusion of initial- and final-state parton showers. Fragmentation into hadrons is performed using the Lund string model [31] in the case of Pythia, and a modified version of the cluster model [32] in the case of Sherpa. For the samples generated with Pythia (Sherpa), the proton structure is parameterised using the LO NNPDF2.3 [33] (NLO CT10 [34]) PDFs. Both samples include a simulation of the underlying event (UE). The event generator parameters are set according to the “A14” [35] tune for PYTHIA and the tune developed by the authors for use in conjunction with the NLO CT10 PDF set for SHERPA.

The PYTHIA simulation of the signal includes LO matrix elements for photon plus jet production from both direct processes (the subprocesses $qg \to q\gamma$ and $q\bar{q} \to g\gamma$) and photon bremsstrahlung in QCD dijet events to simulate the fragmentation process. The contribution from the $qg \to q\gamma$ subprocess is dominant over most of the measured phase-space region. The SHERPA samples are generated with LO matrix elements for photon plus jet final states with up to three additional partons. The photon bremsstrahlung component is simulated differently in PYTHIA and SHERPA. In PYTHIA, photons can be radiated in the parton shower without a restriction on the opening angle with respect to the parent parton and, as a result, the photons can be emitted very close to the parton direction. In SHERPA, photons are not emitted in the parton shower and the photon bremsstrahlung component is simulated through matrix elements of $2 \to N$ processes, with $N \geq 3$. In this case, divergencies in the calculation are avoided by restricting the emission through an implementation of the Frixione requirement; as a result, photons are not emitted close to the parent parton. Frixione's criterion requires the total transverse energy inside a cone of size $\mathfrak{r}$ in the $\eta - \phi$ plane around the generated final-state photon, excluding the photon itself, to be below a certain threshold, $E_{\mathrm{T}}^{\mathrm{max}}(\mathfrak{r}) = \epsilon E_{\mathrm{T}}^{\gamma}((1-\cos\mathfrak{r})/(1-\cos\mathcal{R}))^n$, for all $\mathfrak{r} < \mathcal{R}$, where $\mathcal{R}$ is the maximal cone size, n is a parameter which modifies the dependence of the threshold from the radius $\mathfrak{r}$ and ϵ is a constant such that $\epsilon E_{\mathrm{T}}^{\gamma}$ represents the threshold for $\mathfrak{r} = \mathcal{R}$. The parameters used for the generation of these SHERPA samples are chosen to be $\mathcal{R} = 0.3$, $n = 2$ and $\epsilon = 0.025$. The resulting Frixione isolation requirement applied at the generation level in SHERPA is looser than the ones applied in this analysis at particle and reconstruction levels (see section 6).

The second main background after misidentification of jets as photons arises from electrons or positrons misidentified as photons and is evaluated using MC samples generated with the program SHERPA 2.2.1 [20, 36–40]. The $pp \to Z/\gamma^* \to e^+e^- + \mathrm{X}$ and $pp \to W \to e\nu + \mathrm{X}$ processes are generated with matrix elements calculated with up to two additional partons at NLO and up to four partons at LO. The NNLO NNPDF3.0 PDF set [41] is used in conjunction with a dedicated set of parton-shower-generator parameters [20] developed by the SHERPA authors.

For all these MC samples, pile-up from additional pp collisions in the same and neighbouring bunch crossings is simulated by overlaying each MC event with a variable number of simulated inelastic pp collisions generated using PYTHIA 8.186 with the ATLAS set of tuned parameters for minimum bias events (A3 tune) [42]. The MC events are weighted ("pile-up reweighting") so that the distribution of the average number of interactions per bunch crossing matches the one observed in data. All the samples of generated events were passed through the GEANT 4-based [43] ATLAS detector- and trigger-simulation programs [44]. The simulated event samples were reconstructed and analysed by the same program chain as the data.

In addition, dedicated MC samples without UE were generated at particle and parton levels to correct the fixed-order pQCD calculations for hadronisation and UE effects (see section 8.1).

JHEP07(2023)086

4 Event and photon selection

Event selection. The data sample used consists of events recorded by a single-photon high-level trigger with a nominal transverse energy threshold of 140 GeV and "loose" photon identification requirements [25, 45, 46]. The efficiency of the trigger for photons with $E_{\mathrm{T}}^{\gamma} > 250$ GeV is found to be close to 100%. The inefficiency of the high-level trigger with respect to the first-level trigger is found to be subpercent and taken as a systematic uncertainty (see section 7.5).

The initial data sample of isolated-photon events is selected offline from those events recorded by the trigger mentioned above and by requiring the events to have at least one reconstructed primary vertex, which has at least two associated tracks of $p_{\mathrm{T}} > 500$ MeV and is consistent with the average beam-spot position.

Photon reconstruction. The offline electron- and photon-candidate reconstruction is based on dynamic variable-size clusters of EM calorimeter cells, called superclusters [47], which change in size as needed to recover energy from bremsstrahlung photons or from electrons from photon conversions. The calibration techniques exploit this advantage of the dynamic clustering algorithm, while achieving similar linearity and stability as for the fixed-size clusters used previously [45]. Superclusters are based on topoclusters, which are built using a dynamical topological cell-clustering algorithm in the three-dimensional space [48] and calibrated at the EM scale. An electron candidate is defined as an object consisting of a supercluster built from energy deposits in the calorimeter and a matched track. A converted photon candidate is a supercluster matched to a conversion vertex (or vertices) or a track consistent with a photon conversion, and an unconverted photon candidate is a supercluster matched to neither an electron track nor a conversion vertex. About 20% of photons at low $|\eta|$ ($|\eta| \lesssim 0.8$) convert in the inner detector, while up to about 65% of photons convert at $|\eta| \approx 2.3$ [47] due to the non-uniform amount of material versus $|\eta|$ upstream of the calorimeter.

Photon calibration. The energy calibration of electrons and photons is updated for the new energy reconstruction [47]. The energy response and resolution of the electrons and photons are optimised using a multivariate regression algorithm, which exploits the properties of the cluster energy deposit in the EM calorimeter. The energy scale corrections extracted from $Z \to ee$ decays are applied to correct the photon energy scale [47]. A data-driven validation of the photon energy scale corrections is performed using radiative decays of the Z boson, probing the region $E_{\mathrm{T}}^{\gamma} \lesssim 80$ GeV. The possible nonlinear energy response for higher E_{T}^{γ} is covered by the systematic uncertainties, determined from auxiliary measurements [49], that are propagated up to 3 TeV using MC simulations.

Several systematic uncertainties impact the measurement of the energy of electrons and photons in a way that depends on their transverse energy, pseudorapidity and, for photons, whether they are reconstructed as converted or unconverted candidates [47]. Some of these uncertainties were re-evaluated with respect to the ones [49] used in the previous publication [8] to reflect the changes in the reconstruction described above. The sensitivity of the calibrated energy to the detector material was also re-evaluated. The systematic uncertain-

JHEP07(2023)086

ties due to the material description of the innermost pixel detector layer and the services of the pixel detector were also updated using a more accurate description of these systems.

Photon identification. Photon candidates are identified by using variables that characterise the lateral and longitudinal electromagnetic shower development in the EM calorimeter and the energy fraction leaking into the hadronic calorimeter.

The photon identification used in this analysis starts with a loose selection [47]. The signal selection is based on the "tight" [47] photon identification criteria; tight requirements are imposed on the shower shapes in the second layer and in the finely segmented first layer of the EM calorimeter as well as on the energy deposited in the hadronic calorimeter. These requirements are optimised separately to ensure the compatibility of the measured shower profile with that originating from unconverted or converted photon candidates. Small differences in the average values of the shower-shape variables between data and simulation are observed and corrected for in simulated events prior to the application of the photon identification criteria. Non-tight photon candidates, used for the data-driven background subtraction (see section 5), are defined as those photons which satisfy the loose criteria, but fail a given subset of tight requirements [8].

Photon isolation. Photon candidates are required to be isolated by using the isolation transverse energy, $E_{\mathrm{T}}^{\mathrm{iso}}$. The $E_{\mathrm{T}}^{\mathrm{iso}}$ variable is constructed by summing up the transverse energies of all topoclusters within a cone of radius $R = 0.4$ or $R = 0.2$ in the $\eta - \phi$ plane around the photon cluster barycenter. Only positive energy topoclusters are used.[3] The topoclusters include cells from the EM and hadronic calorimeters. The energy from the core of the cone in the electromagnetic calorimeter (an area of size $\Delta\eta \times \Delta\phi = 0.125 \times 0.175$ centred on the barycenter of the photon cluster), as well as the small energy leakage into the isolation cone, evaluated as functions of E_{T}^{γ} on simulated samples of single photons, are subtracted from $E_{\mathrm{T}}^{\mathrm{iso}}$.

To match the definition between data and theory (i.e., fixed-order pQCD calculations, which do not include pile-up or UE effects), a correction to $E_{\mathrm{T}}^{\mathrm{iso}}$ is applied to account for the effects from the UE and pile-up. This correction comes from the so-called "jet-area" method [50, 51]. In this method, low-energy jets are used to compute an ambient transverse energy density on an event-by-event basis, which is then multiplied by the area of the isolation cone and subtracted from the isolation transverse energy.

A data-driven correction is applied to the simulated $E_{\mathrm{T}}^{\mathrm{iso}}$ variable to improve the agreement between MC and data [47]. The $E_{\mathrm{T}}^{\mathrm{iso}}$ distributions of photon-enriched samples in data and MC are fitted using a Crystal-Ball function and the correction is computed as the difference in the fitted mean between the two functions. After all these corrections to the MC events, an improved description of the measured $E_{\mathrm{T}}^{\mathrm{iso}}$ distribution is obtained.

Corrections are also applied to the simulated events to match the overall event conditions of the data sample and to account for known differences between data and simulation.

[3] Negative topocluster energies can arise due to the presence of negative cell signals in the ATLAS calorimeters, which are the result of fluctuations introduced predominantly by pile-up and, to a lesser extent, by electronic noise.

JHEP07(2023)086

These additional corrections include pile-up effects and photon identification, isolation and reconstruction efficiency [47].

Photon selection. The photon-candidate selection criteria applied are:

- The starting point of the selection is the photons reconstructed and calibrated as described above. Both converted and unconverted candidates are kept. Photons reconstructed near regions of the calorimeter affected by read-out or high-voltage failures are not considered.

- The candidates are required to pass the tight identification criterion described above.

- Photons with $E_{\mathrm{T}}^{\gamma} > 250$ GeV and $|\eta^{\gamma}| < 2.37$ are selected, excluding those in the transition region ($1.37 < |\eta^{\gamma}| < 1.56$) between the barrel and endcap calorimeters. The threshold in E_{T}^{γ} at 250 GeV is chosen since this is the region most sensitive to the proton PDFs. Isolated-photon production cross sections at lower E_{T}^{γ} were measured by the ATLAS Collaboration in previous publications [3–8].

- In events with multiple candidates satisfying these requirements, the candidate with highest transverse energy (leading photon) is retained for further study.

- The $E_{\mathrm{T}}^{\mathrm{iso}}$ of the leading photon is required to be lower than $4.2 \cdot 10^{-3} \cdot E_{\mathrm{T}}^{\gamma} + 4.8$ GeV. This requirement was optimised to retain most of the photons satisfying the identification criteria, to obtain the best signal-to-background ratio and to keep high and constant the fraction of photon candidates that satisfy the isolation selection on top of the identification criteria [6]. Two different samples are selected using $R = 0.4$ and $R = 0.2$ for the radius of the isolation cone.

The number of data events selected by using the requirements listed above amounts to 3 652 433 for the $R = 0.2$ sample and 3 289 941 for the $R = 0.4$ sample. Each data sample is separated in six η^{γ} regions to perform the cross section measurements individually in each region, namely $|\eta^{\gamma}| < 0.6$, $0.6 < |\eta^{\gamma}| < 0.8$, $0.8 < |\eta^{\gamma}| < 1.37$, $1.56 < |\eta^{\gamma}| < 1.81$, $1.81 < |\eta^{\gamma}| < 2.01$ and $2.01 < |\eta^{\gamma}| < 2.37$. The edges of these η^{γ} regions are driven by the structure of the EM calorimeter. Each region in $|\eta^{\gamma}|$ is divided into 12 bins of E_{T}^{γ} with boundaries (in GeV) set at 250, 300, 350, 400, 470, 550, 650, 750, 900, 1100, 1500, 2000 and 2500. The binning is optimised according to the photon energy resolution and the number of events per bin both in data and MC. Some of the high-E_{T}^{γ} bins are not measured depending on the $|\eta^{\gamma}|$ region.

5 Background evaluation and signal extraction

The main background to isolated-photon production arises from multi-jet processes, in which a jet is misidentified as a photon. Such a jet usually contains a light neutral meson, mainly a π^0, that carries most of the energy of the jet and decays into two collimated photons. A very small contribution from electrons or positrons misidentified as photons is also present in the selected data samples.

5.1 Multi-jet background

For this study, a sample is obtained by applying all the selection criteria described in section 4, except for the tight identification and isolation requirements. Two subsamples are selected: the subsample of candidates that fulfill the requirements (tight subsample) and the subsample of candidates that pass the loose criteria but fail some of the tight requirements (non-tight subsample) [8]. The non-tight subsample is expected to be enriched in background candidates.

A clear signal peak of prompt photons can be observed in the $E_{\mathrm{T}}^{\mathrm{iso}}$ distribution of tight photon candidates in data as shown in figure 1. In this figure, for illustrative purposes, the result of a χ^2 fit of the sum of the $E_{\mathrm{T}}^{\mathrm{iso}}$ templates from Sherpa tight (signal) and data non-tight (background) photon candidates to that of the tight photon data candidates is also included. The signal and background components normalised according to the fit are reported in the same figure. The signal of prompt photons centred at $E_{\mathrm{T}}^{\mathrm{iso}} = 0$ GeV is observed in both data and MC simulation. For the $R = 0.4$ tight data set, the signal peak around zero is wider and the tail at high values of $E_{\mathrm{T}}^{\mathrm{iso}}$ is more populated than for the $R = 0.2$ tight data set. The non-tight $E_{\mathrm{T}}^{\mathrm{iso}}$ data distribution has a broad peak around $E_{\mathrm{T}}^{\mathrm{iso}} \approx 15$ GeV. This data set saturates the tail of the distribution for larger $E_{\mathrm{T}}^{\mathrm{iso}}$ values and shows a tail towards low values, which indicates the presence of background in the signal region. A similar description of the data is obtained by using the Pythia simulations for the signal instead of Sherpa. To avoid having to rely on the $E_{\mathrm{T}}^{\mathrm{iso}}$ MC distribution for the signal, the multi-jet background is subtracted using the data-driven method described below.

The multi-jet background is subtracted using the same data-driven method already employed in previous publications [6–8]. The application of this method to the tight and non-tight subsamples is briefly explained in the following. The multi-jet background contamination is estimated and then subtracted by using a counting technique based on the observed number of events in control regions of the two-dimensional plane defined by using the photon identification variable (γ_{ID}) and the $E_{\mathrm{T}}^{\mathrm{iso}}$ variable. These two variables are chosen because they are expected to be uncorrelated for the background. In the following, the correlation correction factor between the two variables in background events is denoted by R^{bg}. The background subtraction is performed in each bin of E_{T}^{γ} separately for each η^{γ} region and each value of R.

Four regions are defined in the $\gamma_{\mathrm{ID}} - E_{\mathrm{T}}^{\mathrm{iso}}$ plane based on the tight/non-tight γ_{ID} criteria and the isolation ($E_{\mathrm{T}}^{\mathrm{iso}} < 4.2 \cdot 10^{-3} \cdot E_{\mathrm{T}}^{\gamma} + 4.8$ GeV) and non-isolation ($E_{\mathrm{T}}^{\mathrm{iso}} > 4.2 \cdot 10^{-3} \cdot E_{\mathrm{T}}^{\gamma} + 6.8$ GeV) requirements on the photon candidates. These four regions are defined as: "A" is the signal region, which contains tight and isolated photon candidates; "B" is the control region with non-isolated background events, which contains tight and non-isolated photon candidates; "C" is the control region with non-tight background events, which contains isolated and non-tight photon candidates; "D" is the control region that contains non-isolated and non-tight photon candidates. In addition, an upper limit on $E_{\mathrm{T}}^{\mathrm{iso}}$ of 50 GeV is also imposed in regions B and D to make the background subtraction less dependent on the MC description of the data for higher $E_{\mathrm{T}}^{\mathrm{iso}}$ values. These regions are defined with a "gap" of 2 GeV in $E_{\mathrm{T}}^{\mathrm{iso}}$ from region A, to have well separated background-

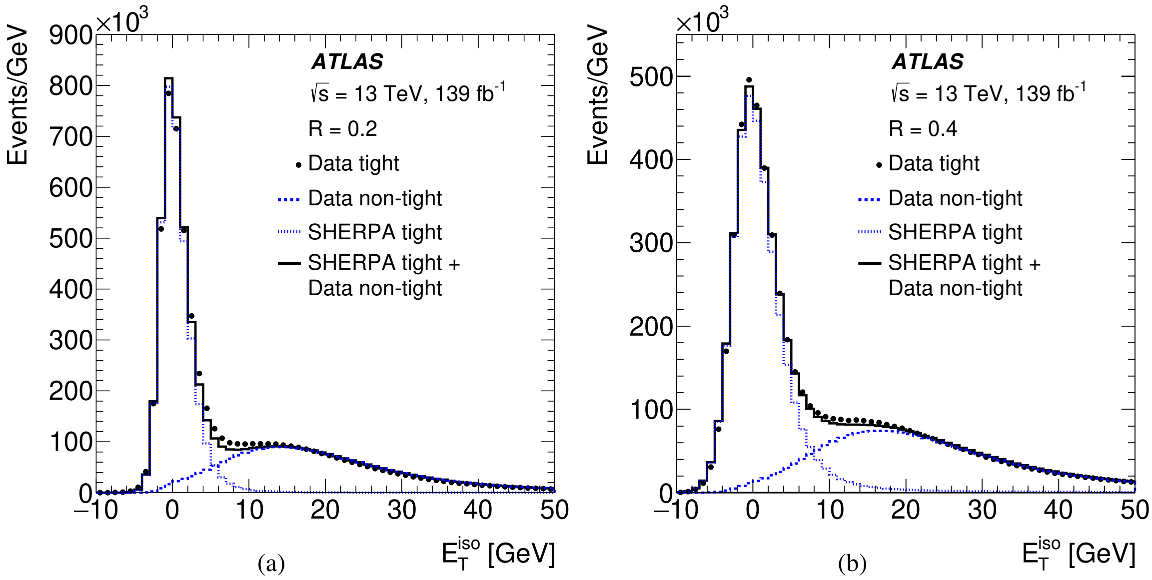

Figure 1. The $E_T^{\rm iso}$ distributions with tight (dots) and non-tight (dashed histograms, normalised according to the χ^2 fit described in the text) photon candidates in data with $E_T^\gamma > 250$ GeV and $|\eta^\gamma| < 1.37$ or $1.56 < |\eta^\gamma| < 2.37$ for $R = 0.2$ (a) and $R = 0.4$ (b). The MC simulation of the signal using Sherpa is also shown (dotted histogram, normalised according to the χ^2 fit described in the text). The solid histogram is the sum of the contributions of the MC simulation of the signal using Sherpa and that of the non-tight photon candidates and normalised according to the χ^2 fit described in the text.

control and signal regions and minimise migrations across the borders; the gap is chosen to be large enough in comparison to any difference between data and simulations, while still providing a sufficiently large number of events in the control regions to perform the data-driven subtraction. Other choices for the size of this gap and for the upper limit in $E_T^{\rm iso}$ are used to assess the corresponding systematic uncertainties (see section 7.2.1).

The relation between the number of signal events in region A ($N_A^{\rm sig}$) and the number of events in the control regions is given by

$$N_A^{\rm sig} = N_A - R^{\rm bg} \cdot (N_B - f_B N_A^{\rm sig}) \cdot \frac{(N_C - f_C N_A^{\rm sig})}{(N_D - f_D N_A^{\rm sig})}, \tag{5.1}$$

where N_K with $K = A, B, C, D$ is the number of observed events in each region and

$$R^{\rm bg} = \frac{N_A^{\rm bg} \cdot N_D^{\rm bg}}{N_B^{\rm bg} \cdot N_C^{\rm bg}},$$

where $N_K^{\rm bg}$ with $K = A, B, C, D$ is the number of background events in each region; $R^{\rm bg}$ is set to unity for the nominal results, the only assumption in this method. This assumption is checked to be valid within $(10 - 25)\%$, depending on the E_T^γ and η^γ region and the isolation cone radius R. The differences of $R^{\rm bg}$ with respect to unity are included as systematic uncertainties in the final results (see section 7.2.2). Equation (5.1) takes into account the expected number of signal events in the three background control regions via the signal leakage fractions, $f_K = N_K^{\mathrm{sig,MC}}/N_A^{\mathrm{sig,MC}}$ with $K = B, C, D$.

The signal leakage fractions are extracted from the MC simulations of the signal, independently for each isolation-cone radius, using SHERPA and PYTHIA. Differences in the values of the signal leakage fractions extracted from PYTHIA and SHERPA are observed. They are due to the different treatment of the fragmentation component in the two MC generators (see section 3).

The signal yield is determined from the observed number of events in the data in the four regions of the $\gamma_{\mathrm{ID}} - E_{\mathrm{T}}^{\mathrm{iso}}$ plane and the signal leakage fractions determined from the simulated signal events using equation (5.1). The signal purity, computed as $P = N_A^{\mathrm{sig}}/N_A$, is shown in figure 2 using the signal leakage fractions from the SHERPA and PYTHIA signal samples. The purity is $\gtrsim 90\%$ and very similar regardless of whether SHERPA or PYTHIA samples are used to compute the signal leakage fractions. The signal purity for $R = 0.4$ is higher than for $R = 0.2$. The nominal signal yield is extracted using the signal leakage fractions from SHERPA; the signal yield extracted from the signal leakage fractions of PYTHIA is used to assess a systematic uncertainty in the purity determination (see section 7.1).

JHEP07(2023)086

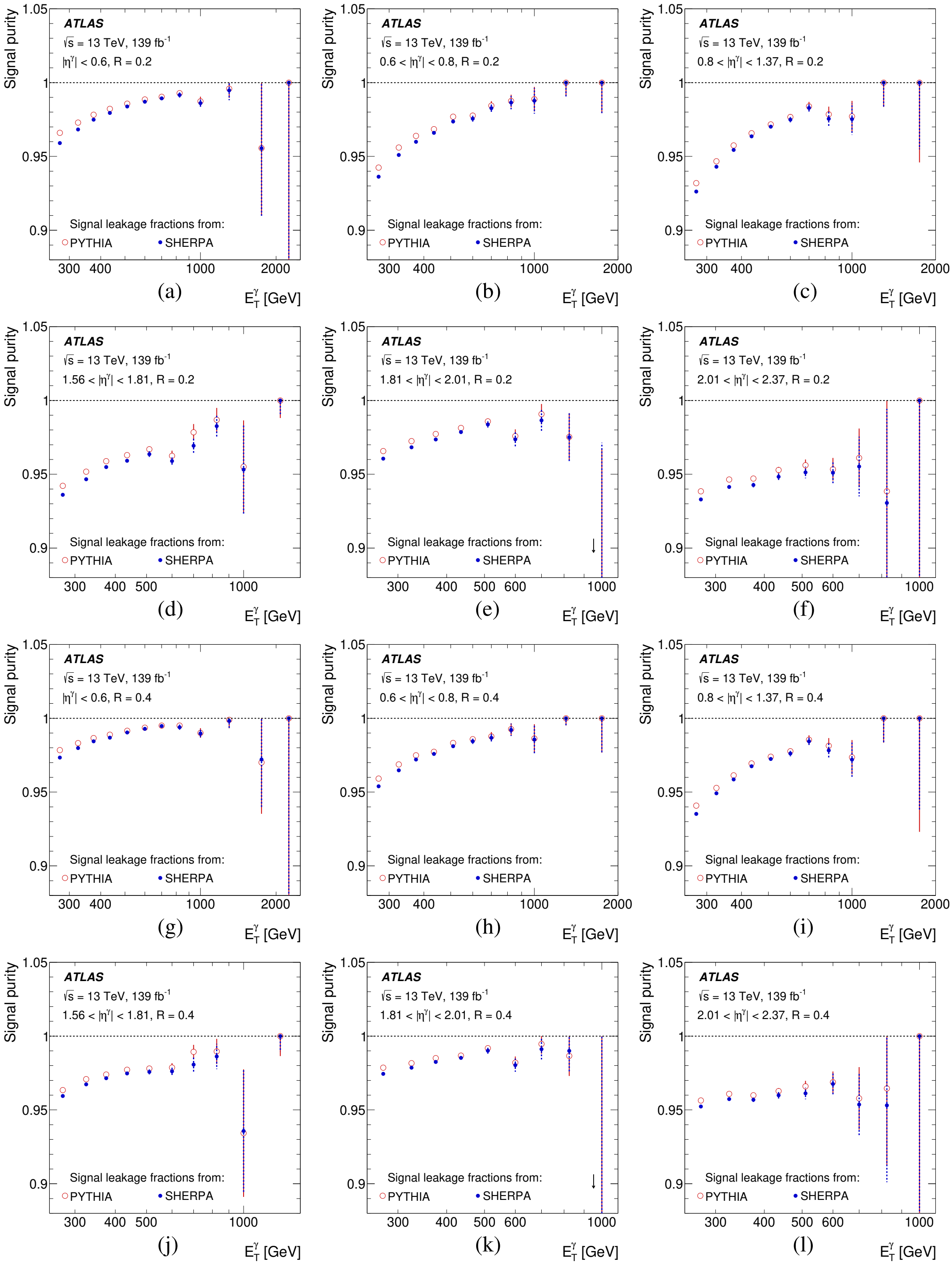

Figure 2. Estimated signal purities in data using the signal leakage fractions from SHERPA (dots) and PYTHIA (open circles) as functions of E_{T}^{γ} in different regions of η^{γ} for $R = 0.2$ (a, b, c, d, e, f) and $R = 0.4$ (g, h, i, j, k, l). The data statistical uncertainties in the signal purity are represented as solid (dashed) error bars for the determination using the signal leakage fractions of PYTHIA (SHERPA). The arrows in (e) and (k) indicate the direction in which the central values of the estimated signal purities are located since they are outside of the plotted range in these bins.

5.2 Background from electrons faking photons

Electrons and positrons can be misidentified as photons and they represent an additional source of background. This background is largely suppressed by the photon selection. The residual background contribution is evaluated using the MC simulations from SHERPA 2.2.1 (see section 3) of the $pp \to Z/\gamma^* \to e^+e^-$ and $pp \to W \to e\nu$ processes. The electron background is estimated separately in each η^γ region as a function of E_{T}^{γ} and found to be at a sub-percent level in the phase-space region of this analysis, except for $1.81 < |\eta^\gamma| < 2.37$ where it reaches $\sim 1\%$. The fraction of electrons faking photons is found to be very similar for $R = 0.2$ and $R = 0.4$. Given the small impact of this background, no attempt to subtract it is performed, and a conservative systematic uncertainty equal to the size of the evaluated background is assigned (see section 7.2.3).

5.3 Signal yields

The estimated signal yields using the signal leakage fractions from SHERPA are shown in figure 3 as functions of E_{T}^{γ} in diffferent regions of η^γ for $R = 0.2$ and $R = 0.4$. The signal yields using the signal leakage fractions from PYTHIA are very similar, as evidenced by the similar signal purity (see figure 2). The measured distributions decrease with increasing E_{T}^{γ} by approximately six orders of magnitude within the measured range. As expected, the signal yield for $R = 0.2$ is larger than for $R = 0.4$. For comparison, the simulations of PYTHIA and SHERPA are also included in these figures; both PYTHIA and SHERPA provide a reasonable description of the shape of the data distribution within statistical uncertainties, except at high E_{T}^{γ}. These predictions are based on tree-level calculations and, therefore, are affected by a theoretical uncertainty due to missing higher-order terms that can be as large as 50%.

JHEP07(2023)086

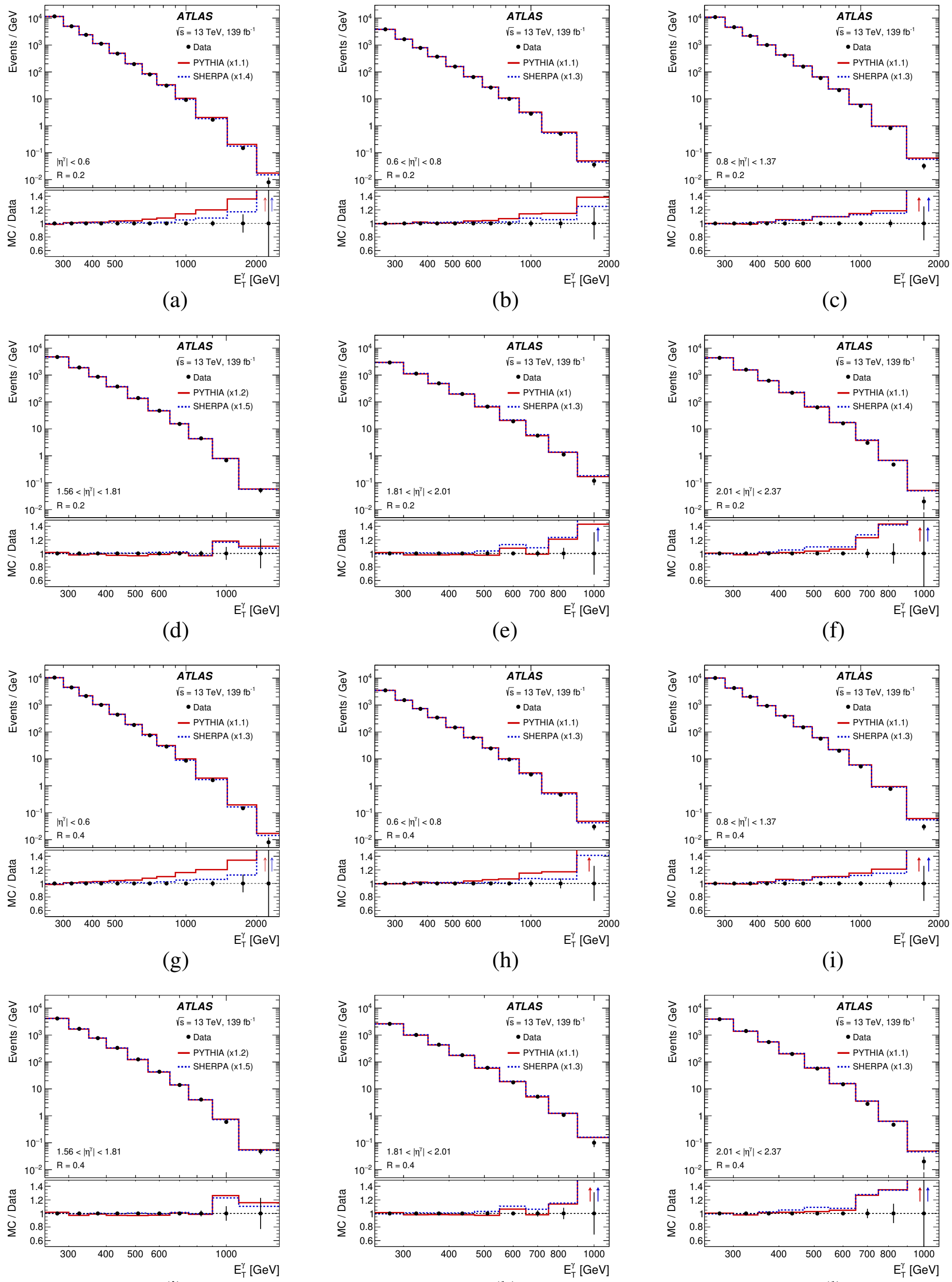

Figure 3. Estimated signal yields per GeV in data (dots) using the signal leakage fractions from Sherpa as functions of E_T^γ in different regions of η^γ for $R = 0.2$ (a, b, c, d, e, f) and $R = 0.4$ (g, h, i, j, k, l). For comparison, the MC simulations of the signal from Sherpa (dashed histograms) and Pythia (solid histograms) are also included. The MC distributions are normalised to the number of data events in each η^γ region using the factors shown in parenthesis. The ratio of the normalised MC and data distributions is shown in the lower part of the figures. The error bars display the statistical uncertainty of the data. The arrows in (a), (c), (e) (f), (g), (h), (i), (k) and (l) indicate the direction in which the ratio of the normalised MC and data distributions are located since they are outside of the plotted range in these bins.

6 Cross section measurement

The inclusive isolated-photon differential cross sections are measured as functions of E_{T}^{γ} in the η^{γ} regions given by $|\eta^{\gamma}| < 0.6$, $0.6 < |\eta^{\gamma}| < 0.8$, $0.8 < |\eta^{\gamma}| < 1.37$, $1.56 < |\eta^{\gamma}| < 1.81$, $1.81 < |\eta^{\gamma}| < 2.01$ and $2.01 < |\eta^{\gamma}| < 2.37$ for the two isolation-cone radii, $R = 0.2$ and $R = 0.4$, separately. The data are unfolded to particle level, as explained below, to the region of fiducial phase space given by isolated photons with $E_{\mathrm{T}}^{\gamma} > 250$ GeV and $|\eta^{\gamma}| < 2.37$, excluding the region $1.37 < |\eta^{\gamma}| < 1.56$. The particle-level isolation ($E_{\mathrm{T}}^{\mathrm{iso}}$(particle)) on the photon is built by summing the transverse energy of all stable particles, except for muons and neutrinos, in a cone of radius $R = 0.4$ or $R = 0.2$ around the photon direction, after the contribution from the UE is subtracted; the same subtraction procedure used on data is applied at the MC particle level. The particles associated with the overlaid *pp* collisions are not considered in the calculation of the particle-level isolation transverse energy; this is done to compare the measurements to theoretical predictions without such an effect. Isolation is ensured by requiring $E_{\mathrm{T}}^{\mathrm{iso}}(\text{particle}) < 4.2 \cdot 10^{-3} \cdot E_{\mathrm{T}}^{\gamma} + 4.8$ GeV. The fiducial phase-space region of the measurements follows closely the detector-level event selection and it is indicated in table 1.

To study the dependence of isolated-photon production on the isolation-cone radius, two additional measurements are performed, both of which are based on the differential cross sections described above. The first measurement is performed by integrating the differential cross sections in each region of η^{γ} ('fiducial integrated cross sections') and dividing by the width of each $|\eta^{\gamma}|$ region for each isolation-cone radius. These measurements are sensitive to the dependence of the inclusive isolated-photon cross section on R. The second measurement comprises the ratio of the differential cross sections with $R = 0.2$ and $R = 0.4$ as a function of E_{T}^{γ} in each η^{γ} region. These ratios are performed using directly the measurements of the differential cross sections for each isolation-cone radius. In the evaluation of the statistical uncertainties in data and MC simulations, the correlation between the sample of photon candidates selected with $R = 0.2$ and that with $R = 0.4$ is taken into account. Thanks to the cancellation of most of the systematic uncertainties, this ratio provides a very stringent test of the evolution of the R-dependence of the inclusive isolated-photon differential cross section in E_{T}^{γ} for each η^{γ} region.

6.1 Unfolding procedure for the measurement of the differential cross sections

The data distributions, after background subtraction, as functions of E_{T}^{γ} in the different η^{γ} regions defined above are unfolded to the particle level, separately for $R = 0.2$ and $R = 0.4$. The unfolding is performed independently for each value of R and each η^{γ} region. The iterative application of Bayes' theorem is used to obtain the measured differential cross sections. The Bayesian unfolding [52] method as implemented in RooUnfold [53] is used. In this method, the repeated application of Bayes' theorem is used to invert the response matrix. The response matrix is built from the two-dimensional distribution in the E_{T}^{γ}(reconstructed)–E_{T}^{γ}(particle) plane of the simulated events which fulfill simultaneously the full event selection at reconstruction and particle levels; furthermore, in each event the reconstructed photon is required to match the generated photon within $\Delta R < 0.2$. The two-

JHEP07(2023)086

Requirement	Phase-space region					
E_T^γ	$E_T^\gamma > 250$ GeV					
Isolation	$E_T^{\rm iso}$(particle) $< 4.2 \cdot 10^{-3} \cdot E_T^\gamma + 4.8$ GeV					
η^γ	$\lvert\eta^\gamma\rvert < 0.6$	$0.6 < \lvert\eta^\gamma\rvert < 0.8$	$0.8 < \lvert\eta^\gamma\rvert < 1.37$	$1.56 < \lvert\eta^\gamma\rvert < 1.81$	$1.81 < \lvert\eta^\gamma\rvert < 2.01$	$2.01 < \lvert\eta^\gamma\rvert < 2.37$

Table 1. Definition of the fiducial phase-space region for the measurements and predictions.

dimensional distribution is then used to calculate the probability for a photon generated with E_T^γ(particle) and η^γ(particle) values to be reconstructed with E_T^γ(reconstructed) and η^γ(reconstructed) values. The method also accounts for the reconstructed photons which are not matched to a truth photon because they are outside of the fiducial region ("reco unmatched") as well as reconstruction inefficiencies due to truth photons which are not matched to a reconstructed photon ("truth unmatched"). The regularisation parameter is the number of iterations ($N_{\rm iter}$), therefore regularisation is achieved by stopping the iterative procedure at a given value of $N_{\rm iter}$. The results are found to be fairly insensitive to $N_{\rm iter}$; two iterations, i.e. $N_{\rm iter} = 2$, are used in this analysis.

The nominal cross sections are measured using the response matrices from the Sherpa samples and the deviations in the results obtained by using Pythia instead are taken to represent systematic uncertainties of the effect of the parton-shower and hadronisation models in the corrections (see section 7.4).

7 Systematic uncertainties

The sources of systematic uncertainties that affect the measurements are the signal modelling, the background subtraction, the photon reconstruction, the unfolding procedure, the running conditions and the photon calibration. Each source is discussed in detail below. For some of the systematic uncertainties, the Bootstrap technique [54] is used to evaluate the statistical uncertainty in the calculated values. The dependence of the systematic uncertainties on E_T^γ is then fitted with smooth functions using the estimated statistical uncertainties as inputs. Each contribution to the systematic uncertainty is assumed to be fully correlated between measurements when calculating the uncertainties of the ratios of the cross sections, except for the $E_T^{\rm iso}$ modelling (see section 7.3.3). In the following text, an average value in η^γ of the resulting uncertainty in the measured fiducial integrated cross sections is quoted in parentheses for $R = 0.2$ and $R = 0.4$, except in the cases for which the systematic uncertainty is independent of R. The total systematic uncertainty and the main contributions for the differential cross sections and the ratios are discussed in section 7.7.

7.1 Signal modelling

The uncertainty due to the signal modelling in the signal purity calculation (see section 5) is evaluated as the deviations observed from the nominal result when using Pythia to compute the signal leakage fractions. The resulting uncertainty in the measured cross sections is similar for both radii ($\pm 0.5\%$ for $R = 0.2$ and $\pm 0.4\%$ for $R = 0.4$).

7.2 Background subtraction

7.2.1 Choice of background control regions

A data-driven method is used to subtract the multi-jet background in the signal region. The estimation of the background contamination in the signal region is affected by the choice of the background-enriched control regions. For each modification of the background control regions, the signal leakage fractions are recalculated.

$E_{\mathrm{T}}^{\mathrm{iso}}$ requirement to define the control regions. The uncertainty due to the choice of the $E_{\mathrm{T}}^{\mathrm{iso}}$ requirement to define the control regions is estimated by varying the E_{T}^{γ}-dependent isolation requirement from the nominal cut ($E_{\mathrm{T}}^{\mathrm{iso}} > E_{\mathrm{T,cut}}^{\mathrm{iso}} + 2$ GeV, see section 5) by ± 1 GeV. The resulting uncertainty in the measured cross sections for $R = 0.2$ is larger than for $R = 0.4$ ($\pm 0.05\%$ for $R = 0.2$ and $\pm 0.01\%$ for $R = 0.4$).

Upper requirement on $E_{\mathrm{T}}^{\mathrm{iso}}$. The dependence of the results on the upper requirement on $E_{\mathrm{T}}^{\mathrm{iso}}$ for regions B and D is estimated by removing it. Small differences are observed on the resulting uncertainties in the measured cross sections between $R = 0.2$ and $R = 0.4$ (-0.06% for $R = 0.2$ and -0.1% for $R = 0.4$).

Identification criteria. The nominal non-tight photon control region is defined by photons which pass loose, but fail some of the tight identification criteria. The uncertainty due to this choice is estimated by repeating the analysis with three different non-tight definitions [7]. The final uncertainty is estimated as the envelope of these variations. The resulting uncertainty in the measured cross sections for $R = 0.2$ is somewhat larger than for $R = 0.4$ ($\pm 0.8\%$ for $R = 0.2$ and $\pm 0.6\%$ for $R = 0.4$).

7.2.2 Identification and isolation correlation in the background

The isolation and identification photon variables used to define the plane in the 2D side-band method to subtract the background (see section 5) are assumed to be uncorrelated for background events ($R^{\mathrm{bg}} = 1$ in equation (5.1)). Any correlation between these variables would affect the estimation of the signal purity and lead to systematic uncertainties in the background-subtraction procedure. The same data-driven method as used in previous analyses [7, 8] is applied for the current analysis, using the same four validation regions. Region B is subdivided into two regions: region B' of tight photon candidates with $E_{\mathrm{T,cut}}^{\mathrm{iso}} + 2$ GeV $< E_{\mathrm{T}}^{\mathrm{iso}} < E_{\mathrm{T,cut}}^{\mathrm{iso}} + 10$ GeV and region B'' of tight photon candidates with $E_{\mathrm{T}}^{\mathrm{iso}} > E_{\mathrm{T,cut}}^{\mathrm{iso}} + 10$ GeV. Likewise, region D is subdivided into two regions, D' and D'', using the same separation in $E_{\mathrm{T}}^{\mathrm{iso}}$ as above. The four regions B', B'', D' and D'' are used to extract values of R^{bg} from the data after accounting for the signal leakage fractions in those regions extracted either from Pythia or Sherpa MC simulations. The dependence on the signal leakage is investigated by increasing the lower limits on $E_{\mathrm{T}}^{\mathrm{iso}}$ for the validation regions, $E_{\mathrm{T,cut}}^{\mathrm{iso}} + 2$ GeV ($E_{\mathrm{T,cut}}^{\mathrm{iso}} + 10$ GeV), each time by 1 GeV up to $E_{\mathrm{T,cut}}^{\mathrm{iso}} + 7$ GeV ($E_{\mathrm{T,cut}}^{\mathrm{iso}} + 15$ GeV) for regions B' and D' (B'' and D''), keeping the width in $E_{\mathrm{T}}^{\mathrm{iso}}$ fixed to 8 GeV for the regions

B' and D'. As a result of this study, the range of variation from unity for $R^{\rm bg}$ is $0.10 - 0.25$. These maximum deviations are used to re-evaluate the signal yields before the unfolding procedure and are very similar for $R = 0.2$ and $R = 0.4$, showing that the effects are largely correlated. The symmetrised resulting uncertainty in the measured cross sections for $R = 0.2$ is somewhat larger than for $R = 0.4$ ($\pm 0.8\%$ for $R = 0.2$ and $\pm 0.6\%$ for $R = 0.4$).

7.2.3 Background from electrons faking photons

As discussed in section 5.2, the background from electrons faking photons is at a sub-percent level and no background subtraction is performed. A systematic uncertainty is included by taking the full size of this background, after adding W + jets and Z + jets contributions linearly, depending on the $E_{\rm T}^{\gamma}$ and η^{γ} region. The resulting uncertainty in the measured cross sections ranges from $\pm 0.4\%$ to $\pm 1.3\%$ for both $R = 0.2$ and $R = 0.4$.

7.3 Photon reconstruction

7.3.1 Photon-reconstruction efficiency

The impact of the uncertainty in the photon-reconstruction efficiency is estimated by propagating the uncertainties in the scale factors applied to the MC events to match the reconstruction efficiency between data and simulation (see section 4) [55] through the unfolding. The resulting uncertainty in the measured cross sections is $\pm 0.3\%$ for both radii.

7.3.2 Photon-identification efficiency

The impact of the uncertainty in the photon-identification efficiency is estimated by propagating the uncertainties in the scale factors, which are applied to the MC events to match the tight identification efficiency between data and simulation, to the final results. The resulting uncertainty in the measured cross sections is $\pm 0.6\%$ for both radii. The size of this systematic uncertainty is significantly reduced [47] with respect to the previous analysis [8] ($1\% - 3\%$).

7.3.3 $E_{\rm T}^{\rm iso}$ modelling

The systematic uncertainty due to the modelling of the $E_{\rm T}^{\rm iso}$ distribution is obtained by propagating the uncertainties in the data-driven corrections to $E_{\rm T}^{\rm iso}$ applied to the MC samples discussed in section 4. The resulting uncertainty in the measured cross sections for $R = 0.4$ is somewhat larger than for $R = 0.2$ ($\pm 0.02\%$ for $R = 0.2$ and $\pm 0.07\%$ for $R = 0.4$). This source of uncertainty, in contrast to the others, is conservatively taken as uncorrelated when performing the ratios of the measured differential cross sections since the extraction procedures for the two isolation radii are completely independent.

7.4 Unfolding procedure

7.4.1 Parton-shower and hadronisation model dependence

The effect of the parton-shower and hadronisation models in the unfolding is estimated as the change in the measured cross section between the results using the response matrices of Sherpa (default MC used for unfolding) and Pythia. Some differences are observed

JHEP07(2023)086

between the resulting uncertainties in the measured cross sections for $R = 0.2$ and $R = 0.4$ ($\pm 0.7\%$ for $R = 0.2$ and $\pm 0.5\%$ for $R = 0.4$). The uncertainties due to the scale variations, the strong coupling constant and PDFs in the MC samples of events used for unfolding are also investigated and found to have a negligible impact in the measured cross sections.

7.4.2 Unfolding closure

An uncertainty due to the non-closure of the unfolding procedure is estimated in the following way. The MC SHERPA distributions are weighted to the data after background subtraction. The nominal MC SHERPA samples are used as pseudo-data and unfolded with the weighted samples. The unfolded results are compared to the SHERPA predictions at particle level and the differences are taken as the non-closure uncertainties. The resulting uncertainties in the measured cross sections are typically much smaller than 0.1%, except in the tails of the most forward η^{γ} region, where they reach up to 0.3%, for both $R = 0.2$ and $R = 0.4$.

7.4.3 MC statistical uncertainties

The statistical uncertainty due to the limited number of simulated events mainly affects the estimation of the response matrices. The resulting uncertainties in the measured cross sections are very small for both radii ($\pm 0.09\%$ for $R = 0.2$ and $\pm 0.1\%$ for $R = 0.4$).

7.5 Running conditions

7.5.1 Pile-up

The uncertainty related to pile-up weighting of the simulated events is propagated to the final results. The resulting uncertainty in the measured cross sections for $R = 0.4$ is larger than for $R = 0.2$ ($\pm 0.4\%$ for $R = 0.2$ and $\pm 1.0\%$ for $R = 0.4$).

7.5.2 Trigger efficiency

The uncertainty in the trigger efficiency is estimated using the same methodology as in ref. [25] and it is propagated to the measured cross sections. The uncertainty is estimated to be between 0.05% and 0.15%, depending on the η^{γ} and E_{T}^{γ} regions and independent of R.

7.5.3 Measurement of the integrated luminosity

The uncertainty in the integrated luminosity is $\pm 1.7\%$ [28]. This uncertainty is fully correlated in all bins of all the measured cross sections.

7.6 Photon calibration: energy scale and resolution

The assessment of the systematic uncertainty in the photon energy scale and resolution is performed following the model originally presented in ref. [56] and subsequently updated in ref. [47] for Run 2 data-taking conditions.

The sources of uncertainty in the photon energy scale include: the uncertainty in the overall energy scale adjustment using $Z \to e^+e^-$ events; the uncertainty in the non-linearity of the energy measurement at the cell level of the EM calorimeter; the uncertainty in the relative calibration of the different calorimeter layers; the uncertainty in the amount of material in front of the calorimeter; the uncertainty in the modelling of the reconstruction of photon conversions; and the uncertainty in the modelling of the lateral shower shape. The sources of uncertainty in the photon energy resolution include: the uncertainty in the modelling of the sampling term and the uncertainty in the measurement of the constant term in Z-boson decays. The sources of uncertainty are modelled using independent components to account for their η dependence. All the uncertainty components are propagated separately through the analysis to keep track of the information about the correlations between different bins. The systematic uncertainty in the measured cross section is evaluated by varying each individual source of uncertainty separately by $\pm 1\sigma$ in the MC simulations and then adding the uncertainty contributions in quadrature. The resulting uncertainties in the measured integrated fiducial cross sections are $\pm 0.09\%$ for the energy resolution and $\pm 3.7\%$ for the energy scale, independent of R. For the differential cross sections, the energy scale uncertainty is $\approx (2-6)\%$ at $E_{\mathrm{T}}^{\gamma} = 250$ GeV and rises up to $\approx (6-20)\%$ at high E_{T}^{γ}, depending on the η^{γ} region, for both isolation-cone radii. This constitutes the dominant contribution to the total systematic uncertainty (see section 7.7).

7.7 Total systematic uncertainty

The total systematic uncertainty is computed by adding in quadrature the sources of uncertainty listed in the previous sections. Figure 4 shows the resulting relative total systematic uncertainties in the differential cross sections as functions of E_{T}^{γ} in different regions of η^{γ} and for the two isolation radii. There are bin-to-bin correlations of the systematic uncertainties for each source. For instance, the systematic uncertainty due to the photon energy scale and resolution is partially correlated bin-to-bin and its decomposition into independent sources is used (see section 7.6). The following uncertainties are considered as uncorrelated bin-to-bin: photon-identification efficiency, choice of background control regions, $E_{\mathrm{T}}^{\mathrm{iso}}$ modelling and MC statistical uncertainties.

The three dominant uncertainties in the measured differential cross sections, namely, the photon energy scale and luminosity uncertainties for both $R = 0.2$ and $R = 0.4$, and the uncertainty due to the background correlation for $R = 0.2$ and the pile-up uncertainty for $R = 0.4$, are also included in figure 4. The total systematic uncertainty varies in the range $(3-20)\%$, depending on E_{T}^{γ} and η^{γ}. The systematic uncertainty in the photon-energy scale is larger in the regions $0.8 < |\eta^{\gamma}| < 1.37$ and $1.56 < |\eta^{\gamma}| < 1.81$ due to the presence of more material upstream of the calorimeter than in $|\eta^{\gamma}| < 0.8$. The systematic uncertainties dominate the total uncertainty for E_{T}^{γ} up to 1.5 TeV for $|\eta^{\gamma}| < 0.6$ and $0.8 < |\eta^{\gamma}| < 1.37$, up to 1.1 TeV for $0.6 < |\eta^{\gamma}| < 0.8$ and $1.56 < |\eta^{\gamma}| < 1.81$, and up to 0.9 TeV for $1.81 < |\eta^{\gamma}| < 2.37$. For higher E_{T}^{γ} values, the statistical uncertainty of the data limits the precision of the measurements. Previously [8], the E_{T}^{γ} values up to which the systematic uncertainties dominated were: 1.1 TeV for $|\eta^{\gamma}| < 1.37$, 0.9 TeV for $1.56 < |\eta^{\gamma}| < 1.81$, and 0.75 TeV for $1.81 < |\eta^{\gamma}| < 2.37$.

The resulting relative total systematic uncertainties in the ratios of the differential cross sections for $R = 0.2$ and $R = 0.4$ as functions of E_{T}^{γ} in different regions of η^{γ} are shown in figure 5. Some residual statistical effects might remain in the individual contributions to the total systematic uncertainty in the ratios after taking into account the correlations between the measurements of the differential cross sections with the different radii. The main contributions to the total systematic uncertainty in the ratios of the measured differential cross sections are also included in figure 5; the dominant components are the pile-up modelling, the MC modelling used for unfolding and the R^{bg} correlation. In these measurements, the luminosity and other contributions which yield uncertainties in the differential cross sections that are independent of the isolation radius cancel out. In particular, the photon energy scale is no longer the dominant contribution. Since the different sources of uncertainty, except for the $E_{\mathrm{T}}^{\mathrm{iso}}$ modelling, are taken as fully correlated, there is a significant reduction both in the total systematic uncertainty (typically $< 1\%$) and the data statistical uncertainty. Thus, the ratios of the differential cross sections constitute a compelling measurement for precise testing of the underlying pQCD theory.

JHEP07(2023)086

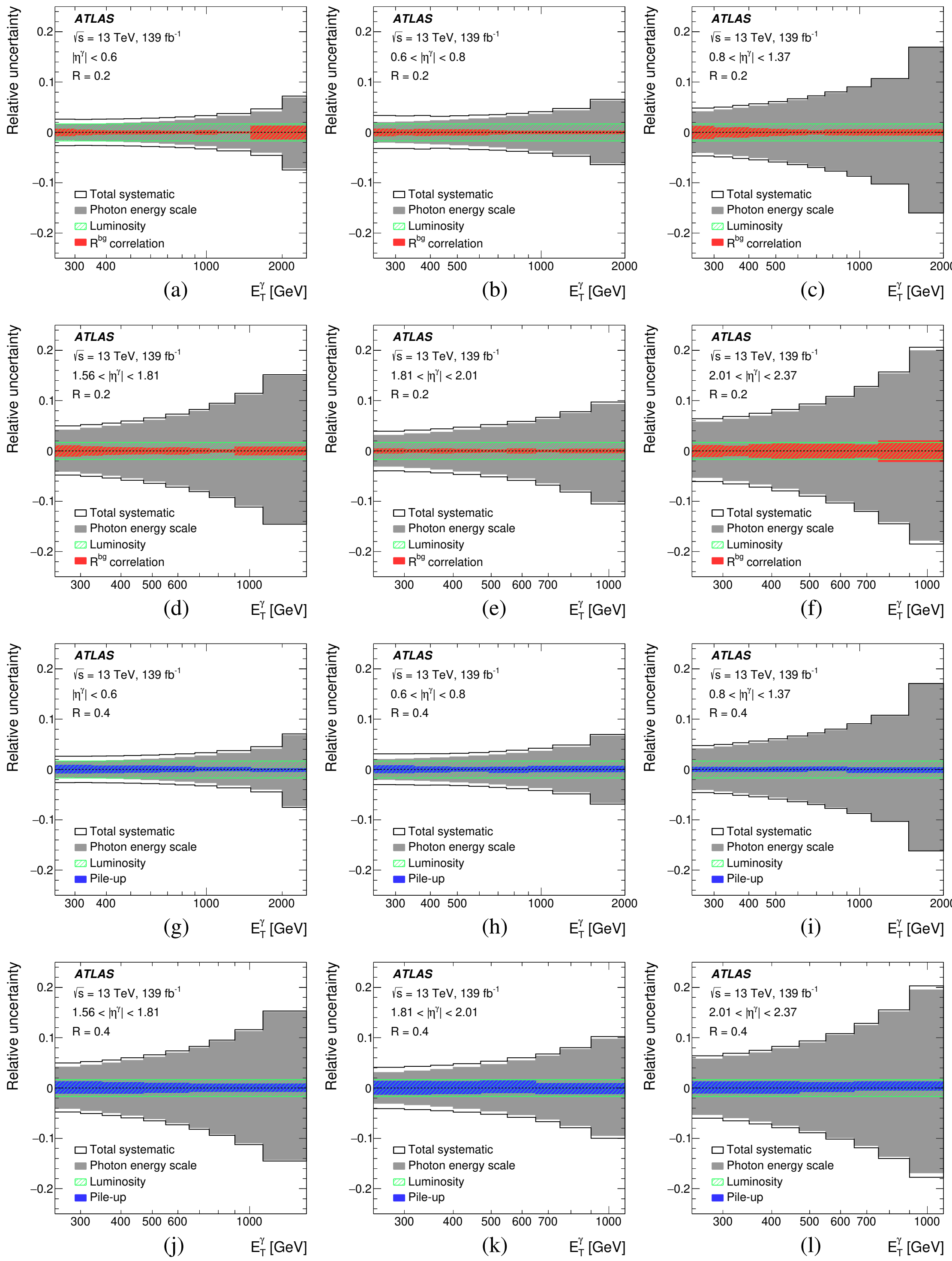

Figure 4. Relative systematic uncertainties in the differential cross sections as functions of E_T^γ in different regions of η^γ for $R = 0.2$ (a, b, c, d, e, f) and $R = 0.4$ (g, h, i, j, k, l): total (black histograms), and main contributions from photon energy scale (grey areas), luminosity (green hatched areas), R^{bg} correlation (red areas, only for $R = 0.2$) and pile-up modelling (blue areas, only for $R = 0.4$).

JHEP07(2023)086

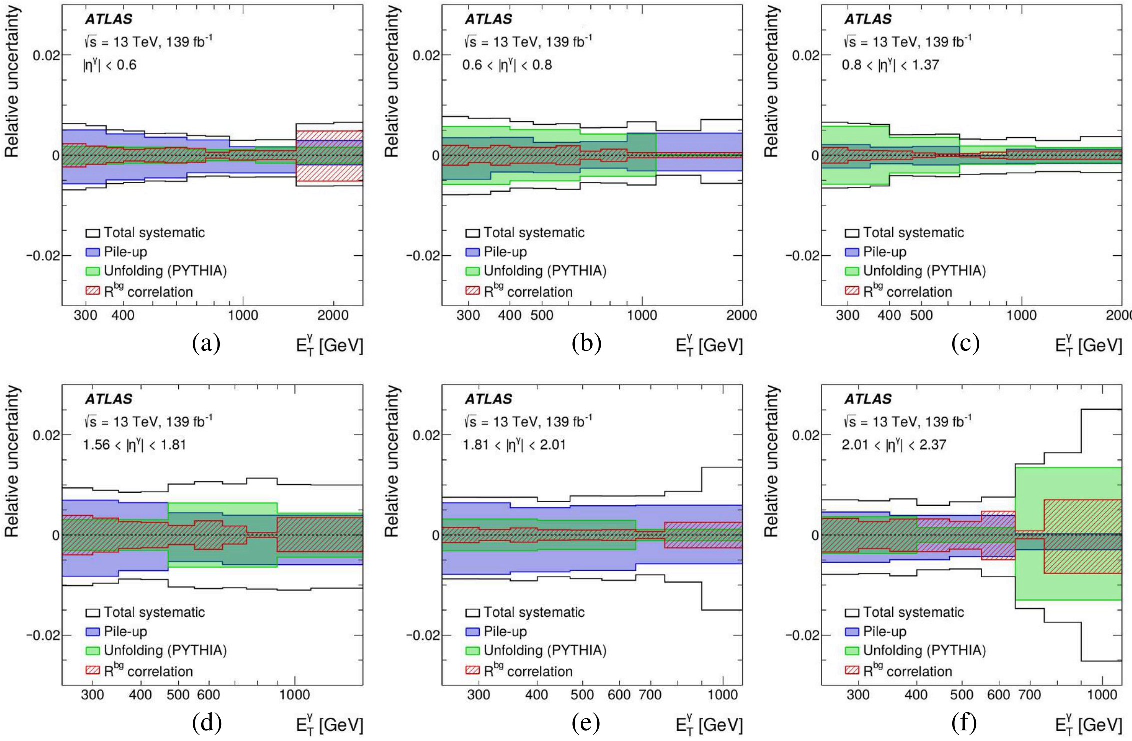

Figure 5. Relative total systematic uncertainty in the ratios of the differential cross sections for $R = 0.2$ and $R = 0.4$ (black histograms), relative uncertainty due to the pile-up modelling (blue areas), relative uncertainty due to the MC modelling used for unfolding (green areas) and relative uncertainty due to the R^{bg} correlation (red hatched areas) as functions of E_{T}^{γ} in different regions of η^{γ}.

8 Theoretical predictions

The NLO pQCD calculations presented in this paper are computed using the programs JETPHOX 1.3.1_2 and SHERPA 2.2.2. The NNLO pQCD predictions are calculated in the NNLOJET framework. The comparison of these predictions to the measurements is presented in section 9.

Jetphox predictions. The JETPHOX program includes a full NLO pQCD calculation of both the direct and the fragmentation contributions to the cross section for the $pp \to \gamma + \text{jet} + X$ process. The number of massless quark flavours is set to five. The renormalisation scale μ_{R}, the factorisation scale μ_{F} and the fragmentation scale μ_{f} are chosen to be $\mu_{\mathrm{R}} = \mu_{\mathrm{F}} = \mu_{\mathrm{f}} = \mu = E_{\mathrm{T}}^{\gamma}/2$. For the nominal predictions, the calculations are performed using the MMHT2014 [57] PDF set and the BFG set II of parton-to-photon fragmentation functions [58], both at NLO. The strong coupling constant is set to $\alpha_{\mathrm{s}}(m_{\mathrm{Z}}) = 0.120$; for consistency, in this calculation as well as in those described below, the value of $\alpha_{\mathrm{s}}(m_{\mathrm{Z}})$ is set to that assumed in the PDF set. For the electromagnetic coupling (α_{EM}), the low-energy limit value of $1/137.036$ is used. The calculations are performed using the fixed-cone isolation criterion at parton level which requires the total transverse energy from the partons inside a cone of radius $R = 0.4$ or $R = 0.2$ around the photon direction to be below

JHEP07(2023)086

$4.2 \cdot 10^{-3} \cdot E_{\mathrm{T}}^{\gamma} + 4.8$ GeV. Predictions based on other PDF sets are also performed to test the sensitivity of the observables to each different PDF set from the comparison to the data.

Sherpa predictions. The SHERPA 2.2.2 program consistently combines parton-level calculations of $\gamma + (1,\ 2) -$ jet events at NLO and $\gamma + (3,\ 4) -$ jet events at LO [37, 38] supplemented with a parton shower [39] while avoiding double-counting effects [40]. A requirement on the photon isolation at the matrix-element level is imposed using Frixione's criterion with $\mathcal{R} = 0.1$, $n = 2$ and $\epsilon = 0.1$. The prescription employed is referred to as 'hybrid-cone isolation' [16, 59] since it includes the application of the Frixione's criterion at a small value of ΔR ($\mathcal{R} = 0.1$) and the fixed-cone isolation at $R = 0.4$ or $R = 0.2$ used for the fiducial region of the measurement. Dynamic μ_{R} and μ_{F} scales are adopted ($\mu_{\mathrm{R}} = \mu_{\mathrm{F}} = E_{\mathrm{T}}^{\gamma}$) as well as a dynamical merging scale with $\bar{Q}_{\mathrm{cut}} = 20$ GeV [59]. The strong coupling constant is set to $\alpha_{\mathrm{s}}(m_{\mathrm{Z}}) = 0.118$. The same prescription for the electromagnetic coupling as for the JETPHOX prediction is used. Fragmentation into hadrons and simulation of the UE are performed using the same models as for the LO SHERPA samples. The NNPDF3.0 NNLO PDF set [41] is used in conjunction with the corresponding SHERPA tuning. These predictions are referred to as 'SHERPA NLO' in the following.

Nnlojet predictions. The NNLO corrections include three types of parton-level contributions, namely the two-loop corrections to the Born-level processes, the one-loop Feynman diagrams with an additional parton radiation, and the emission of two additional partons. The three contributions to the NNLO corrections are individually infrared divergent, but these divergencies cancel when all contributions are considered together. Direct and fragmentation processes are included in this calculation. The fragmentation component is treated using the parton-to-photon fragmentation functions BFG set II in the antenna approximation, as described in ref. [60]. Therefore, fixed-cone requirements, as in the experiment, can be applied on these parton-level calculations. The renormalisation and factorisation scales are set to $\mu_{\mathrm{R}} = \mu_{\mathrm{F}} = E_{\mathrm{T}}^{\gamma}$, whereas the fragmentation scale is set to $\mu_{\mathrm{f}} = \sqrt{E_{\mathrm{T}}^{\gamma} \cdot E_{\mathrm{T}}^{\mathrm{max}}} \cdot R$ [19], where $E_{\mathrm{T}}^{\mathrm{max}}$ is the maximal hadronic transverse energy in the isolation cone of radius R. The CT18NNLO PDF set [61] is used. The strong coupling constant is set to $\alpha_{\mathrm{s}}(m_{\mathrm{Z}}) = 0.118$ while the electromagnetic coupling is set to $\alpha_{\mathrm{EM}} = 1/137.036$. The photon is required to be isolated by demanding that the transverse energy within a cone of $R = 0.4$ or $R = 0.2$ around the photon direction is smaller than $4.2 \cdot 10^{-3} \cdot E_{\mathrm{T}}^{\gamma} + 4.8$ GeV. The prediction at NLO pQCD in the NNLOJET framework is also calculated to illustrate the improvements achieved by including the NNLO pQCD corrections.

Differences between the theoretical calculations. There are several differences between the calculations using JETPHOX, SHERPA NLO and NNLOJET: the calculations from NNLOJET include NNLO pQCD corrections and adopt a different scheme to include the fragmentation contribution as well as a different choice of μ_{f} than JETPHOX; the calculations using SHERPA NLO include higher-order contributions as well as parton showers. The application of the Frixione's criterion in SHERPA NLO at matrix-element level allows the fragmentation contribution to be ignored. The prediction for the cross section using

Program	Order in α_s	Fragmentation	Parton shower	Isolation method	PDF	Particle level
JETPHOX	NLO	yes	no	fixed cone	– MMHT2014 – CT18 – NNPDF3.1 – HERAPDF2.0 – ATLASpdf21	no
SHERPA NLO	NLO for $\gamma+(1,2)$-jet LO for $\gamma+(3,4)$-jet	no	yes	hybrid	NNPDF3.0	yes
NNLOJET	(N)NLO	yes	no	fixed cone	CT18NNLO	no

Table 2. Major features of the three predictions used for inclusive isolated-photon production.

SHERPA NLO is at particle level and includes UE effects. A compilation of the major features of the three different approaches is shown in table 2.

Sensitivity of the NLO predictions to the PDFs. The sensitivity of the differential cross sections to the proton PDFs is investigated by comparing the calculations of JETPHOX based on MMHT2014 with alternative calculations based on other PDF sets, namely CT18NLO [61], NNPDF3.1 [62], HERAPDF2.0 [63] and ATLASpdf21 [64]. The ATLASpdf21 PDFs are at NNLO, whereas the other PDF sets are at NLO, and were extracted including as input the ratios of the measured differential cross sections for inclusive-photon production at 13 TeV over those at 8 TeV [65]. Figure 6 shows the relative difference between these alternative predictions of JETPHOX for $R = 0.2$ or $R = 0.4$ and the prediction based on MMHT2014 as functions of E_T^γ in different regions of η^γ. Differences between the PDF sets are observed: the predictions based on the ATLASpdf21 and on the HERAPDF2.0 PDF sets show differences of up to $\approx 10\%$ with respect to those based on the MMHT2014 PDF set, whereas those from CT18NLO (NNPDF3.1) are within 2% of those based on MMHT2014 at low E_T^γ but tend to be somewhat higher (lower) than MMHT2014 at high E_T^γ values in each η^γ region. As expected, the sensitivity of the observables to the PDF set is largely independent of the isolation cone radius.

JHEP07(2023)086

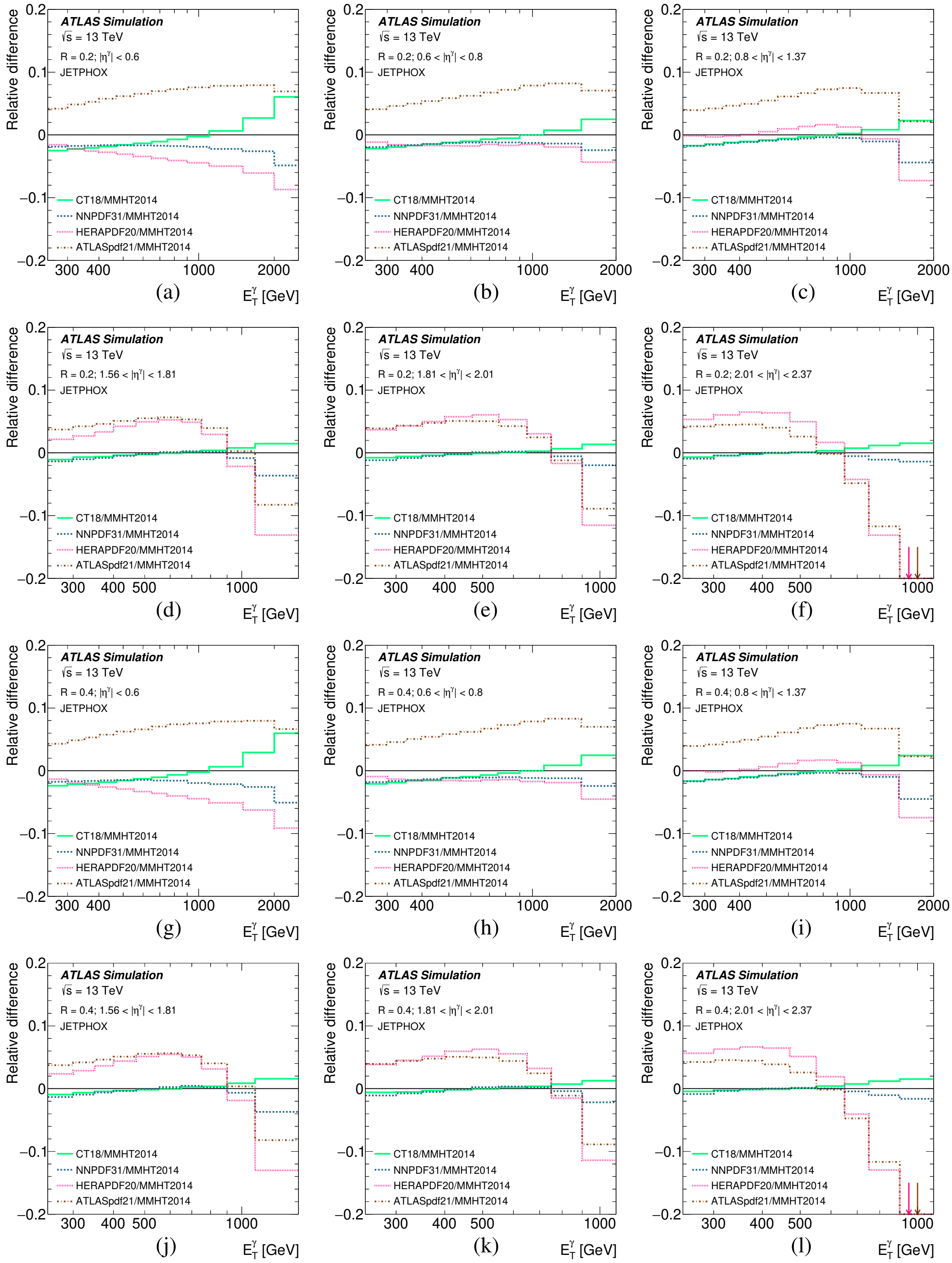

Figure 6. Relative difference between the JETPHOX predictions based on the CT18 (solid lines), NNPDF3.1 (dashed lines), HERAPDF2.0 (dotted lines) and ATLASpdf21 (dot-dashed lines) and those based on the MMHT2014 PDFs for $R = 0.2$ (a, b, c, d, e, f) and $R = 0.4$ (g, h, i, j, k, l) as functions of E_{T}^{γ} in different regions of η^{γ}. The arrows in (f) and (l) indicate the direction in which the relative differences are located since they are outside of the plotted range in these bins.

8.1 Hadronisation and underlying-event corrections to the fixed-order pQCD calculations

The NLO pQCD predictions from JETPHOX and the (N)NLO predictions from NNLOJET are at the parton level, while the measurements are unfolded at the particle level. Thus, there can be differences between the two levels concerning the photon isolation as well as the photon four-momentum. Since the data are corrected for pile-up and UE effects and the distributions are unfolded to a phase-space definition in which the requirement on $E_{\mathrm{T}}^{\mathrm{iso}}$(particle) is applied after subtraction of the UE, it is expected that the parton-to-hadron corrections to the predictions are small.

Correction factors to the differential cross section predictions are estimated by computing the ratio of the particle-level cross section for a PYTHIA sample generated using version 8.243 with UE effects to the parton-level cross section without UE effects. For the sample with UE, the same jet-area based subtraction method used in data and particle-level MC is applied. The correction factors are found to be consistent with unity within $\pm 1\%$ for both isolation cone radii, and no significant dependence on η^{γ} is observed. Thus, no corrections are applied to the differential cross section predictions and an uncertainty of $\pm 1\%$ is assigned for these effects for both isolation radii.

For the ratio of the differential cross sections with different isolation radii, the non-perturbative correction factors are also very close to unity; a fit to a constant function for the non-perturbative correction for the ratio of cross sections yields 0.9998 ± 0.0008. Also in this case, no correction is applied and an uncertainty is assigned to the ratio predictions given by the difference of the correction factors from unity in each bin of E_{T}^{γ}. This uncertainty ranges from 0.06% to 0.8%, depending on the E_{T}^{γ} bin and the η^{γ} region.

8.2 Theoretical uncertainties

The theoretical uncertainties for the differential cross section predictions are estimated in the following way:

- The uncertainty in the NLO pQCD predictions from JETPHOX due to missing higher-order terms is estimated by repeating the calculations using values of μ_{R}, μ_{F} and μ_{f} scaled by the factors 0.5 and 2. The three scales are either varied simultaneously, individually or by fixing one and varying the other two. In all cases, the condition $0.5 \leq \mu_A/\mu_B \leq 2$ is imposed, where $A, B = \mathrm{R},\ \mathrm{F},\ \mathrm{f}$. The final uncertainty is taken as the largest deviation from the nominal value among the 14 possible variations. A similar method is used for the predictions of NNLOJET [19]. In the case of the SHERPA NLO predictions, which do not include the fragmentation contribution, μ_{R} and μ_{F} are varied as above and the largest deviation from the nominal value among the 6 possible variations is taken as the uncertainty.

- The uncertainty in the NLO pQCD predictions from JETPHOX due to the uncertainty in the proton PDFs is estimated by repeating the calculations using the 50 sets from the MMHT2014 error analysis [57] and applying the Hessian method [66] for the evaluation of the PDF uncertainty. The PDF uncertainty for the NNLOJET calculations is not available; thus, this uncertainty is taken from the corresponding relative uncertainty of the JETPHOX predictions. In the case of SHERPA NLO, this uncertainty is estimated using the 100 replicas from the NNPDF3.0 analysis [41].

- The uncertainty in the NLO pQCD predictions from JETPHOX (SHERPA NLO) due to the uncertainty in α_s is estimated by repeating the calculations using two additional sets of proton PDFs from the MMHT2014 (NNPDF3.0) analysis, for which different values of α_s at m_Z are assumed in the fits, namely 0.118 (0.117) and 0.122 (0.119); in this way, the correlation between α_s and the PDFs is preserved. The α_s uncertainty for the NNLOJET calculations is not available; thus, this uncertainty is taken from the corresponding relative uncertainty of the JETPHOX predictions.

- The uncertainty in the NLO pQCD predictions from JETPHOX due to the uncertainty in the fragmentation functions is evaluated by repeating the calculations using the BFG set I [58] and comparing the results with the nominal predictions. The uncertainty is found to be negligible.

- An uncertainty of $\pm 1\%$ is included in the uncertainty of the JETPHOX and NNLOJET predictions due to the non-perturbative corrections.

The total theoretical uncertainty for the differential cross section predictions is obtained by adding in quadrature the individual uncertainties listed above. Figures 7 and 8 show the relative total theoretical uncertainties and the components as functions of E_T^γ in different regions of η^γ for $R = 0.2$ and $R = 0.4$ for JETPHOX and SHERPA NLO, respectively. The total theoretical uncertainty ranges from $\approx 10\%$ to $\approx 15\%$ for JETPHOX and it is $\approx 20\%$ for SHERPA NLO. No significant difference in the size of the uncertainties is observed between the predictions for $R = 0.2$ and $R = 0.4$. The dominant theoretical uncertainty is the one arising from missing higher-order terms. For large E_T^γ values, the uncertainty coming from the PDFs is the second dominant contribution. Figure 9 shows the uncertainties in the NNLO pQCD prediction due to missing higher-order terms. These uncertainties are in the range $(1-6)\%$ and are smaller than those in the NLO pQCD prediction (also shown in figure 9) by a factor between $2-15$, depending on E_T^γ, η^γ and R.

Figure 10 shows the relative theoretical uncertainty and its components as functions of E_T^γ in different regions of η^γ for the ratio of the differential cross sections for the JETPHOX and SHERPA NLO predictions. The theoretical uncertainties in the ratios are estimated as fully correlated for both isolation-cone radii; as a consequence, a significant reduction of the theoretical uncertainty is obtained: for JETPHOX (SHERPA NLO), the theoretical uncertainty decreases from $\approx (10-15)\%$ ($\approx 20\%$) in the differential cross sections to $\approx 1.5\%$ ($\approx 1.5\%$) in the ratios. Figure 11 shows the relative theoretical uncertainty and its components as functions of E_T^γ in different regions of η^γ for the ratio of the differential cross sections for the NNLO predictions; the uncertainty due to missing higher-order terms decreases to typically less than 1% in the ratio.

JHEP07(2023)086

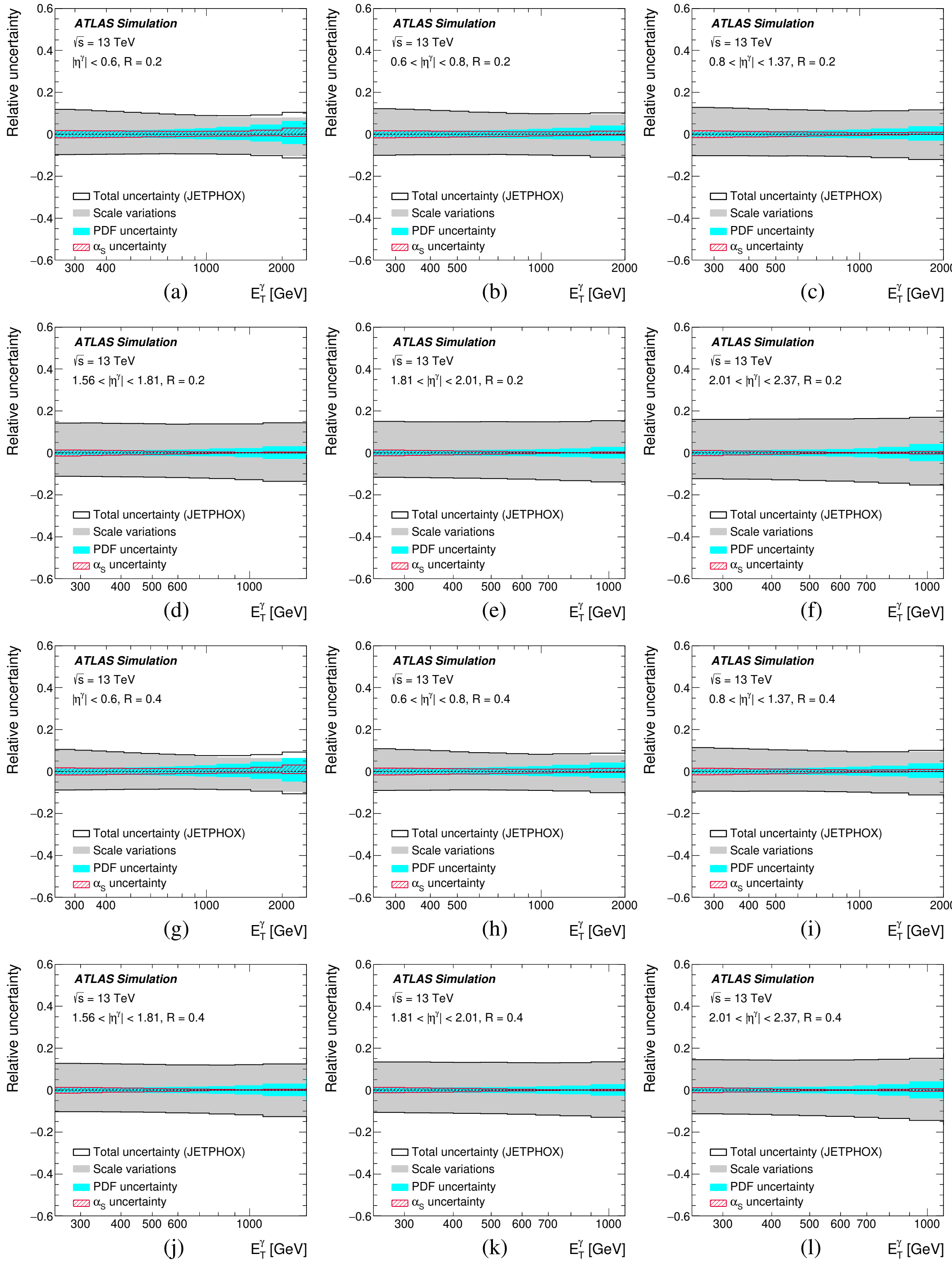

Figure 7. Relative theoretical uncertainty in JETPHOX arising from scale variations (grey areas), PDF uncertainty (cyan areas), α_s uncertainty (red hatched areas) and the total theoretical uncertainty (black histogram, which includes the uncertainty in the non-perturbative corrections) for the differential cross sections with $R = 0.2$ (a, b, c, d, e, f) and $R = 0.4$ (g, h, i, j, k, l) as functions of E_T^γ in different regions of η^γ.

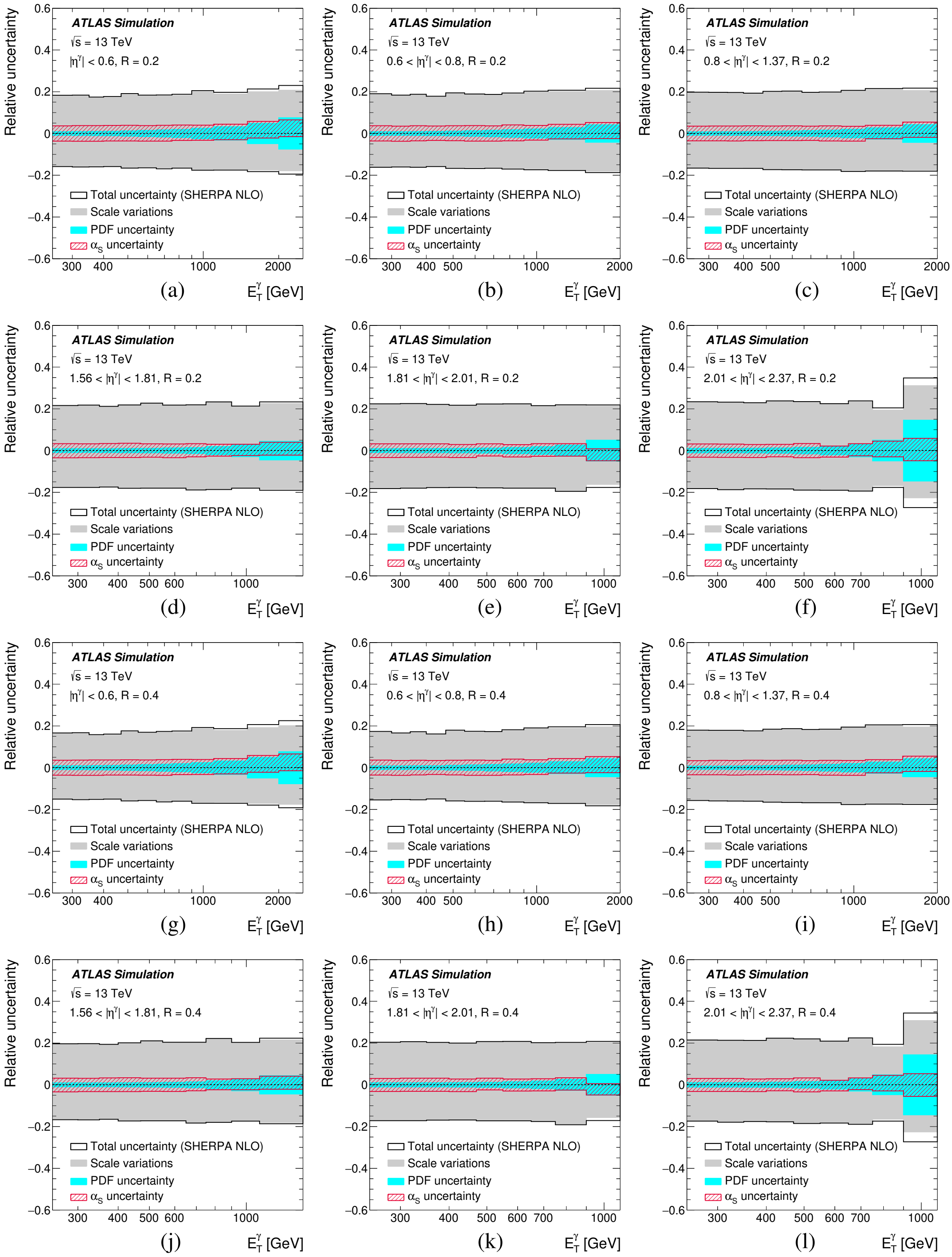

Figure 8. Relative theoretical uncertainty in SHERPA NLO arising from scale variations (grey areas), PDF uncertainty (cyan areas), α_s uncertainty (red hatched areas) and the total theoretical uncertainty (black histogram) for the differential cross sections with $R = 0.2$ (a, b, c, d, e, f) and $R = 0.4$ (g, h, i, j, k, l) as functions of E_T^γ in different regions of η^γ.

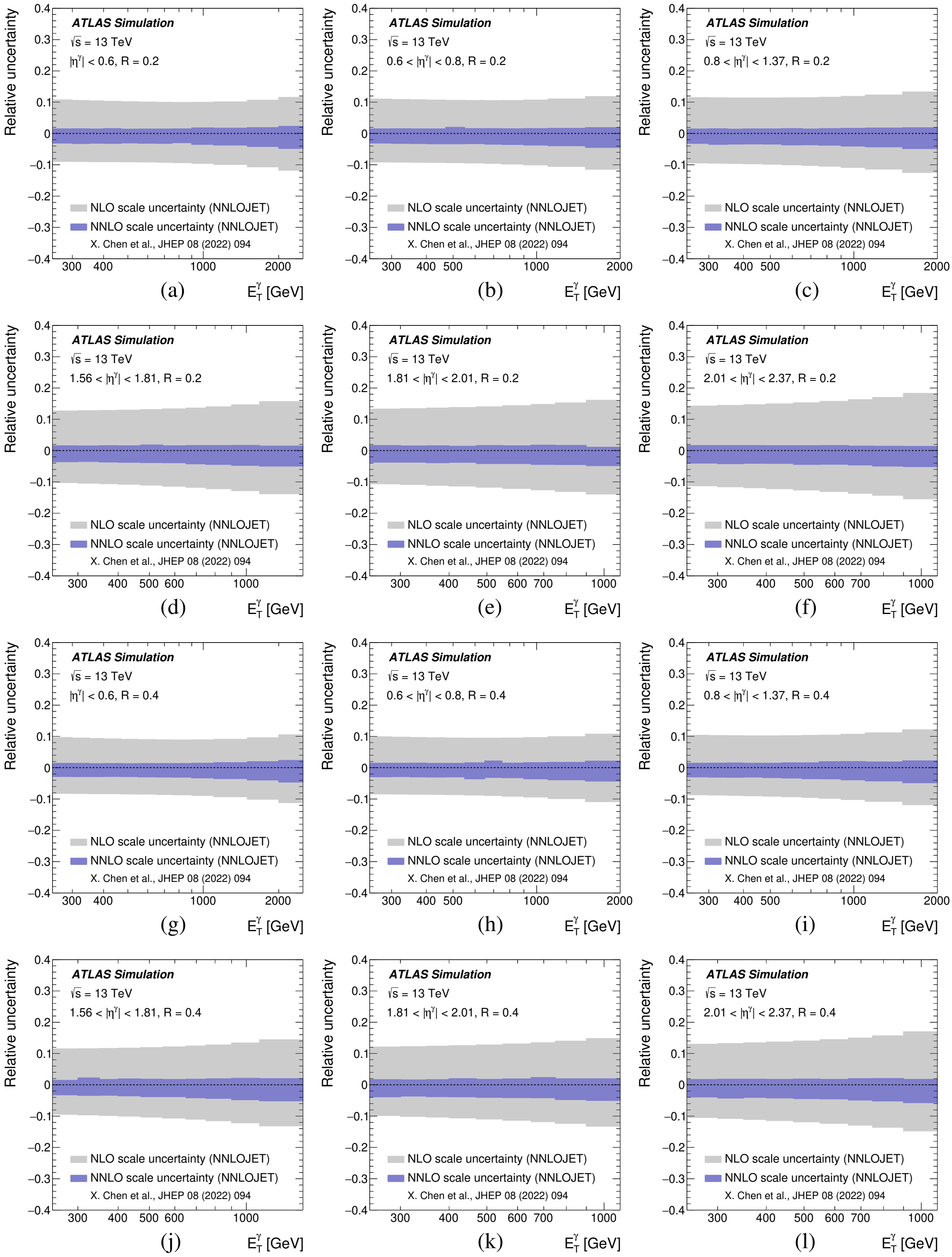

Figure 9. Relative theoretical uncertainty in NNLOJET arising from scale variations in the NLO (grey areas) and NNLO (violet areas) predictions for the differential cross sections with $R = 0.2$ (a, b, c, d, e, f) and $R = 0.4$ (g, h, i, j, k, l) as functions of E_{T}^{γ} in different regions of η^{γ}.

JHEP07(2023)086

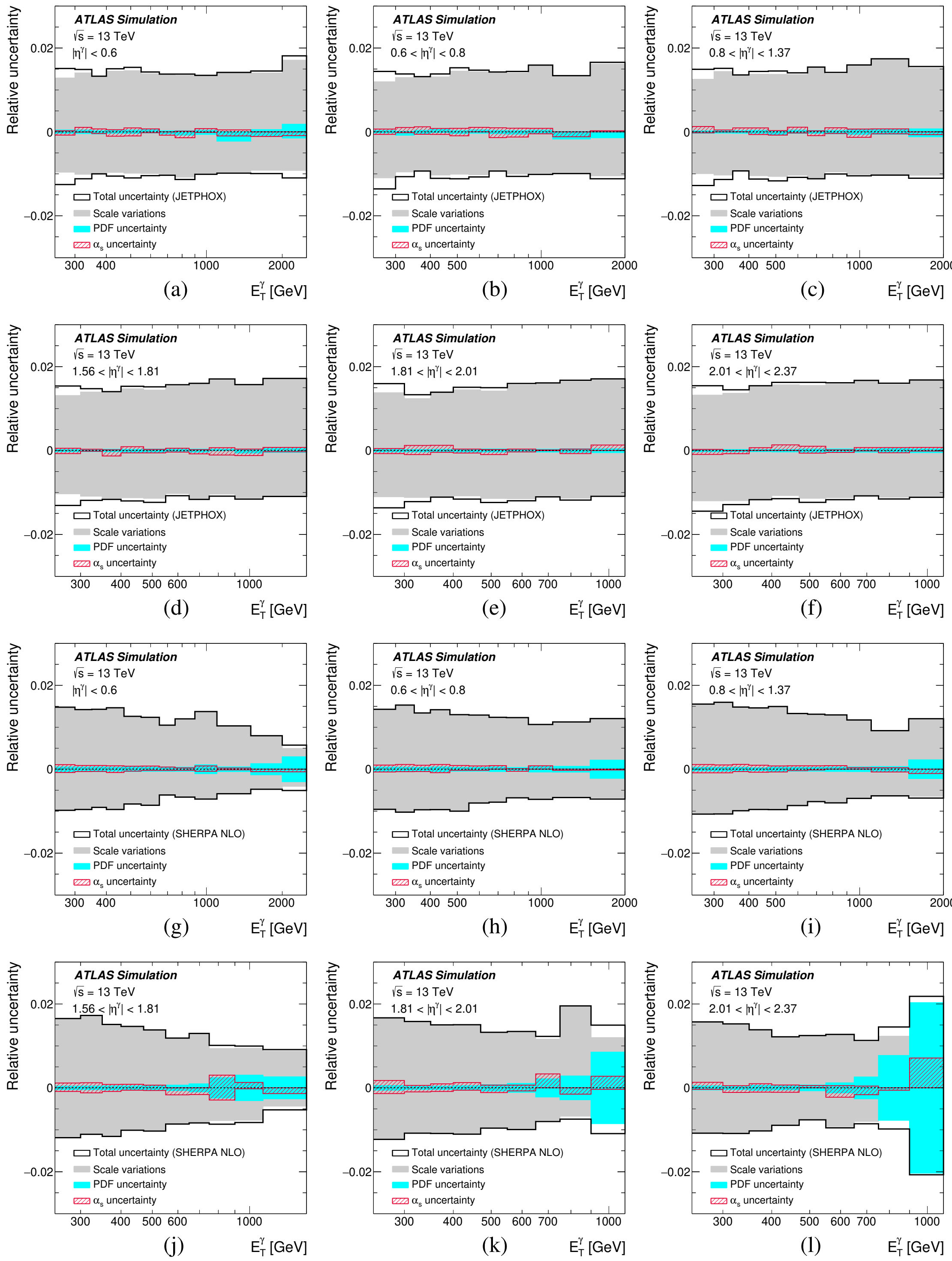

Figure 10. Relative theoretical uncertainty in JETPHOX (a, b, c, d, e, f) and SHERPA NLO (g, h, i, j, k, l) arising from scale variations (grey areas), PDF uncertainty (cyan areas), α_s uncertainty (red hatched areas) and the total theoretical uncertainty (black histogram, which includes the uncertainty in the non-perturbative corrections in the case of JETPHOX) for the ratio of the differential cross sections as functions of E_T^γ in different regions of η^γ.

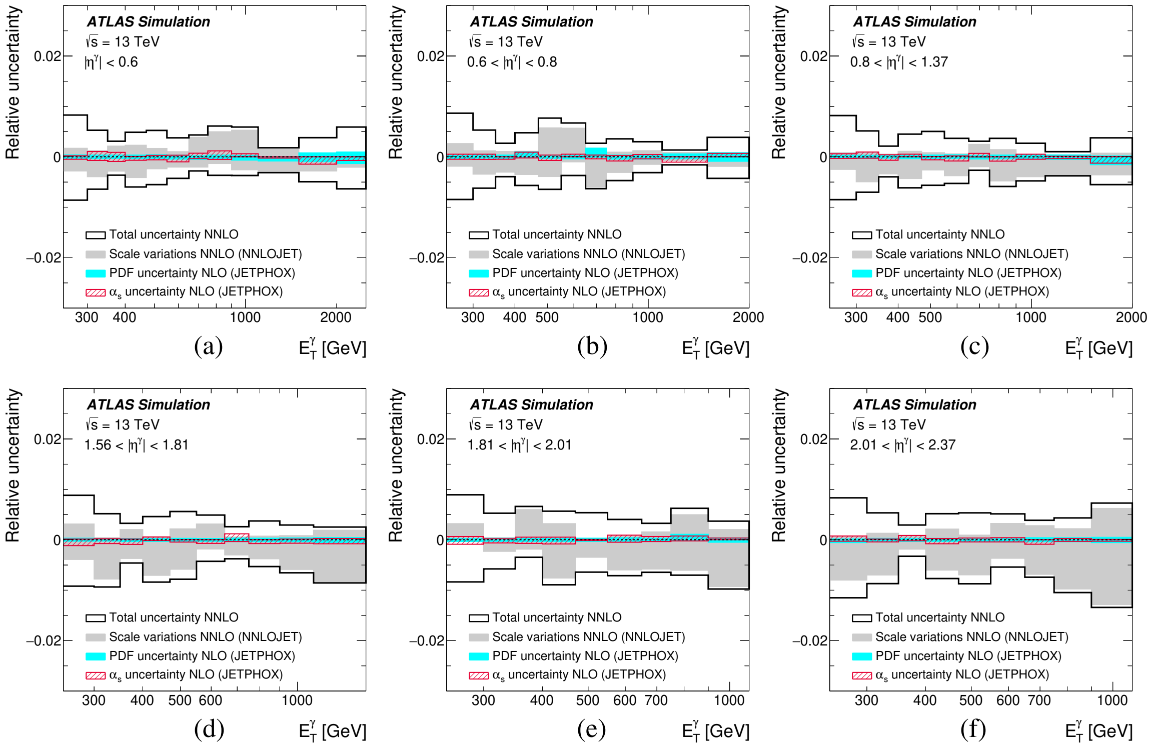

Figure 11. Relative theoretical uncertainty in the NNLO pQCD prediction for the ratio of the differential cross sections as functions of E_{T}^{γ} in different regions of η^{γ} from NNLOJET due to scale variations (grey areas). The relative theoretical uncertainty in the NLO pQCD prediction for the ratio from JETPHOX due to the uncertainty in the PDFs (cyan areas) and the uncertainty in α_{s} (red hatched areas) are also shown. The total relative theoretical uncertainty in the ratio is shown as the black histogram and also includes the uncertainty in the non-perturbative corrections and the statistical uncertainty in the NNLO pQCD predictions.

9 Results

9.1 Differential cross sections as functions of E_{T}^{γ} in different η^{γ} regions

Figure 12 shows the inclusive isolated-photon differential cross sections as functions of E_{T}^{γ} in different regions of η^{γ} for $R = 0.2$ and $R = 0.4$. The measured cross sections decrease by approximately six orders of magnitude in the investigated range. The shape of the measured cross sections is similar for different η^{γ} regions and radii, though the normalisation of the measurements for $R = 0.2$ is higher than for $R = 0.4$. Values of E_{T}^{γ} up to 2.5 TeV are measured with the full Run 2 ATLAS data set.

The NLO pQCD predictions of SHERPA NLO and JETPHOX and the NNLO pQCD predictions of NNLOJET are compared to the measurements in figure 12. These predictions are consistent with each other within the theoretical uncertainties.

The ratio of the predictions from SHERPA NLO based on the NNPDF3.0 PDF set and the measured cross sections is shown in figure 13 and the ratio of the predictions from JETPHOX based on different PDFs and the measured cross sections is shown in figure 14. Both the predictions from SHERPA NLO and JETPHOX are consistent with the measure-

JHEP07(2023)086

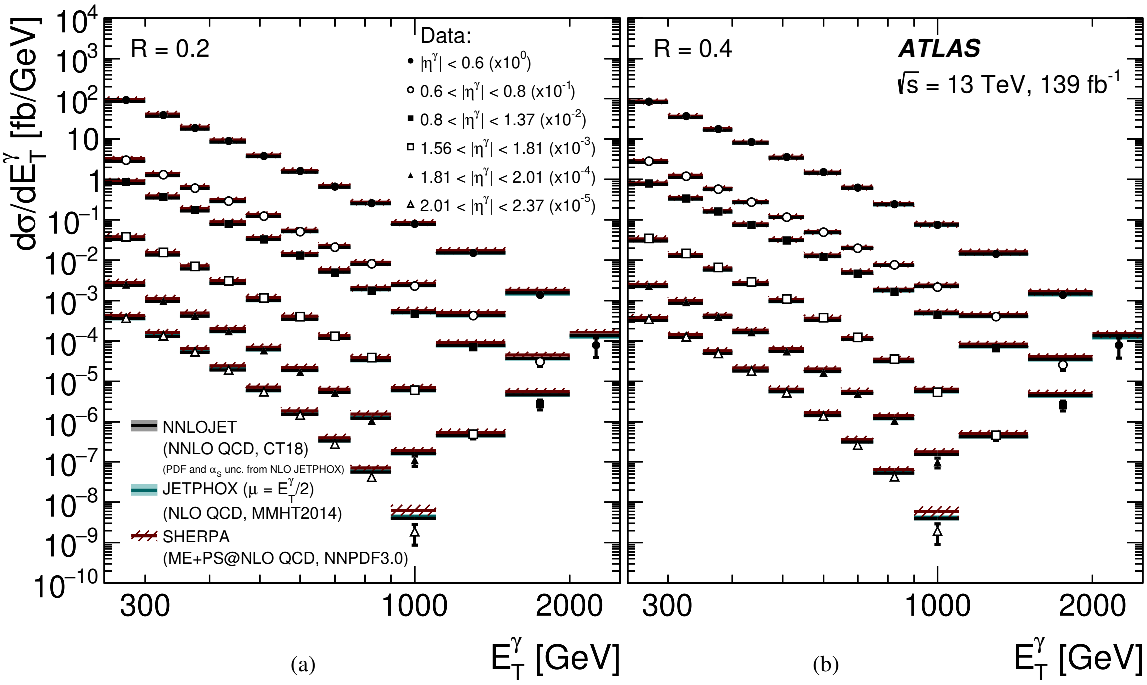

Figure 12. Measured differential cross sections for inclusive isolated-photon production as functions of E_T^γ in $|\eta^\gamma| < 0.6$ (dots), $0.6 < |\eta^\gamma| < 0.8$ (open circles), $0.8 < |\eta^\gamma| < 1.37$ (black squares), $1.56 < |\eta^\gamma| < 1.81$ (open squares), $1.81 < |\eta^\gamma| < 2.01$ (black triangles) and $2.01 < |\eta^\gamma| < 2.37$ (open triangles) for $R = 0.2$ (a) and $R = 0.4$ (b). The NLO pQCD predictions from Jetphox (blue lines) based on the MMHT2014 PDFs, the ME+PS@NLO QCD predictions from Sherpa NLO (brown lines) based on the NNPDF3.0 PDFs and the NNLO pQCD predictions from Nnlojet based on the CT18NNLO PDFs (black lines) are also shown. The measurements and the predictions are normalised by the factors shown in parentheses for each η^γ region to aid visibility. The error bars represent the statistical and systematic uncertainties added in quadrature. For most of the points, the error bars are smaller than the marker size and, thus, not visible. The hatched and shaded bands represent the theoretical uncertainty.

ments within the experimental and theoretical uncertainties. However, the predictions of Sherpa NLO have a normalisation larger than those of Jetphox which is attributed to the fact that the former include contributions from parton showers, virtual corrections for $\gamma + 2$-jet and higher-order tree matrix elements for the processes $2 \to n$ with $n = 4$ and 5, which are not present in the predictions of Jetphox. As seen in figure 14, the Jetphox predictions based on the MMHT2014, CT18 and NNPDF3.1 PDF sets are similar and the closest to the data for $|\eta^\gamma| < 1.37$ and $1.81 < |\eta^\gamma| < 2.37$. For $1.56 < |\eta^\gamma| < 1.81$, the predictions based on the HERAPDF2.0 PDF and ATLASpdf21 sets are the closest to the data. Figure 15 shows the ratio of the NLO and NNLO predictions from Nnlojet based on the CT18 PDF set and the measured cross sections; the predictions are consistent with the measurements within the experimental and theoretical uncertainties, except in the region $1.56 < |\eta^\gamma| < 1.81$, where the NNLO pQCD predictions underestimate the data.

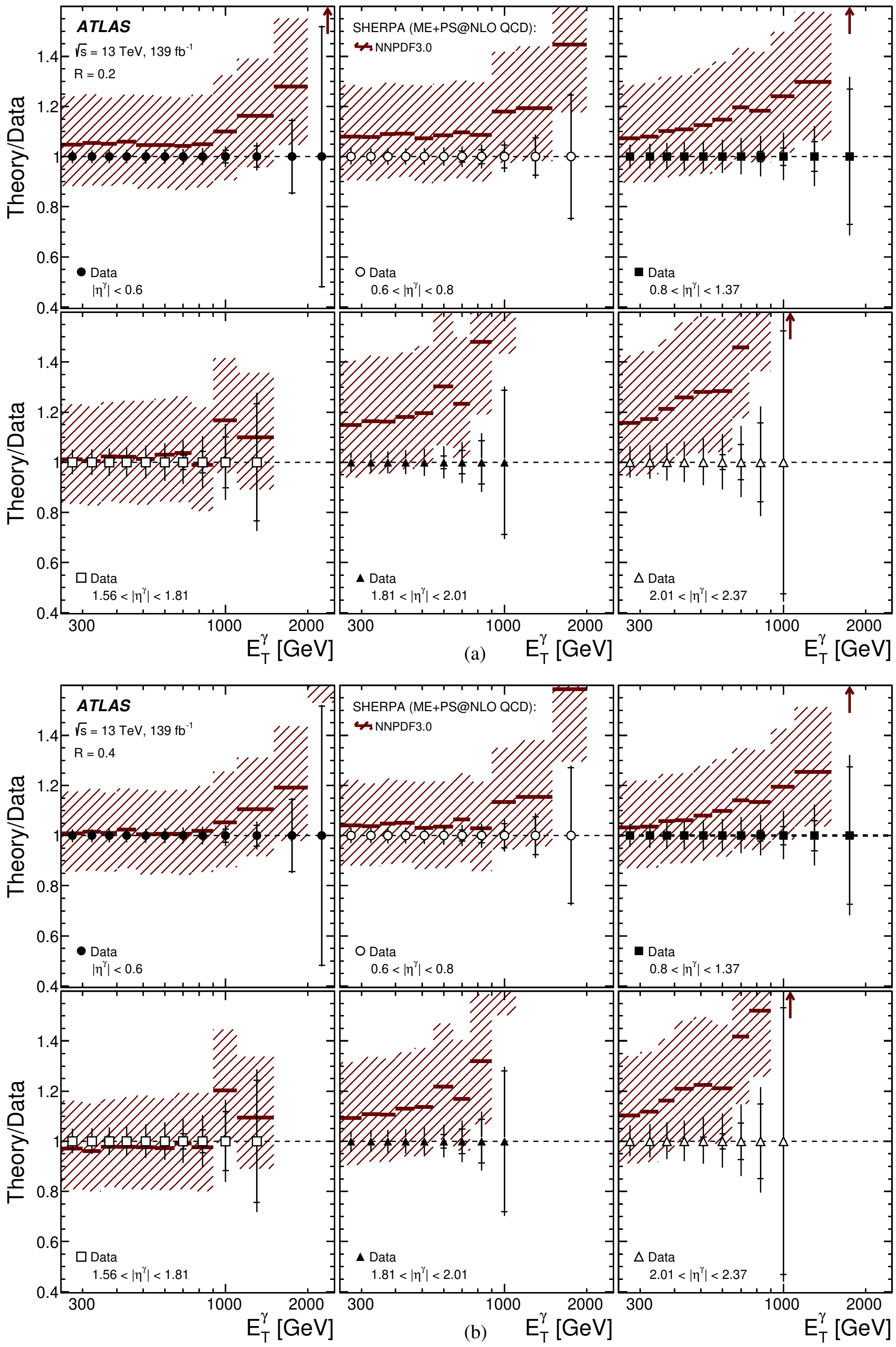

Figure 13. Ratio of the NLO pQCD calculations from SHERPA NLO based on the NNPDF3.0 PDF set and the measured differential cross sections for inclusive isolated-photon production with $R = 0.2$ (a) and $R = 0.4$ (b) as functions of E_{T}^{γ} in different regions of η^{γ}. The inner (outer) error bars represent the statistical uncertainties (statistical and systematic uncertainties added in quadrature). For most of the points, the inner error bars are smaller than the marker size and, thus, not visible. The hatched bands represent the theoretical uncertainty. The arrows indicate the direction in which the ratios of the calculations from SHERPA NLO and the measured differential cross sections are located since they are outside of the plotted range in these bins.

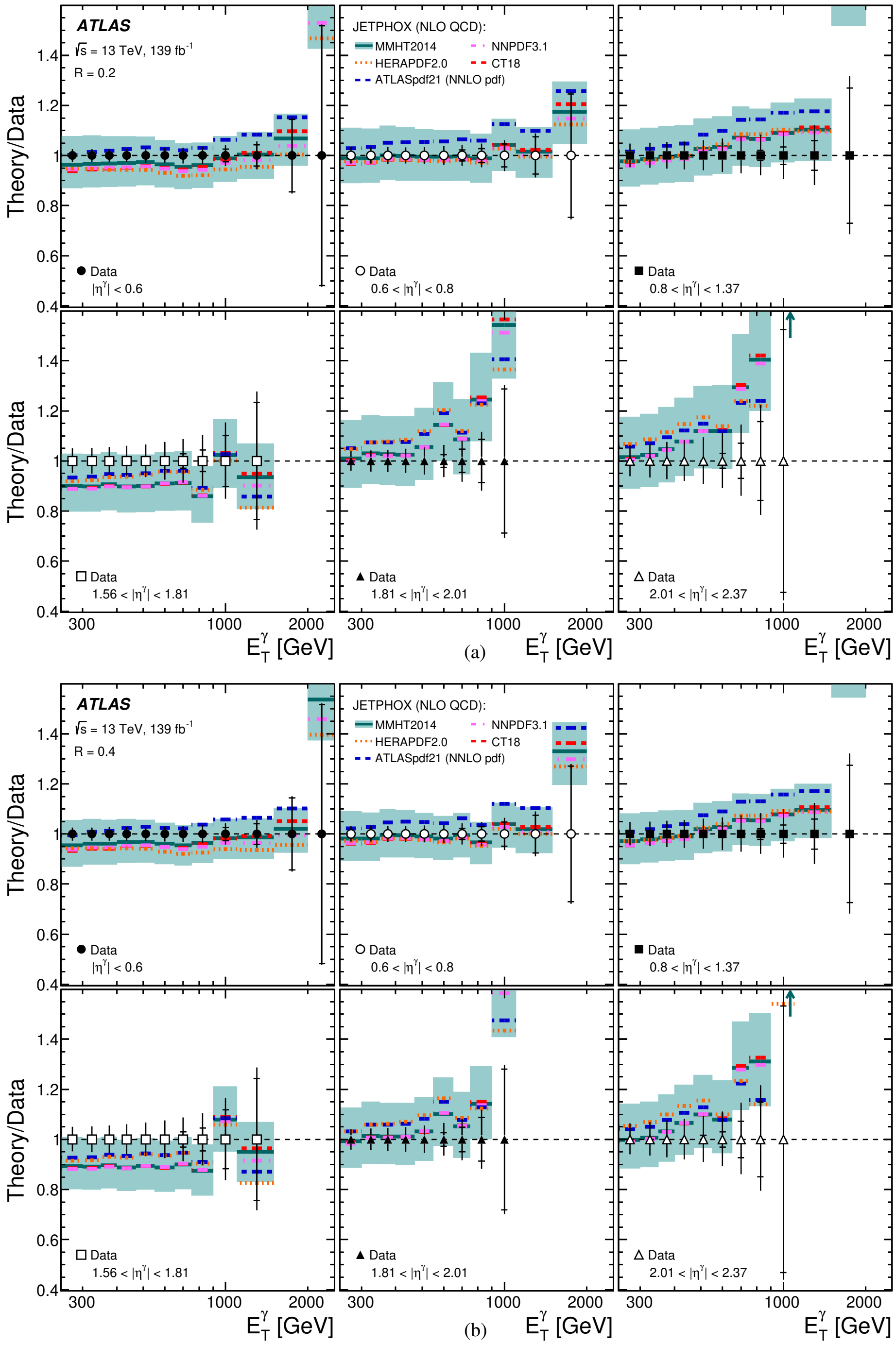

Figure 14. Ratio of the NLO pQCD calculations from JETPHOX based on different PDF sets and the measured differential cross sections for inclusive isolated-photon production with $R = 0.2$ (a) and $R = 0.4$ (b) as functions of E_{T}^{γ} in different regions of η^{γ}. The inner (outer) error bars represent the statistical uncertainties (statistical and systematic uncertainties added in quadrature). For most of the points, the inner error bars are smaller than the marker size and, thus, not visible. The shaded bands represent the theoretical uncertainty. The arrows indicate the direction in which the ratios of the calculations from JETPHOX and the measured differential cross sections are located since they are outside of the plotted range in these bins.

JHEP07(2023)086

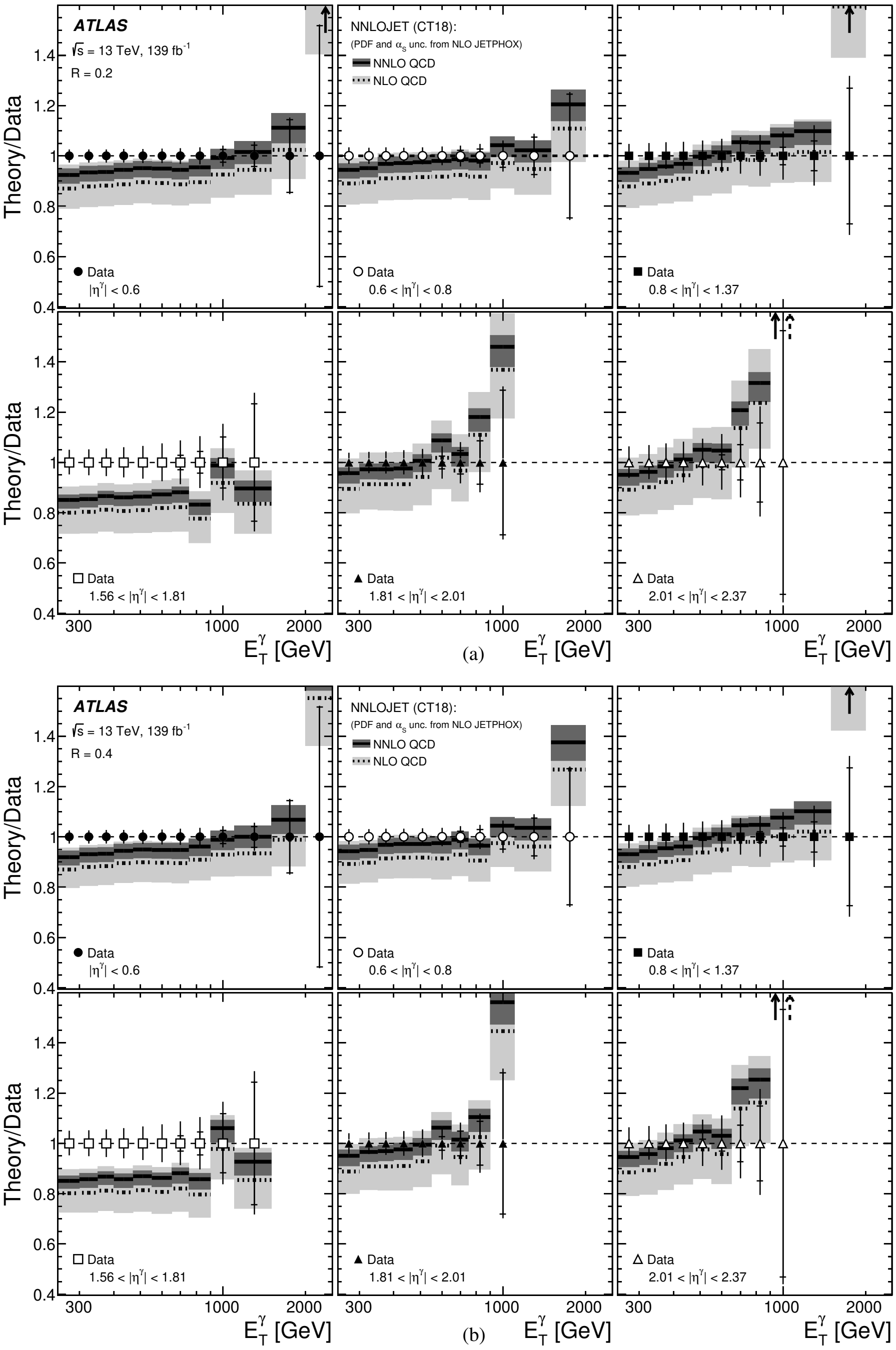

Figure 15. Ratio of the NLO (dotted lines) and NNLO (solid lines) pQCD calculations from NNLOJET based on the CT18 PDF set and the measured differential cross sections for isolated-photon production with $R = 0.2$ (a) and $R = 0.4$ (b) as functions of E_{T}^{γ} in different regions of η^{γ}. The inner (outer) error bars represent the statistical uncertainties (statistical and systematic uncertainties added in quadrature). For most of the points, the inner error bars are smaller than the marker size and, thus, not visible. The shaded bands represent the theoretical uncertainties. The arrows indicate the direction in which the ratios of the calculations from NNLOJET and the measured differential cross sections are located since they are outside of the plotted range in these bins.

9.2 R dependence of the fiducial cross section for inclusive isolated-photon production

The dependence of the inclusive isolated-photon cross section on R is investigated by measuring the fiducial integrated cross section in each η^γ region, divided by the width of the $|\eta^\gamma|$ region, for both R values measured (see figure 16). The measured cross section decreases with increasing R in all η^γ regions and it is approximately constant for $|\eta^\gamma| < 1.37$, but decreases with increasing η^γ in the region $|\eta^\gamma| > 1.37$ for a fixed value of R.

The NLO pQCD predictions of SHERPA NLO and JETPHOX are compared to the data in figures 16 and 17, respectively, and describe within the theoretical and experimental uncertainties the dependence on R of the measured fiducial integrated cross sections. In particular, the nominal predictions of SHERPA NLO tend to be above the data for $R = 0.2$ and $|\eta^\gamma| < 1.37$; in the region $1.56 < |\eta^\gamma| < 1.81$, these predictions describe the data well, but there is a tendency to overestimate the data for $|\eta^\gamma| > 1.81$ for both radii. The NLO pQCD predictions of JETPHOX describe the data well, except in the region $1.56 < |\eta^\gamma| < 1.81$, where the nominal prediction of JETPHOX is below the data. Figure 17 also includes the JETPHOX predictions based on different PDFs; no significant sensitivity to the PDFs is observed for the fiducial integrated cross sections.

Figure 18 shows the comparison of the measured fiducial integrated cross section as a function of R and the predictions from NNLOJET. The NNLO pQCD predictions describe within the theoretical and experimental uncertainties the dependence on R of the measured fiducial cross section, except in the region $1.56 < |\eta^\gamma| < 1.81$, where the predictions underestimate the data; for $|\eta^\gamma| < 1.37$, there is a tendency in the NNLO pQCD predictions to be below the data.

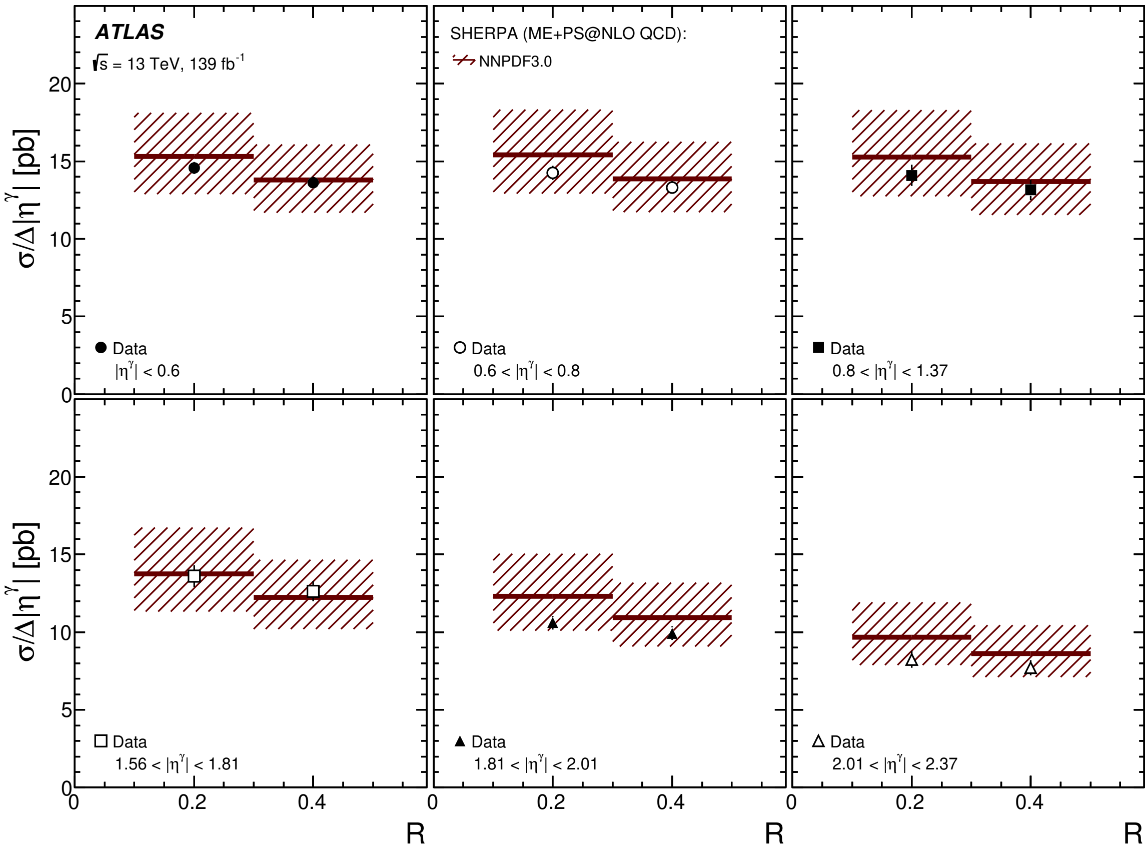

Figure 16. Measured fiducial integrated cross sections for inclusive isolated-photon production as functions of R in different η^γ regions. The NLO pQCD predictions from SHERPA NLO based on the NNPDF3.0 PDF set are also shown. The error bars represent the statistical and systematic uncertainties added in quadrature. For some of the points, the error bars are smaller than the marker size and, thus, not visible. The hatched bands represent the theoretical uncertainties.

JHEP07(2023)086

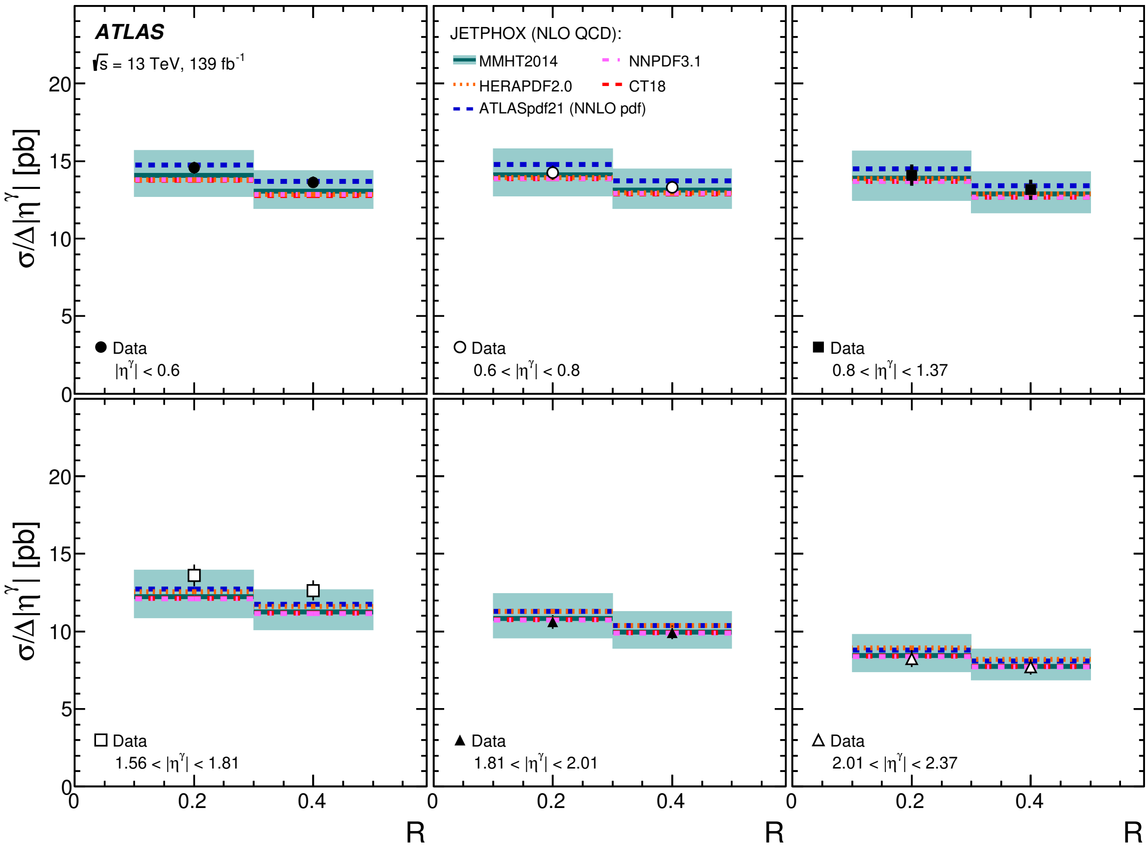

Figure 17. Measured fiducial integrated cross sections for inclusive isolated-photon production as functions of R in different η^{γ} regions. The NLO pQCD predictions from JETPHOX based on different PDF sets are also shown. The error bars represent the statistical and systematic uncertainties added in quadrature. For some of the points, the error bars are smaller than the marker size and, thus, not visible. The shaded bands represent the theoretical uncertainties.

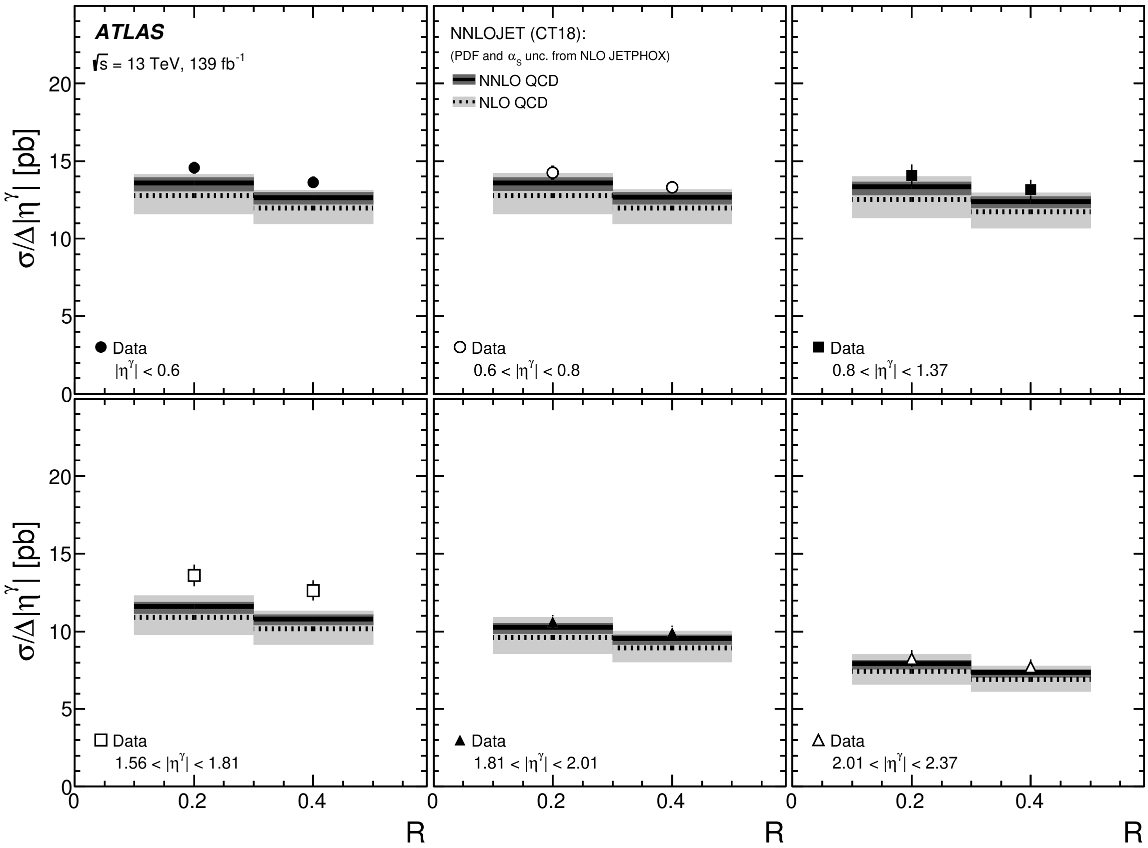

Figure 18. Measured fiducial integrated cross sections for isolated-photon production as functions of R in different η^γ regions. The NLO (dotted lines) and NNLO (solid lines) pQCD predictions from Nnlojet based on the CT18 PDF set are also shown. The error bars represent the statistical and systematic uncertainties added in quadrature. For some of the points, the error bars are smaller than the marker size and, thus, not visible. The shaded bands represent the theoretical uncertainties.

9.3 Ratio of the differential cross sections with different isolation-cone radii

Further investigation of the dependence on R of the inclusive isolated-photon cross sections is performed by measuring the ratios of the differential cross sections for $R = 0.2$ and $R = 0.4$ as functions of E_{T}^{γ} in different regions of η^{γ}. For these measurements, both the experimental, except for the $E_{\mathrm{T}}^{\mathrm{iso}}$ modelling (see section 7.3.3), and the theoretical uncertainties are considered to be fully correlated. Thus, a significant cancellation of the uncertainties is obtained in the ratio (see sections 7.7 and 8.2).

Figures 19 and 20 show the measured ratios together with the predictions of SHERPA NLO and JETPHOX, respectively. The measurements decrease with increasing E_{T}^{γ} in all η^{γ} regions and have approximately the same value in all η^{γ} regions for a fixed E_{T}^{γ} range. In the high-E_{T}^{γ} region, statistical fluctuations distort this tendency in some η^{γ} regions. The NLO pQCD predictions of SHERPA NLO overestimate the data in all E_{T}^{γ} and η^{γ} regions, whereas those from JETPHOX give a good description of the data. These differences between the predictions of JETPHOX and SHERPA NLO might be attributed to the fact that the former includes an explicit calculation of the fragmentation contribution using fragmentation functions, an approach that describes the measurements better. No significant dependence on the proton PDFs is observed in the ratios. Figure 21 shows the measured ratios together with the predictions of NNLOJET. The NNLO pQCD predictions give a good description of the data. These measurements provide a very stringent test of pQCD with reduced experimental and theoretical uncertainties.

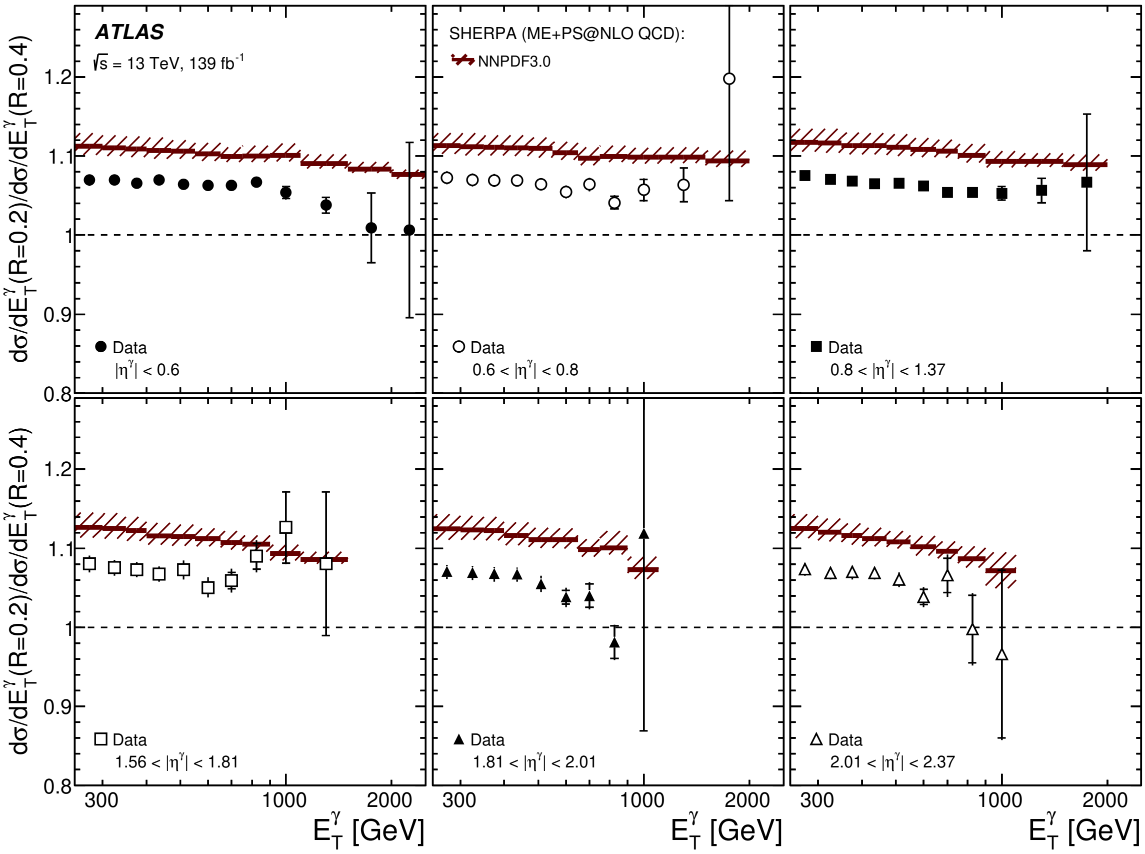

Figure 19. Measured ratios of the differential cross sections for inclusive isolated-photon production for $R = 0.2$ and $R = 0.4$ as functions of E_{T}^{γ} in different η^{γ} regions. The NLO pQCD predictions from SHERPA NLO based on the NNPDF3.0 PDF set are also shown. The inner (outer) error bars represent the statistical uncertainties (statistical and systematic uncertainties added in quadrature) and the hatched bands represent the theoretical uncertainty. For some of the points, the inner and outer error bars are smaller than the marker size and, thus, not visible.

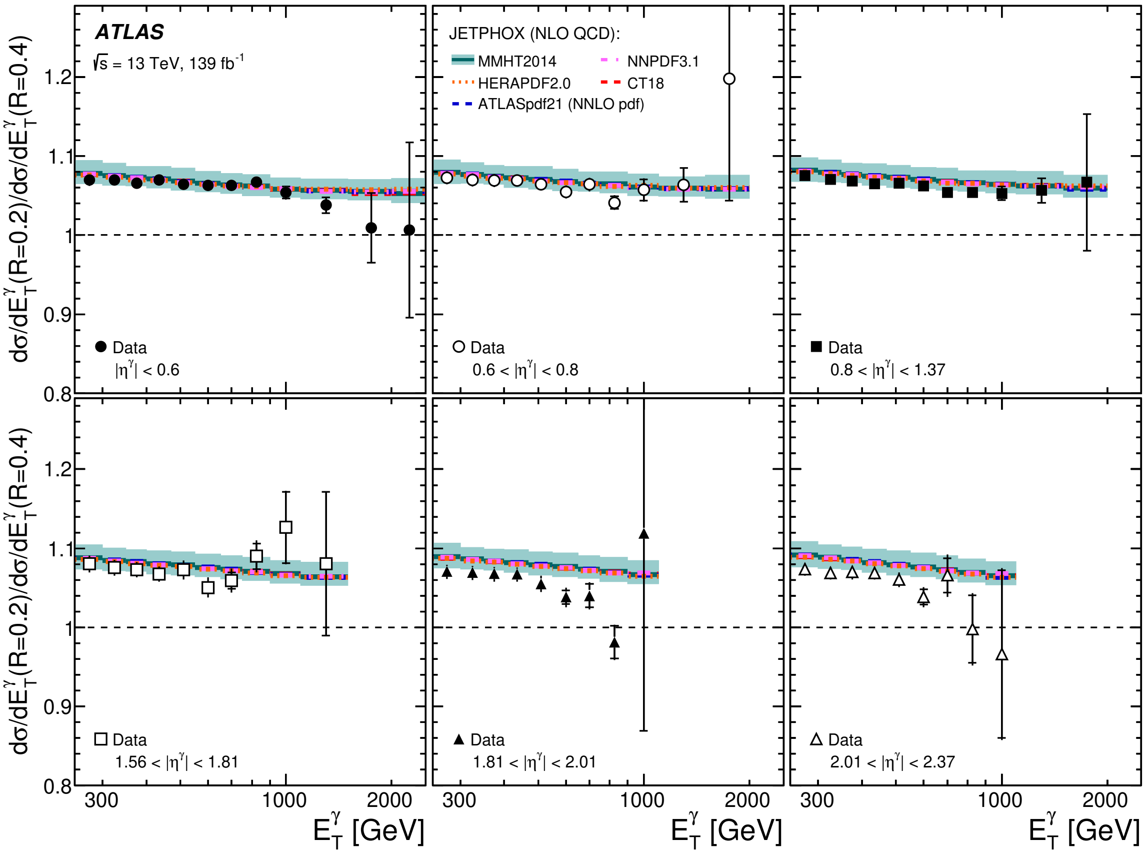

Figure 20. Measured ratios of the differential cross sections for inclusive isolated-photon production for $R = 0.2$ and $R = 0.4$ as functions of E_{T}^{γ} in different η^{γ} regions. The NLO pQCD predictions from JETPHOX based on different PDF sets are also shown. The inner (outer) error bars represent the statistical uncertainties (statistical and systematic uncertainties added in quadrature) and the shaded bands represent the theoretical uncertainties. For some of the points, the inner and outer error bars are smaller than the marker size and, thus, not visible.

JHEP07(2023)086

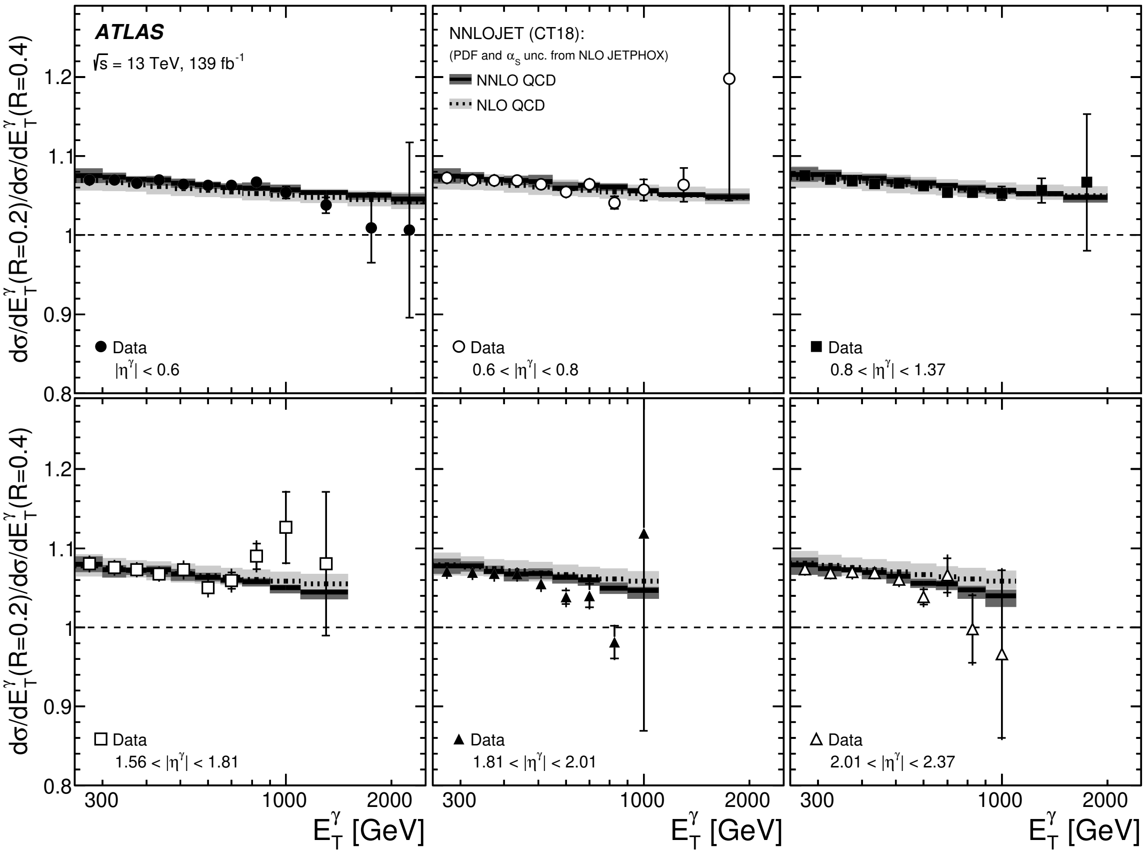

Figure 21. Measured ratios of the differential cross sections for inclusive isolated-photon production for $R = 0.2$ and $R = 0.4$ as functions of E_T^γ in different η^γ regions. The NLO (dotted lines) and NNLO (solid lines) pQCD predictions from NNLOJET based on the CT18 PDF set are also shown. The inner (outer) error bars represent the statistical uncertainties (statistical and systematic uncertainties added in quadrature) and the shaded bands represent the theoretical uncertainties. For some of the points, the inner and outer error bars are smaller than the marker size and, thus, not visible.

10 Summary and conclusions

Measurements of the inclusive isolated-photon production cross sections in *pp* collisions at $\sqrt{s} = 13$ TeV recorded by the ATLAS experiment at the LHC are presented based on $139\,\text{fb}^{-1}$ of 2015–2018 data.

Differential cross sections as functions of E_{T}^{γ} are measured in different regions of η^{γ} for photons with $E_{\text{T}}^{\gamma} > 250$ GeV and $|\eta^{\gamma}| < 2.37$, excluding the region $1.37 < |\eta^{\gamma}| < 1.56$. The photon isolation is ensured by requiring that the transverse energy in a cone of $R = 0.2$ or $R = 0.4$ around the photon direction is smaller than $4.2 \cdot 10^{-3} \cdot E_{\text{T}}^{\gamma} + 4.8$ GeV. Values of E_{T}^{γ} up to 2.5 TeV are measured with the full Run 2 ATLAS data set.

The measurements presented in this paper constitute an improvement with respect to those published earlier in several aspects. The η^{γ} range is subdivided in more regions; this provides more detailed experimental information for the PDF fits. The measurements are performed based on different isolation-cone radii, namely $R = 0.2$ and $R = 0.4$, which provide a test of the dependence of the pQCD predictions on R; these tests are performed in terms of the fiducial integrated cross section as functions of R in different regions of η^{γ} and of the ratio of the differential cross sections for $R = 0.2$ and $R = 0.4$ as functions of E_{T}^{γ} in different regions of η^{γ}.

Next-to-leading-order pQCD predictions using several PDF sets are compared to the differential cross section measurements and found to provide an adequate description of the data within the experimental and theoretical uncertainties. The comparison of data and theory is limited by the theoretical uncertainties due to missing higher-order terms in pQCD; in particular, the predictions from Sherpa NLO have a tendency to be above the data whereas the predictions from Jetphox provide a good description of the data in all η^{γ} for both isolation-cone radii. Experimental systematic uncertainties are smaller than the theoretical uncertainties over the full investigated phase space. The measurements have the potential to further constrain the PDFs, particularly the gluon density in the proton, within a global NNLO QCD fit.

The dependence on R of the measured cross section for inclusive isolated-photon production is described well by the predictions of Jetphox, whereas the predictions of Sherpa NLO for the ratios are above the data in most of the η^{γ} and E_{T}^{γ} regions. No dependence on the proton PDFs of the predictions for the fiducial cross section as functions of R or the ratio of the differential cross sections with $R = 0.2$ and $R = 0.4$ is observed. These ratios provide a very stringent test of pQCD, with significantly reduced experimental and theoretical uncertainties, and validate the underlying theoretical description up to $\mathcal{O}(\alpha_{\text{s}})$.

Next-to-next-to-leading-order pQCD predictions, including direct and fragmentation components, are compared to the differential and fiducial cross sections and to the ratios of the cross sections. For both cone radii, the NNLO predictions give a good description of the data within the uncertainties, except in the region $1.56 < |\eta^{\gamma}| < 1.81$, where the calculations underestimate the data. The comparison of the ratios of the differential cross sections between data and the predictions including NNLO corrections validates the underlying pQCD theoretical description up to $\mathcal{O}(\alpha_{\text{s}}^2)$.

JHEP07(2023)086

Acknowledgments

We thank CERN for the very successful operation of the LHC, as well as the support staff from our institutions without whom ATLAS could not be operated efficiently.

We acknowledge the support of ANPCyT, Argentina; YerPhI, Armenia; ARC, Australia; BMWFW and FWF, Austria; ANAS, Azerbaijan; CNPq and FAPESP, Brazil; NSERC, NRC and CFI, Canada; CERN; ANID, Chile; CAS, MOST and NSFC, China; Minciencias, Colombia; MEYS CR, Czech Republic; DNRF and DNSRC, Denmark; IN2P3-CNRS and CEA-DRF/IRFU, France; SRNSFG, Georgia; BMBF, HGF and MPG, Germany; GSRI, Greece; RGC and Hong Kong SAR, China; ISF and Benoziyo Center, Israel; INFN, Italy; MEXT and JSPS, Japan; CNRST, Morocco; NWO, Netherlands; RCN, Norway; MEiN, Poland; FCT, Portugal; MNE/IFA, Romania; MESTD, Serbia; MSSR, Slovakia; ARRS and MIZŠ, Slovenia; DSI/NRF, South Africa; MICINN, Spain; SRC and Wallenberg Foundation, Sweden; SERI, SNSF and Cantons of Bern and Geneva, Switzerland; MOST, Taiwan; TENMAK, Türkiye; STFC, United Kingdom; DOE and NSF, United States of America. In addition, individual groups and members have received support from BCKDF, CANARIE, Compute Canada and CRC, Canada; PRIMUS 21/SCI/017 and UNCE SCI/013, Czech Republic; COST, ERC, ERDF, Horizon 2020 and Marie Skłodowska-Curie Actions, European Union; Investissements d'Avenir Labex, Investissements d'Avenir Idex and ANR, France; DFG and AvH Foundation, Germany; Herakleitos, Thales and Aristeia programmes co-financed by EU-ESF and the Greek NSRF, Greece; BSF-NSF and MINERVA, Israel; Norwegian Financial Mechanism 2014-2021, Norway; NCN and NAWA, Poland; La Caixa Banking Foundation, CERCA Programme Generalitat de Catalunya and PROMETEO and GenT Programmes Generalitat Valenciana, Spain; Göran Gustafssons Stiftelse, Sweden; The Royal Society and Leverhulme Trust, United Kingdom.

The crucial computing support from all WLCG partners is acknowledged gratefully, in particular from CERN, the ATLAS Tier-1 facilities at TRIUMF (Canada), NDGF (Denmark, Norway, Sweden), CC-IN2P3 (France), KIT/GridKA (Germany), INFN-CNAF (Italy), NL-T1 (Netherlands), PIC (Spain), ASGC (Taiwan), RAL (U.K.) and BNL (U.S.A.), the Tier-2 facilities worldwide and large non-WLCG resource providers. Major contributors of computing resources are listed in ref. [67].

References

[1] T. Pietrycki and A. Szczurek, *Photon-jet correlations in pp and $p\bar{p}$ collisions*, *Phys. Rev. D* **76** (2007) 034003 [arXiv:0704.2158] [INSPIRE].

[2] Z. Belghobsi et al., *Photon-jet correlations and constraints on fragmentation functions*, *Phys. Rev. D* **79** (2009) 114024 [arXiv:0903.4834] [INSPIRE].

[3] ATLAS collaboration, *Measurement of the inclusive isolated prompt photon cross section in pp collisions at $\sqrt{s} = 7$ TeV with the ATLAS detector*, *Phys. Rev. D* **83** (2011) 052005 [arXiv:1012.4389] [INSPIRE].

[4] ATLAS collaboration, *Measurement of the inclusive isolated prompt photon cross-section in pp collisions at $\sqrt{s} = 7$ TeV using $35\,pb^{-1}$ of ATLAS data*, *Phys. Lett. B* **706** (2011) 150 [arXiv:1108.0253] [INSPIRE].

[5] ATLAS collaboration, *Measurement of the inclusive isolated prompt photons cross section in pp collisions at $\sqrt{s} = 7$ TeV with the ATLAS detector using $4.6\,fb^{-1}$*, *Phys. Rev. D* **89** (2014) 052004 [arXiv:1311.1440] [INSPIRE].

[6] ATLAS collaboration, *Measurement of the inclusive isolated prompt photon cross section in pp collisions at $\sqrt{s} = 8$ TeV with the ATLAS detector*, *JHEP* **08** (2016) 005 [arXiv:1605.03495] [INSPIRE].

[7] ATLAS collaboration, *Measurement of the cross section for inclusive isolated-photon production in pp collisions at $\sqrt{s} = 13$ TeV using the ATLAS detector*, *Phys. Lett. B* **770** (2017) 473 [arXiv:1701.06882] [INSPIRE].

[8] ATLAS collaboration, *Measurement of the inclusive isolated-photon cross section in pp collisions at $\sqrt{s} = 13$ TeV using $36\,fb^{-1}$ of ATLAS data*, *JHEP* **10** (2019) 203 [arXiv:1908.02746] [INSPIRE].

[9] CMS collaboration, *Measurement of the isolated prompt photon production cross section in pp collisions at $\sqrt{s} = 7$ TeV*, *Phys. Rev. Lett.* **106** (2011) 082001 [arXiv:1012.0799] [INSPIRE].

[10] CMS collaboration, *Measurement of the differential cross section for isolated prompt photon production in pp collisions at 7 TeV*, *Phys. Rev. D* **84** (2011) 052011 [arXiv:1108.2044] [INSPIRE].

[11] CMS collaboration, *Measurement of differential cross sections for inclusive isolated-photon and photon+jets production in proton-proton collisions at $\sqrt{s} = 13$ TeV*, *Eur. Phys. J. C* **79** (2019) 20 [arXiv:1807.00782] [INSPIRE].

[12] D. d'Enterria and J. Rojo, *Quantitative constraints on the gluon distribution function in the proton from collider isolated-photon data*, *Nucl. Phys. B* **860** (2012) 311 [arXiv:1202.1762] [INSPIRE].

[13] L. Carminati et al., *Sensitivity of the LHC isolated-γ+jet data to the parton distribution functions of the proton*, *EPL* **101** (2013) 61002 [arXiv:1212.5511] [INSPIRE].

[14] J. Gao, L. Harland-Lang and J. Rojo, *The structure of the proton in the LHC precision era*, *Phys. Rept.* **742** (2018) 1 [arXiv:1709.04922] [INSPIRE].

[15] J.M. Campbell, J. Rojo, E. Slade and C. Williams, *Direct photon production and PDF fits reloaded*, *Eur. Phys. J. C* **78** (2018) 470 [arXiv:1802.03021] [INSPIRE].

[16] X. Chen et al., *Isolated photon and photon+jet production at NNLO QCD accuracy*, *JHEP* **04** (2020) 166 [arXiv:1904.01044] [INSPIRE].

[17] S. Catani, M. Fontannaz, J.P. Guillet and E. Pilon, *Cross-section of isolated prompt photons in hadron hadron collisions*, *JHEP* **05** (2002) 028 [hep-ph/0204023] [INSPIRE].

[18] P. Aurenche et al., *A new critical study of photon production in hadronic collisions*, *Phys. Rev. D* **73** (2006) 094007 [hep-ph/0602133] [INSPIRE].

[19] X. Chen et al., *Single photon production at hadron colliders at NNLO QCD with realistic photon isolation*, *JHEP* **08** (2022) 094 [arXiv:2205.01516] [INSPIRE].

[20] SHERPA collaboration, *Event generation with Sherpa* 2.2, *SciPost Phys.* **7** (2019) 034 [arXiv:1905.09127] [INSPIRE].

[21] S. Frixione, *Isolated photons in perturbative QCD*, *Phys. Lett. B* **429** (1998) 369 [hep-ph/9801442] [INSPIRE].

[22] ATLAS collaboration, *The ATLAS experiment at the CERN Large Hadron Collider*, 2008 *JINST* **3** S08003 [INSPIRE].

[23] ATLAS collaboration, *ATLAS Insertable B-Layer technical design report*, CERN-LHCC-2010-013, CERN, Geneva, Switzerland (2010).

[24] ATLAS IBL collaboration, *Production and integration of the ATLAS Insertable B-Layer*, 2018 *JINST* **13** T05008 [arXiv:1803.00844] [INSPIRE].

[25] ATLAS collaboration, *Performance of the ATLAS trigger system in* 2015, *Eur. Phys. J. C* **77** (2017) 317 [arXiv:1611.09661] [INSPIRE].

[26] ATLAS collaboration, *The ATLAS collaboration software and firmware*, ATL-SOFT-PUB-2021-001, CERN, Geneva, Switzerland (2021).

[27] ATLAS collaboration, *ATLAS data quality operations and performance for* 2015–2018 *data-taking*, 2020 *JINST* **15** P04003 [arXiv:1911.04632] [INSPIRE].

[28] ATLAS collaboration, *Luminosity determination in pp collisions at* $\sqrt{s} = 13$ *TeV using the ATLAS detector at the LHC*, ATLAS-CONF-2019-021, CERN, Geneva, Switzerland (2019).

[29] T. Sjöstrand, S. Mrenna and P.Z. Skands, *A brief introduction to PYTHIA* 8.1, *Comput. Phys. Commun.* **178** (2008) 852 [arXiv:0710.3820] [INSPIRE].

[30] T. Gleisberg et al., *Event generation with SHERPA* 1.1, *JHEP* **02** (2009) 007 [arXiv:0811.4622] [INSPIRE].

[31] B. Andersson, G. Gustafson, G. Ingelman and T. Sjöstrand, *Parton fragmentation and string dynamics*, *Phys. Rept.* **97** (1983) 31 [INSPIRE].

[32] J.-C. Winter, F. Krauss and G. Soff, *A modified cluster hadronization model*, *Eur. Phys. J. C* **36** (2004) 381 [hep-ph/0311085] [INSPIRE].

[33] R.D. Ball et al., *Parton distributions with LHC data*, *Nucl. Phys. B* **867** (2013) 244 [arXiv:1207.1303] [INSPIRE].

[34] H.-L. Lai et al., *New parton distributions for collider physics*, *Phys. Rev. D* **82** (2010) 074024 [arXiv:1007.2241] [INSPIRE].

[35] ATLAS collaboration, *ATLAS PYTHIA* 8 *tunes to* 7 *TeV data*, ATL-PHYS-PUB-2014-021, CERN, Geneva, Switzerland (2014).

[36] T. Gleisberg and S. Höche, *Comix, a new matrix element generator*, *JHEP* **12** (2008) 039 [arXiv:0808.3674] [INSPIRE].

[37] F. Krauss, R. Kuhn and G. Soff, *AMEGIC++* 1.0*: a matrix element generator in C++*, *JHEP* **02** (2002) 044 [hep-ph/0109036] [INSPIRE].

[38] F. Cascioli, P. Maierhöfer and S. Pozzorini, *Scattering amplitudes with Open Loops*, *Phys. Rev. Lett.* **108** (2012) 111601 [arXiv:1111.5206] [INSPIRE].

[39] S. Schumann and F. Krauss, *A parton shower algorithm based on Catani-Seymour dipole factorisation*, *JHEP* **03** (2008) 038 [arXiv:0709.1027] [INSPIRE].

[40] S. Höche, F. Krauss, M. Schönherr and F. Siegert, *QCD matrix elements + parton showers: the NLO case*, *JHEP* **04** (2013) 027 [arXiv:1207.5030] [INSPIRE].

[41] NNPDF collaboration, *Parton distributions for the LHC run II*, *JHEP* **04** (2015) 040 [arXiv:1410.8849] [INSPIRE].

[42] ATLAS collaboration, *Summary of ATLAS PYTHIA* 8 *tunes*, ATL-PHYS-PUB-2012-003, CERN, Geneva, Switzerland (2012).

[43] GEANT4 collaboration, *GEANT4 — a simulation toolkit*, *Nucl. Instrum. Meth. A* **506** (2003) 250 [INSPIRE].

[44] ATLAS collaboration, *The ATLAS simulation infrastructure*, *Eur. Phys. J. C* **70** (2010) 823 [arXiv:1005.4568] [INSPIRE].

[45] ATLAS collaboration, *Measurement of the photon identification efficiencies with the ATLAS detector using LHC run* 2 *data collected in* 2015 *and* 2016, *Eur. Phys. J. C* **79** (2019) 205 [arXiv:1810.05087] [INSPIRE].

[46] ATLAS collaboration, *Performance of electron and photon triggers in ATLAS during LHC run* 2, *Eur. Phys. J. C* **80** (2020) 47 [arXiv:1909.00761] [INSPIRE].

[47] ATLAS collaboration, *Electron and photon performance measurements with the ATLAS detector using the* 2015–2017 *LHC proton-proton collision data*, 2019 *JINST* **14** P12006 [arXiv:1908.00005] [INSPIRE].

[48] ATLAS collaboration, *Topological cell clustering in the ATLAS calorimeters and its performance in LHC run* 1, *Eur. Phys. J. C* **77** (2017) 490 [arXiv:1603.02934] [INSPIRE].

[49] ATLAS collaboration, *Electron and photon energy calibration with the ATLAS detector using* 2015–2016 *LHC proton-proton collision data*, 2019 *JINST* **14** P03017 [arXiv:1812.03848] [INSPIRE].

[50] M. Cacciari, G.P. Salam and G. Soyez, *The catchment area of jets*, *JHEP* **04** (2008) 005 [arXiv:0802.1188] [INSPIRE].

[51] M. Cacciari, G.P. Salam and S. Sapeta, *On the characterisation of the underlying event*, *JHEP* **04** (2010) 065 [arXiv:0912.4926] [INSPIRE].

[52] G. D'Agostini, *A multidimensional unfolding method based on Bayes' theorem*, *Nucl. Instrum. Meth. A* **362** (1995) 487 [INSPIRE].

[53] L. Brenner et al., *Comparison of unfolding methods using RooFitUnfold*, *Int. J. Mod. Phys. A* **35** (2020) 2050145 [arXiv:1910.14654] [INSPIRE].

[54] B. Efron, *Bootstrap methods: another look at the jackknife*, *Annals Statist.* **7** (1979) 1 [INSPIRE].

[55] ATLAS collaboration, *Measurement of the production cross section of pairs of isolated photons in pp collisions at* 13 *TeV with the ATLAS detector*, *JHEP* **11** (2021) 169 [arXiv:2107.09330] [INSPIRE].

[56] ATLAS collaboration, *Electron and photon energy calibration with the ATLAS detector using LHC run* 1 *data*, *Eur. Phys. J. C* **74** (2014) 3071 [arXiv:1407.5063] [INSPIRE].

[57] L.A. Harland-Lang, A.D. Martin, P. Motylinski and R.S. Thorne, *Parton distributions in the LHC era: MMHT* 2014 *PDFs*, *Eur. Phys. J. C* **75** (2015) 204 [arXiv:1412.3989] [INSPIRE].

[58] L. Bourhis, M. Fontannaz and J.P. Guillet, *Quarks and gluon fragmentation functions into photons*, *Eur. Phys. J. C* **2** (1998) 529 [hep-ph/9704447] [INSPIRE].

[59] F. Siegert, *A practical guide to event generation for prompt photon production with Sherpa*, *J. Phys. G* **44** (2017) 044007 [arXiv:1611.07226] [INSPIRE].

[60] T. Gehrmann and R. Schürmann, *Photon fragmentation in the antenna subtraction formalism*, *JHEP* **04** (2022) 031 [arXiv:2201.06982] [INSPIRE].

[61] T.-J. Hou et al., *New CTEQ global analysis of quantum chromodynamics with high-precision data from the LHC*, *Phys. Rev. D* **103** (2021) 014013 [arXiv:1912.10053] [INSPIRE].

[62] NNPDF collaboration, *Parton distributions from high-precision collider data*, *Eur. Phys. J. C* **77** (2017) 663 [arXiv:1706.00428] [INSPIRE].

[63] H1 and ZEUS collaborations, *Combination of measurements of inclusive deep inelastic $e^{\pm}p$ scattering cross sections and QCD analysis of HERA data*, *Eur. Phys. J. C* **75** (2015) 580 [arXiv:1506.06042] [INSPIRE].

[64] ATLAS collaboration, *Determination of the parton distribution functions of the proton using diverse ATLAS data from pp collisions at $\sqrt{s} = 7$, 8 and 13 TeV*, *Eur. Phys. J. C* **82** (2022) 438 [arXiv:2112.11266] [INSPIRE].

[65] ATLAS collaboration, *Measurement of the ratio of cross sections for inclusive isolated-photon production in pp collisions at $\sqrt{s} = 13$ and 8 TeV with the ATLAS detector*, *JHEP* **04** (2019) 093 [arXiv:1901.10075] [INSPIRE].

[66] J. Pumplin et al., *Uncertainties of predictions from parton distribution functions. 2. The Hessian method*, *Phys. Rev. D* **65** (2001) 014013 [hep-ph/0101032] [INSPIRE].

[67] ATLAS collaboration, *ATLAS computing acknowledgements*, ATL-SOFT-PUB-2021-003, CERN, Geneva, Switzerland (2021).

JHEP07(2023)086

The ATLAS collaboration

G. Aad[102], B. Abbott[120], K. Abeling[55], S.H. Abidi[29], A. Aboulhorma[35e],
H. Abramowicz[151], H. Abreu[150], Y. Abulaiti[117], A.C. Abusleme Hoffman[137a],
B.S. Acharya[69a,69b,p], C. Adam Bourdarios[4], L. Adamczyk[85a], L. Adamek[155],
S.V. Addepalli[26], J. Adelman[115], A. Adiguzel[21c], S. Adorni[56], T. Adye[134],
A.A. Affolder[136], Y. Afik[36], M.N. Agaras[13], J. Agarwala[73a,73b], A. Aggarwal[100],
C. Agheorghiesei[27c], J.A. Aguilar-Saavedra[130f], A. Ahmad[36], F. Ahmadov[38,z],
W.S. Ahmed[104], S. Ahuja[95], X. Ai[48], G. Aielli[76a,76b], M. Ait Tamlihat[35e],
B. Aitbenchikh[35a], I. Aizenberg[169], M. Akbiyik[100], T.P.A. Åkesson[98], A.V. Akimov[37],
K. Al Khoury[41], G.L. Alberghi[23b], J. Albert[165], P. Albicocco[53], S. Alderweireldt[52],
M. Aleksa[36], I.N. Aleksandrov[38], C. Alexa[27b], T. Alexopoulos[10], A. Alfonsi[114],
F. Alfonsi[23b], M. Alhroob[120], B. Ali[132], S. Ali[148], M. Aliev[37], G. Alimonti[71a],
W. Alkakhi[55], C. Allaire[66], B.M.M. Allbrooke[146], C.A. Allendes Flores[137f],
P.P. Allport[20], A. Aloisio[72a,72b], F. Alonso[90], C. Alpigiani[138], M. Alvarez Estevez[99],
A. Alvarez Fernandez[100], M.G. Alviggi[72a,72b], M. Aly[101], Y. Amaral Coutinho[82b],
A. Ambler[104], C. Amelung[36], M. Amerl[1], C.G. Ames[109], D. Amidei[106],
S.P. Amor Dos Santos[130a], K.R. Amos[163], V. Ananiev[125], C. Anastopoulos[139],
T. Andeen[11], J.K. Anders[36], S.Y. Andrean[47a,47b], A. Andreazza[71a,71b], S. Angelidakis[9],
A. Angerami[41,ab], A.V. Anisenkov[37], A. Annovi[74a], C. Antel[56], M.T. Anthony[139],
E. Antipov[145], M. Antonelli[53], D.J.A. Antrim[17a], F. Anulli[75a], M. Aoki[83],
T. Aoki[153], J.A. Aparisi Pozo[163], M.A. Aparo[146], L. Aperio Bella[48], C. Appelt[18],
N. Aranzabal[36], V. Araujo Ferraz[82a], C. Arcangeletti[53], A.T.H. Arce[51], E. Arena[92],
J-F. Arguin[108], S. Argyropoulos[54], J.-H. Arling[48], A.J. Armbruster[36], O. Arnaez[4],
H. Arnold[114], Z.P. Arrubarrena Tame[109], G. Artoni[75a,75b], H. Asada[111], K. Asai[118],
S. Asai[153], N.A. Asbah[61], J. Assahsah[35d], K. Assamagan[29], R. Astalos[28a],
R.J. Atkin[33a], M. Atkinson[162], N.B. Atlay[18], H. Atmani[62b], P.A. Atmasiddha[106],
K. Augsten[132], S. Auricchio[72a,72b], A.D. Auriol[20], V.A. Austrup[171], G. Avner[150],
G. Avolio[36], K. Axiotis[56], G. Azuelos[108,ad], D. Babal[28a], H. Bachacou[135],
K. Bachas[152,r], A. Bachiu[34], F. Backman[47a,47b], A. Badea[61], P. Bagnaia[75a,75b],
M. Bahmani[18], A.J. Bailey[163], V.R. Bailey[162], J.T. Baines[134], C. Bakalis[10],
O.K. Baker[172], P.J. Bakker[114], E. Bakos[15], D. Bakshi Gupta[8], R. Balasubramanian[114],
E.M. Baldin[37], P. Balek[133], E. Ballabene[71a,71b], F. Balli[135], L.M. Baltes[63a],
W.K. Balunas[32], J. Balz[100], E. Banas[86], M. Bandieramonte[129], A. Bandyopadhyay[24],
S. Bansal[24], L. Barak[151], E.L. Barberio[105], D. Barberis[57b,57a], M. Barbero[102],
G. Barbour[96], K.N. Barends[33a], T. Barillari[110], M-S. Barisits[36], T. Barklow[143],
P. Baron[122], D.A. Baron Moreno[101], A. Baroncelli[62a], G. Barone[29], A.J. Barr[126],
L. Barranco Navarro[47a,47b], F. Barreiro[99], J. Barreiro Guimarães da Costa[14a],
U. Barron[151], M.G. Barros Teixeira[130a], S. Barsov[37], F. Bartels[63a], R. Bartoldus[143],
A.E. Barton[91], P. Bartos[28a], A. Basan[100], M. Baselga[49], I. Bashta[77a,77b],
A. Bassalat[66,b], M.J. Basso[155], C.R. Basson[101], R.L. Bates[59], S. Batlamous[35e],
J.R. Batley[32], B. Batool[141], M. Battaglia[136], D. Battulga[18], M. Bauce[75a,75b],
P. Bauer[24], J.B. Beacham[51], T. Beau[127], P.H. Beauchemin[158], F. Becherer[54],

JHEP07(2023)086

P. Bechtle[24], H.P. Beck[19,q], K. Becker[167], A.J. Beddall[21d], V.A. Bednyakov[38], C.P. Bee[145], L.J. Beemster[15], T.A. Beermann[36], M. Begalli[82d,82d], M. Begel[29], A. Behera[145], J.K. Behr[48], C. Beirao Da Cruz E Silva[36], J.F. Beirer[55,36], F. Beisiegel[24], M. Belfkir[159], G. Bella[151], L. Bellagamba[23b], A. Bellerive[34], P. Bellos[20], K. Beloborodov[37], N.L. Belyaev[37], D. Benchekroun[35a], F. Bendebba[35a], Y. Benhammou[151], M. Benoit[29], J.R. Bensinger[26], S. Bentvelsen[114], L. Beresford[36], M. Beretta[53], E. Bergeaas Kuutmann[161], N. Berger[4], B. Bergmann[132], J. Beringer[17a], S. Berlendis[7], G. Bernardi[5], C. Bernius[143], F.U. Bernlochner[24], T. Berry[95], P. Berta[133], A. Berthold[50], I.A. Bertram[91], S. Bethke[110], A. Betti[75a,75b], A.J. Bevan[94], M. Bhamjee[33c], S. Bhatta[145], D.S. Bhattacharya[166], P. Bhattarai[26], V.S. Bhopatkar[121], R. Bi[29,ag], R.M. Bianchi[129], O. Biebel[109], R. Bielski[123], M. Biglietti[77a], T.R.V. Billoud[132], M. Bindi[55], A. Bingul[21b], C. Bini[75a,75b], A. Biondini[92], C.J. Birch-sykes[101], G.A. Bird[20,134], M. Birman[169], M. Biros[133], T. Bisanz[36], E. Bisceglie[43b,43a], D. Biswas[170], A. Bitadze[101], K. Bjørke[125], I. Bloch[48], C. Blocker[26], A. Blue[59], U. Blumenschein[94], J. Blumenthal[100], G.J. Bobbink[114], V.S. Bobrovnikov[37], M. Boehler[54], D. Bogavac[36], A.G. Bogdanchikov[37], C. Bohm[47a], V. Boisvert[95], P. Bokan[48], T. Bold[85a], M. Bomben[5], M. Bona[94], M. Boonekamp[135], C.D. Booth[95], A.G. Borbély[59], H.M. Borecka-Bielska[108], L.S. Borgna[96], G. Borissov[91], D. Bortoletto[126], D. Boscherini[23b], M. Bosman[13], J.D. Bossio Sola[36], K. Bouaouda[35a], N. Bouchhar[163], J. Boudreau[129], E.V. Bouhova-Thacker[91], D. Boumediene[40], R. Bouquet[5], A. Boveia[119], J. Boyd[36], D. Boye[29], I.R. Boyko[38], J. Bracinik[20], N. Brahimi[62d], G. Brandt[171], O. Brandt[32], F. Braren[48], B. Brau[103], J.E. Brau[123], K. Brendlinger[48], R. Brener[169], L. Brenner[114], R. Brenner[161], S. Bressler[169], D. Britton[59], D. Britzger[110], I. Brock[24], G. Brooijmans[41], W.K. Brooks[137f], E. Brost[29], L.M. Brown[165], T.L. Bruckler[126], P.A. Bruckman de Renstrom[86], B. Brüers[48], D. Bruncko[28b,*], A. Bruni[23b], G. Bruni[23b], M. Bruschi[23b], N. Bruscino[75a,75b], T. Buanes[16], Q. Buat[138], A.G. Buckley[59], I.A. Budagov[38,*], M.K. Bugge[125], O. Bulekov[37], B.A. Bullard[143], S. Burdin[92], C.D. Burgard[49], A.M. Burger[40], B. Burghgrave[8], J.T.P. Burr[32], C.D. Burton[11], J.C. Burzynski[142], E.L. Busch[41], V. Büscher[100], P.J. Bussey[59], J.M. Butler[25], C.M. Buttar[59], J.M. Butterworth[96], W. Buttinger[134], C.J. Buxo Vazquez[107], A.R. Buzykaev[37], G. Cabras[23b], S. Cabrera Urbán[163], D. Caforio[58], H. Cai[129], Y. Cai[14a,14d], V.M.M. Cairo[36], O. Cakir[3a], N. Calace[36], P. Calafiura[17a], G. Calderini[127], P. Calfayan[68], G. Callea[59], L.P. Caloba[82b], D. Calvet[40], S. Calvet[40], T.P. Calvet[102], M. Calvetti[74a,74b], R. Camacho Toro[127], S. Camarda[36], D. Camarero Munoz[26], P. Camarri[76a,76b], M.T. Camerlingo[72a,72b], D. Cameron[125], C. Camincher[165], M. Campanelli[96], A. Camplani[42], V. Canale[72a,72b], A. Canesse[104], M. Cano Bret[80], J. Cantero[163], Y. Cao[162], F. Capocasa[26], M. Capua[43b,43a], A. Carbone[71a,71b], R. Cardarelli[76a], J.C.J. Cardenas[8], F. Cardillo[163], T. Carli[36], G. Carlino[72a], J.I. Carlotto[13], B.T. Carlson[129,s], E.M. Carlson[165,156a], L. Carminati[71a,71b], M. Carnesale[75a,75b], S. Caron[113], E. Carquin[137f], S. Carrá[71a,71b], G. Carratta[23b,23a], F. Carrio Argos[33g], J.W.S. Carter[155], T.M. Carter[52], M.P. Casado[13,j], A.F. Casha[155], M. Caspar[48], E.G. Castiglia[172], F.L. Castillo[63a], L. Castillo Garcia[13],

V. Castillo Gimenez[163], N.F. Castro[130a,130e], A. Catinaccio[36], J.R. Catmore[125], V. Cavaliere[29], N. Cavalli[23b,23a], V. Cavasinni[74a,74b], E. Celebi[21a], F. Celli[126], M.S. Centonze[70a,70b], K. Cerny[122], A.S. Cerqueira[82a], A. Cerri[146], L. Cerrito[76a,76b], F. Cerutti[17a], A. Cervelli[23b], G. Cesarini[53], S.A. Cetin[21d], Z. Chadi[35a], D. Chakraborty[115], M. Chala[130f], J. Chan[170], W.Y. Chan[153], J.D. Chapman[32], B. Chargeishvili[149b], D.G. Charlton[20], T.P. Charman[94], M. Chatterjee[19], S. Chekanov[6], S.V. Chekulaev[156a], G.A. Chelkov[38,a], A. Chen[106], B. Chen[151], B. Chen[165], H. Chen[14c], H. Chen[29], J. Chen[62c], J. Chen[142], S. Chen[153], S.J. Chen[14c], X. Chen[62c], X. Chen[14b,ac], Y. Chen[62a], C.L. Cheng[170], H.C. Cheng[64a], S. Cheong[143], A. Cheplakov[38], E. Cheremushkina[48], E. Cherepanova[114], R. Cherkaoui El Moursli[35e], E. Cheu[7], K. Cheung[65], L. Chevalier[135], V. Chiarella[53], G. Chiarelli[74a], N. Chiedde[102], G. Chiodini[70a], A.S. Chisholm[20], A. Chitan[27b], M. Chitishvili[163], M.V. Chizhov[38], K. Choi[11], A.R. Chomont[75a,75b], Y. Chou[103], E.Y.S. Chow[114], T. Chowdhury[33g], L.D. Christopher[33g], K.L. Chu[64a], M.C. Chu[64a], X. Chu[14a,14d], J. Chudoba[131], J.J. Chwastowski[86], D. Cieri[110], K.M. Ciesla[85a], V. Cindro[93], A. Ciocio[17a], F. Cirotto[72a,72b], Z.H. Citron[169,m], M. Citterio[71a], D.A. Ciubotaru[27b], B.M. Ciungu[155], A. Clark[56], P.J. Clark[52], J.M. Clavijo Columbie[48], S.E. Clawson[101], C. Clement[47a,47b], J. Clercx[48], L. Clissa[23b,23a], Y. Coadou[102], M. Cobal[69a,69c], A. Coccaro[57b], R.F. Coelho Barrue[130a], R. Coelho Lopes De Sa[103], S. Coelli[71a], H. Cohen[151], A.E.C. Coimbra[71a,71b], B. Cole[41], J. Collot[60], P. Conde Muiño[130a,130g], M.P. Connell[33c], S.H. Connell[33c], I.A. Connelly[59], E.I. Conroy[126], F. Conventi[72a,ae], H.G. Cooke[20], A.M. Cooper-Sarkar[126], F. Cormier[164], L.D. Corpe[36], M. Corradi[75a,75b], F. Corriveau[104,x], A. Cortes-Gonzalez[18], M.J. Costa[163], F. Costanza[4], D. Costanzo[139], B.M. Cote[119], G. Cowan[95], J.W. Cowley[32], K. Cranmer[117], S. Crépé-Renaudin[60], F. Crescioli[127], M. Cristinziani[141], M. Cristoforetti[78a,78b,d], V. Croft[114], G. Crosetti[43b,43a], A. Cueto[36], T. Cuhadar Donszelmann[160], H. Cui[14a,14d], Z. Cui[7], W.R. Cunningham[59], F. Curcio[43b,43a], P. Czodrowski[36], M.M. Czurylo[63b], M.J. Da Cunha Sargedas De Sousa[62a], J.V. Da Fonseca Pinto[82b], C. Da Via[101], W. Dabrowski[85a], T. Dado[49], S. Dahbi[33g], T. Dai[106], C. Dallapiccola[103], M. Dam[42], G. D'amen[29], V. D'Amico[109], J. Damp[100], J.R. Dandoy[128], M.F. Daneri[30], M. Danninger[142], V. Dao[36], G. Darbo[57b], S. Darmora[6], S.J. Das[29], S. D'Auria[71a,71b], C. David[156b], T. Davidek[133], B. Davis-Purcell[34], I. Dawson[94], K. De[8], R. De Asmundis[72a], N. De Biase[48], S. De Castro[23b,23a], N. De Groot[113], P. de Jong[114], H. De la Torre[107], A. De Maria[14c], A. De Salvo[75a], U. De Sanctis[76a,76b], A. De Santo[146], J.B. De Vivie De Regie[60], D.V. Dedovich[38], J. Degens[114], A.M. Deiana[44], F. Del Corso[23b,23a], J. Del Peso[99], F. Del Rio[63a], F. Deliot[135], C.M. Delitzsch[49], M. Della Pietra[72a,72b], D. Della Volpe[56], A. Dell'Acqua[36], L. Dell'Asta[71a,71b], M. Delmastro[4], P.A. Delsart[60], S. Demers[172], M. Demichev[38], S.P. Denisov[37], L. D'Eramo[115], D. Derendarz[86], F. Derue[127], P. Dervan[92], K. Desch[24], K. Dette[155], C. Deutsch[24], F.A. Di Bello[57b,57a], A. Di Ciaccio[76a,76b], L. Di Ciaccio[4], A. Di Domenico[75a,75b], C. Di Donato[72a,72b], A. Di Girolamo[36], G. Di Gregorio[5], A. Di Luca[78a,78b], B. Di Micco[77a,77b], R. Di Nardo[77a,77b], C. Diaconu[102], F.A. Dias[114], T. Dias Do Vale[142], M.A. Diaz[137a,137b],

JHEP07(2023)086

F.G. Diaz Capriles[24], M. Didenko[163], E.B. Diehl[106], L. Diehl[54], S. Díez Cornell[48],
C. Diez Pardos[141], C. Dimitriadi[24,161], A. Dimitrievska[17a], J. Dingfelder[24],
I-M. Dinu[27b], S.J. Dittmeier[63b], F. Dittus[36], F. Djama[102], T. Djobava[149b],
J.I. Djuvsland[16], C. Doglioni[101,98], J. Dolejsi[133], Z. Dolezal[133], M. Donadelli[82c],
B. Dong[107], J. Donini[40], A. D'Onofrio[77a,77b], M. D'Onofrio[92], J. Dopke[134],
A. Doria[72a], M.T. Dova[90], A.T. Doyle[59], M.A. Draguet[126], E. Drechsler[142],
E. Dreyer[169], I. Drivas-koulouris[10], A.S. Drobac[158], M. Drozdova[56], D. Du[62a],
T.A. du Pree[114], F. Dubinin[37], M. Dubovsky[28a], E. Duchovni[169], G. Duckeck[109],
O.A. Ducu[27b], D. Duda[110], A. Dudarev[36], E.R. Duden[26], M. D'uffizi[101], L. Duflot[66],
M. Dührssen[36], C. Dülsen[171], A.E. Dumitriu[27b], M. Dunford[63a], S. Dungs[49],
K. Dunne[47a,47b], A. Duperrin[102], H. Duran Yildiz[3a], M. Düren[58], A. Durglishvili[149b],
B.L. Dwyer[115], G.I. Dyckes[17a], M. Dyndal[85a], S. Dysch[101], B.S. Dziedzic[86],
Z.O. Earnshaw[146], B. Eckerova[28a], S. Eggebrecht[55], M.G. Eggleston[51],
E. Egidio Purcino De Souza[127], L.F. Ehrke[56], G. Eigen[16], K. Einsweiler[17a],
T. Ekelof[161], P.A. Ekman[98], Y. El Ghazali[35b], H. El Jarrari[35e,148], A. El Moussaouy[35a],
V. Ellajosyula[161], M. Ellert[161], F. Ellinghaus[171], A.A. Elliot[94], N. Ellis[36],
J. Elmsheuser[29], M. Elsing[36], D. Emeliyanov[134], Y. Enari[153], I. Ene[17a], S. Epari[13],
J. Erdmann[49], P.A. Erland[86], M. Errenst[171], M. Escalier[66], C. Escobar[163],
E. Etzion[151], G. Evans[130a], H. Evans[68], M.O. Evans[146], A. Ezhilov[37],
S. Ezzarqtouni[35a], F. Fabbri[59], L. Fabbri[23b,23a], G. Facini[96], V. Fadeyev[136],
R.M. Fakhrutdinov[37], S. Falciano[75a], L.F. Falda Ulhoa Coelho[36], P.J. Falke[24],
S. Falke[36], J. Faltova[133], Y. Fan[14a], Y. Fang[14a,14d], G. Fanourakis[46], M. Fanti[71a,71b],
M. Faraj[69a,69b], Z. Farazpay[97], A. Farbin[8], A. Farilla[77a], T. Farooque[107],
S.M. Farrington[52], F. Fassi[35e], D. Fassouliotis[9], M. Faucci Giannelli[76a,76b],
W.J. Fawcett[32], L. Fayard[66], P. Federic[133], P. Federicova[131], O.L. Fedin[37,a],
G. Fedotov[37], M. Feickert[170], L. Feligioni[102], A. Fell[139], D.E. Fellers[123], C. Feng[62b],
M. Feng[14b], Z. Feng[114], M.J. Fenton[160], A.B. Fenyuk[37], L. Ferencz[48],
R.A.M. Ferguson[91], S.I. Fernandez Luengo[137f], J. Ferrando[48], A. Ferrari[161],
P. Ferrari[114,113], R. Ferrari[73a], D. Ferrere[56], C. Ferretti[106], F. Fiedler[100],
A. Filipčič[93], E.K. Filmer[1], F. Filthaut[113], M.C.N. Fiolhais[130a,130c,c], L. Fiorini[163],
F. Fischer[141], W.C. Fisher[107], T. Fitschen[101], I. Fleck[141], P. Fleischmann[106],
T. Flick[171], L. Flores[128], M. Flores[33d], L.R. Flores Castillo[64a], F.M. Follega[78a,78b],
N. Fomin[16], J.H. Foo[155], B.C. Forland[68], A. Formica[135], A.C. Forti[101], E. Fortin[102],
A.W. Fortman[61], M.G. Foti[17a], L. Fountas[9], D. Fournier[66], H. Fox[91],
P. Francavilla[74a,74b], S. Francescato[61], S. Franchellucci[56], M. Franchini[23b,23a],
S. Franchino[63a], D. Francis[36], L. Franco[113], L. Franconi[19], M. Franklin[61], G. Frattari[26],
A.C. Freegard[94], W.S. Freund[82b], Y.Y. Frid[151], N. Fritzsche[50], A. Froch[54],
D. Froidevaux[36], J.A. Frost[126], Y. Fu[62a], M. Fujimoto[118], E. Fullana Torregrosa[163,*],
J. Fuster[163], A. Gabrielli[23b,23a], A. Gabrielli[155], P. Gadow[48], G. Gagliardi[57b,57a],
L.G. Gagnon[17a], G.E. Gallardo[126], E.J. Gallas[126], B.J. Gallop[134], R. Gamboa Goni[94],
K.K. Gan[119], S. Ganguly[153], J. Gao[62a], Y. Gao[52], F.M. Garay Walls[137a,137b],
B. Garcia[29,ag], C. García[163], J.E. García Navarro[163], M. Garcia-Sciveres[17a],
R.W. Gardner[39], D. Garg[80], R.B. Garg[143], C.A. Garner[155], V. Garonne[29],

S.J. Gasiorowski[138], P. Gaspar[82b], G. Gaudio[73a], V. Gautam[13], P. Gauzzi[75a,75b], I.L. Gavrilenko[37], A. Gavrilyuk[37], C. Gay[164], G. Gaycken[48], E.N. Gazis[10], A.A. Geanta[27b,27e], C.M. Gee[136], C. Gemme[57b], M.H. Genest[60], S. Gentile[75a,75b], S. George[95], W.F. George[20], T. Geralis[46], L.O. Gerlach[55], P. Gessinger-Befurt[36], M.E. Geyik[171], M. Ghneimat[141], K. Ghorbanian[94], A. Ghosal[141], A. Ghosh[160], A. Ghosh[7], B. Giacobbe[23b], S. Giagu[75a,75b], P. Giannetti[74a], A. Giannini[62a], S.M. Gibson[95], M. Gignac[136], D.T. Gil[85b], A.K. Gilbert[85a], B.J. Gilbert[41], D. Gillberg[34], G. Gilles[114], N.E.K. Gillwald[48], L. Ginabat[127], D.M. Gingrich[2,ad], M.P. Giordani[69a,69c], P.F. Giraud[135], G. Giugliarelli[69a,69c], D. Giugni[71a], F. Giuli[36], I. Gkialas[9,k], L.K. Gladilin[37], C. Glasman[99], G.R. Gledhill[123], M. Glisic[123], I. Gnesi[43b,g], Y. Go[29,ag], M. Goblirsch-Kolb[26], B. Gocke[49], D. Godin[108], B. Gokturk[21a], S. Goldfarb[105], T. Golling[56], M.G.D. Gololo[33g], D. Golubkov[37], J.P. Gombas[107], A. Gomes[130a,130b], G. Gomes Da Silva[141], A.J. Gomez Delegido[163], R. Gonçalo[130a,130c], G. Gonella[123], L. Gonella[20], A. Gongadze[38], F. Gonnella[20], J.L. Gonski[41], R.Y. González Andana[52], S. González de la Hoz[163], S. Gonzalez Fernandez[13], R. Gonzalez Lopez[92], C. Gonzalez Renteria[17a], R. Gonzalez Suarez[161], S. Gonzalez-Sevilla[56], G.R. Gonzalvo Rodriguez[163], L. Goossens[36], P.A. Gorbounov[37], B. Gorini[36], E. Gorini[70a,70b], A. Gorišek[93], A.T. Goshaw[51], M.I. Gostkin[38], S. Goswami[121], C.A. Gottardo[36], M. Gouighri[35b], V. Goumarre[48], A.G. Goussiou[138], N. Govender[33c], C. Goy[4], I. Grabowska-Bold[85a], K. Graham[34], E. Gramstad[125], S. Grancagnolo[18], M. Grandi[146], V. Gratchev[37,*], P.M. Gravila[27f], F.G. Gravili[70a,70b], H.M. Gray[17a], M. Greco[70a,70b], C. Grefe[24], I.M. Gregor[48], P. Grenier[143], C. Grieco[13], A.A. Grillo[136], K. Grimm[31,n], S. Grinstein[13,u], J.-F. Grivaz[66], E. Gross[169], J. Grosse-Knetter[55], C. Grud[106], J.C. Grundy[126], L. Guan[106], W. Guan[170], C. Gubbels[164], J.G.R. Guerrero Rojas[163], G. Guerrieri[69a,69b], F. Guescini[110], R. Gugel[100], J.A.M. Guhit[106], A. Guida[48], T. Guillemin[4], E. Guilloton[167,134], S. Guindon[36], F. Guo[14a,14d], J. Guo[62c], L. Guo[66], Y. Guo[106], R. Gupta[48], S. Gurbuz[24], S.S. Gurdasani[54], G. Gustavino[36], M. Guth[56], P. Gutierrez[120], L.F. Gutierrez Zagazeta[128], C. Gutschow[96], C. Gwenlan[126], C.B. Gwilliam[92], E.S. Haaland[125], A. Haas[117], M. Habedank[48], C. Haber[17a], H.K. Hadavand[8], A. Hadef[100], S. Hadzic[110], E.H. Haines[96], M. Haleem[166], J. Haley[121], J.J. Hall[139], G.D. Hallewell[102], L. Halser[19], K. Hamano[165], H. Hamdaoui[35e], M. Hamer[24], G.N. Hamity[52], J. Han[62b], K. Han[62a], L. Han[14c], L. Han[62a], S. Han[17a], Y.F. Han[155], K. Hanagaki[83], M. Hance[136], D.A. Hangal[41,ab], H. Hanif[142], M.D. Hank[39], R. Hankache[101], J.B. Hansen[42], J.D. Hansen[42], P.H. Hansen[42], K. Hara[157], D. Harada[56], T. Harenberg[171], S. Harkusha[37], Y.T. Harris[126], N.M. Harrison[119], P.F. Harrison[167], N.M. Hartman[143], N.M. Hartmann[109], Y. Hasegawa[140], A. Hasib[52], S. Haug[19], R. Hauser[107], M. Havranek[132], C.M. Hawkes[20], R.J. Hawkings[36], S. Hayashida[111], D. Hayden[107], C. Hayes[106], R.L. Hayes[114], C.P. Hays[126], J.M. Hays[94], H.S. Hayward[92], F. He[62a], Y. He[154], Y. He[127], N.B. Heatley[94], V. Hedberg[98], A.L. Heggelund[125], N.D. Hehir[94], C. Heidegger[54], K.K. Heidegger[54], W.D. Heidorn[81], J. Heilman[34], S. Heim[48], T. Heim[17a], J.G. Heinlein[128], J.J. Heinrich[123], L. Heinrich[110], J. Hejbal[131],

JHEP07(2023)086

L. Helary[48], A. Held[170], S. Hellesund[125], C.M. Helling[164], S. Hellman[47a,47b], C. Helsens[36], R.C.W. Henderson[91], L. Henkelmann[32], A.M. Henriques Correia[36], H. Herde[98], Y. Hernández Jiménez[145], L.M. Herrmann[24], T. Herrmann[50], G. Herten[54], R. Hertenberger[109], L. Hervas[36], N.P. Hessey[156a], H. Hibi[84], S.J. Hillier[20], F. Hinterkeuser[24], M. Hirose[124], S. Hirose[157], D. Hirschbuehl[171], T.G. Hitchings[101], B. Hiti[93], J. Hobbs[145], R. Hobincu[27e], N. Hod[169], M.C. Hodgkinson[139], B.H. Hodkinson[32], A. Hoecker[36], J. Hofer[48], T. Holm[24], M. Holzbock[110], L.B.A.H. Hommels[32], B.P. Honan[101], J. Hong[62c], T.M. Hong[129], J.C. Honig[54], B.H. Hooberman[162], W.H. Hopkins[6], Y. Horii[111], S. Hou[148], A.S. Howard[93], J. Howarth[59], J. Hoya[6], M. Hrabovsky[122], A. Hrynevich[48], T. Hryn'ova[4], P.J. Hsu[65], S.-C. Hsu[138], Q. Hu[41], Y.F. Hu[14a,14d,af], D.P. Huang[96], S. Huang[64b], X. Huang[14c], Y. Huang[62a], Y. Huang[14a], Z. Huang[101], Z. Hubacek[132], M. Huebner[24], F. Huegging[24], T.B. Huffman[126], M. Huhtinen[36], S.K. Huiberts[16], R. Hulsken[104], N. Huseynov[12,a], J. Huston[107], J. Huth[61], R. Hyneman[143], G. Iacobucci[56], G. Iakovidis[29], I. Ibragimov[141], L. Iconomidou-Fayard[66], P. Iengo[72a,72b], R. Iguchi[153], T. Iizawa[56], Y. Ikegami[83], A. Ilg[19], N. Ilic[155], H. Imam[35a], T. Ingebretsen Carlson[47a,47b], G. Introzzi[73a,73b], M. Iodice[77a], V. Ippolito[75a,75b], M. Ishino[153], W. Islam[170], C. Issever[18,48], S. Istin[21a], H. Ito[168], J.M. Iturbe Ponce[64a], R. Iuppa[78a,78b], A. Ivina[169], J.M. Izen[45], V. Izzo[72a], P. Jacka[131,132], P. Jackson[1], R.M. Jacobs[48], B.P. Jaeger[142], C.S. Jagfeld[109], P. Jain[54], G. Jäkel[171], K. Jakobs[54], T. Jakoubek[169], J. Jamieson[59], K.W. Janas[85a], A.E. Jaspan[92], M. Javurkova[103], F. Jeanneau[135], L. Jeanty[123], J. Jejelava[149a,aa], P. Jenni[54,h], C.E. Jessiman[34], S. Jézéquel[4], C. Jia[62b], J. Jia[145], X. Jia[61], X. Jia[14a,14d], Z. Jia[14c], Y. Jiang[62a], S. Jiggins[52], J. Jimenez Pena[110], S. Jin[14c], A. Jinaru[27b], O. Jinnouchi[154], P. Johansson[139], K.A. Johns[7], J.W. Johnson[136], D.M. Jones[32], E. Jones[167], P. Jones[32], R.W.L. Jones[91], T.J. Jones[92], R. Joshi[119], J. Jovicevic[15], X. Ju[17a], J.J. Junggeburth[36], T. Junkermann[63a], A. Juste Rozas[13,u], S. Kabana[137e], A. Kaczmarska[86], M. Kado[110], H. Kagan[119], M. Kagan[143], A. Kahn[41], A. Kahn[128], C. Kahra[100], T. Kaji[168], E. Kajomovitz[150], N. Kakati[169], C.W. Kalderon[29], A. Kamenshchikov[155], S. Kanayama[154], N.J. Kang[136], D. Kar[33g], K. Karava[126], M.J. Kareem[156b], E. Karentzos[54], I. Karkanias[152,f], S.N. Karpov[38], Z.M. Karpova[38], V. Kartvelishvili[91], A.N. Karyukhin[37], E. Kasimi[152,f], J. Katzy[48], S. Kaur[34], K. Kawade[140], T. Kawamoto[135], G. Kawamura[55], E.F. Kay[165], F.I. Kaya[158], S. Kazakos[13], V.F. Kazanin[37], Y. Ke[145], J.M. Keaveney[33a], R. Keeler[165], G.V. Kehris[61], J.S. Keller[34], A.S. Kelly[96], D. Kelsey[146], J.J. Kempster[146], K.E. Kennedy[41], P.D. Kennedy[100], O. Kepka[131], B.P. Kerridge[167], S. Kersten[171], B.P. Kerševan[93], S. Keshri[66], L. Keszeghova[28a], S. Ketabchi Haghighat[155], M. Khandoga[127], A. Khanov[121], A.G. Kharlamov[37], T. Kharlamova[37], E.E. Khoda[138], T.J. Khoo[18], G. Khoriauli[166], J. Khubua[149b], Y.A.R. Khwaira[66], M. Kiehn[36], A. Kilgallon[123], D.W. Kim[47a,47b], E. Kim[154], Y.K. Kim[39], N. Kimura[96], A. Kirchhoff[55], C. Kirfel[24], J. Kirk[134], A.E. Kiryunin[110], T. Kishimoto[153], D.P. Kisliuk[155], C. Kitsaki[10], O. Kivernyk[24], M. Klassen[63a], C. Klein[34], L. Klein[166], M.H. Klein[106], M. Klein[92], S.B. Klein[56], U. Klein[92], P. Klimek[36], A. Klimentov[29],

F. Klimpel[110], T. Klioutchnikova[36], P. Kluit[114], S. Kluth[110], E. Kneringer[79], T.M. Knight[155], A. Knue[54], R. Kobayashi[87], M. Kocian[143], P. Kodyš[133], D.M. Koeck[146], P.T. Koenig[24], T. Koffas[34], M. Kolb[135], I. Koletsou[4], T. Komarek[122], K. Köneke[54], A.X.Y. Kong[1], T. Kono[118], N. Konstantinidis[96], B. Konya[98], R. Kopeliansky[68], S. Koperny[85a], K. Korcyl[86], K. Kordas[152,f], G. Koren[151], A. Korn[96], S. Korn[55], I. Korolkov[13], N. Korotkova[37], B. Kortman[114], O. Kortner[110], S. Kortner[110], W.H. Kostecka[115], V.V. Kostyukhin[141], A. Kotsokechagia[135], A. Kotwal[51], A. Koulouris[36], A. Kourkoumeli-Charalampidi[73a,73b], C. Kourkoumelis[9], E. Kourlitis[6], O. Kovanda[146], R. Kowalewski[165], W. Kozanecki[135], A.S. Kozhin[37], V.A. Kramarenko[37], G. Kramberger[93], P. Kramer[100], M.W. Krasny[127], A. Krasznahorkay[36], J.A. Kremer[100], T. Kresse[50], J. Kretzschmar[92], K. Kreul[18], P. Krieger[155], S. Krishnamurthy[103], M. Krivos[133], K. Krizka[17a], K. Kroeninger[49], H. Kroha[110], J. Kroll[131], J. Kroll[128], K.S. Krowpman[107], U. Kruchonak[38], H. Krüger[24], N. Krumnack[81], M.C. Kruse[51], J.A. Krzysiak[86], O. Kuchinskaia[37], S. Kuday[3a], S. Kuehn[36], R. Kuesters[54], T. Kuhl[48], V. Kukhtin[38], Y. Kulchitsky[37,a], S. Kuleshov[137d,137b], M. Kumar[33g], N. Kumari[102], A. Kupco[131], T. Kupfer[49], A. Kupich[37], O. Kuprash[54], H. Kurashige[84], L.L. Kurchaninov[156a], Y.A. Kurochkin[37], A. Kurova[37], M. Kuze[154], A.K. Kvam[103], J. Kvita[122], T. Kwan[104], N.G. Kyriacou[106], L.A.O. Laatu[102], C. Lacasta[163], F. Lacava[75a,75b], H. Lacker[18], D. Lacour[127], N.N. Lad[96], E. Ladygin[38], B. Laforge[127], T. Lagouri[137e], S. Lai[55], I.K. Lakomiec[85a], N. Lalloue[60], J.E. Lambert[120], S. Lammers[68], W. Lampl[7], C. Lampoudis[152,f], A.N. Lancaster[115], E. Lançon[29], U. Landgraf[54], M.P.J. Landon[94], V.S. Lang[54], R.J. Langenberg[103], A.J. Lankford[160], F. Lanni[36], K. Lantzsch[24], A. Lanza[73a], A. Lapertosa[57b,57a], J.F. Laporte[135], T. Lari[71a], F. Lasagni Manghi[23b], M. Lassnig[36], V. Latonova[131], A. Laudrain[100], A. Laurier[150], S.D. Lawlor[95], Z. Lawrence[101], M. Lazzaroni[71a,71b], B. Le[101], E.M. Le Boulicaut[51], B. Leban[93], A. Lebedev[81], M. LeBlanc[36], F. Ledroit-Guillon[60], A.C.A. Lee[96], G.R. Lee[16], S.C. Lee[148], S. Lee[47a,47b], T.F. Lee[92], L.L. Leeuw[33c], H.P. Lefebvre[95], M. Lefebvre[165], C. Leggett[17a], K. Lehmann[142], G. Lehmann Miotto[36], M. Leigh[56], W.A. Leight[103], A. Leisos[152,t], M.A.L. Leite[82c], C.E. Leitgeb[48], R. Leitner[133], K.J.C. Leney[44], T. Lenz[24], S. Leone[74a], C. Leonidopoulos[52], A. Leopold[144], C. Leroy[108], R. Les[107], C.G. Lester[32], M. Levchenko[37], J. Levêque[4], D. Levin[106], L.J. Levinson[169], M.P. Lewicki[86], D.J. Lewis[4], A. Li[5], B. Li[62b], C. Li[62a], C-Q. Li[62c], H. Li[62a], H. Li[62b], H. Li[14c], H. Li[62b], J. Li[62c], K. Li[138], L. Li[62c], M. Li[14a,14d], Q.Y. Li[62a], S. Li[14a,14d], S. Li[62d,62c,e], T. Li[62b], X. Li[104], Z. Li[62b], Z. Li[126], Z. Li[104], Z. Li[92], Z. Li[14a,14d], Z. Liang[14a], M. Liberatore[48], B. Liberti[76a], K. Lie[64c], J. Lieber Marin[82b], H. Lien[68], K. Lin[107], R.A. Linck[68], R.E. Lindley[7], J.H. Lindon[2], A. Linss[48], E. Lipeles[128], A. Lipniacka[16], A. Lister[164], J.D. Little[4], B. Liu[14a], B.X. Liu[142], D. Liu[62d,62c], J.B. Liu[62a], J.K.K. Liu[32], K. Liu[62d,62c], M. Liu[62a], M.Y. Liu[62a], P. Liu[14a], Q. Liu[62d,138,62c], X. Liu[62a], Y. Liu[14c,14d], Y.L. Liu[106], Y.W. Liu[62a], M. Livan[73a,73b], J. Llorente Merino[142], S.L. Lloyd[94], E.M. Lobodzinska[48], P. Loch[7], S. Loffredo[76a,76b], T. Lohse[18], K. Lohwasser[139], E. Loiacono[48], M. Lokajicek[131], J.D. Long[162], I. Longarini[160], L. Longo[70a,70b], R. Longo[162],

JHEP07(2023)086

I. Lopez Paz[67], A. Lopez Solis[48], J. Lorenz[109], N. Lorenzo Martinez[4], A.M. Lory[109], X. Lou[47a,47b], X. Lou[14a,14d], A. Lounis[66], J. Love[6], P.A. Love[91], G. Lu[14a,14d], M. Lu[80], S. Lu[128], Y.J. Lu[65], H.J. Lubatti[138], C. Luci[75a,75b], F.L. Lucio Alves[14c], A. Lucotte[60], F. Luehring[68], I. Luise[145], O. Lukianchuk[66], O. Lundberg[144], B. Lund-Jensen[144], N.A. Luongo[123], M.S. Lutz[151], D. Lynn[29], H. Lyons[92], R. Lysak[131], E. Lytken[98], F. Lyu[14a], V. Lyubushkin[38], T. Lyubushkina[38], M.M. Lyukova[145], H. Ma[29], L.L. Ma[62b], Y. Ma[96], D.M. Mac Donell[165], G. Maccarrone[53], J.C. MacDonald[139], R. Madar[40], W.F. Mader[50], J. Maeda[84], T. Maeno[29], M. Maerker[50], H. Maguire[139], A. Maio[130a,130b,130d], K. Maj[85a], O. Majersky[48], S. Majewski[123], N. Makovec[66], V. Maksimovic[15], B. Malaescu[127], Pa. Malecki[86], V.P. Maleev[37], F. Malek[60], D. Malito[43b,43a], U. Mallik[80], C. Malone[32], S. Maltezos[10], S. Malyukov[38], J. Mamuzic[13], G. Mancini[53], G. Manco[73a,73b], J.P. Mandalia[94], I. Mandić[93], L. Manhaes de Andrade Filho[82a], I.M. Maniatis[169], J. Manjarres Ramos[102], D.C. Mankad[169], A. Mann[109], B. Mansoulie[135], S. Manzoni[36], A. Marantis[152], G. Marchiori[5], M. Marcisovsky[131], C. Marcon[71a,71b], M. Marinescu[20], M. Marjanovic[120], E.J. Marshall[91], Z. Marshall[17a], S. Marti-Garcia[163], T.A. Martin[167], V.J. Martin[52], B. Martin dit Latour[16], L. Martinelli[75a,75b], M. Martinez[13,u], P. Martinez Agullo[163], V.I. Martinez Outschoorn[103], P. Martinez Suarez[13], S. Martin-Haugh[134], V.S. Martoiu[27b], A.C. Martyniuk[96], A. Marzin[36], S.R. Maschek[110], D. Mascione[78a,78b], L. Masetti[100], T. Mashimo[153], J. Masik[101], A.L. Maslennikov[37], L. Massa[23b], P. Massarotti[72a,72b], P. Mastrandrea[74a,74b], A. Mastroberardino[43b,43a], T. Masubuchi[153], T. Mathisen[161], N. Matsuzawa[153], J. Maurer[27b], B. Maček[93], D.A. Maximov[37], R. Mazini[148], I. Maznas[152,f], M. Mazza[107], S.M. Mazza[136], C. Mc Ginn[29], J.P. Mc Gowan[104], S.P. Mc Kee[106], E.F. McDonald[105], A.E. McDougall[114], J.A. Mcfayden[146], G. Mchedlidze[149b], R.P. Mckenzie[33g], T.C. Mclachlan[48], D.J. Mclaughlin[96], K.D. McLean[165], S.J. McMahon[134], P.C. McNamara[105], C.M. Mcpartland[92], R.A. McPherson[165,x], T. Megy[40], S. Mehlhase[109], A. Mehta[92], D. Melini[150], B.R. Mellado Garcia[33g], A.H. Melo[55], F. Meloni[48], A.M. Mendes Jacques Da Costa[20], H.Y. Meng[155], L. Meng[91], S. Menke[110], M. Mentink[36], E. Meoni[43b,43a], C. Merlassino[126], L. Merola[72a,72b], C. Meroni[71a], G. Merz[106], O. Meshkov[37], J. Metcalfe[6], A.S. Mete[6], C. Meyer[68], J-P. Meyer[135], R.P. Middleton[134], L. Mijović[52], G. Mikenberg[169], M. Mikestikova[131], M. Mikuž[93], H. Mildner[139], A. Milic[36], C.D. Milke[44], D.W. Miller[39], L.S. Miller[34], A. Milov[169], D.A. Milstead[47a,47b], T. Min[14c], A.A. Minaenko[37], I.A. Minashvili[149b], L. Mince[59], A.I. Mincer[117], B. Mindur[85a], M. Mineev[38], Y. Mino[87], L.M. Mir[13], M. Miralles Lopez[163], M. Mironova[126], M.C. Missio[113], T. Mitani[168], A. Mitra[167], V.A. Mitsou[163], O. Miu[155], P.S. Miyagawa[94], Y. Miyazaki[89], A. Mizukami[83], T. Mkrtchyan[63a], M. Mlinarevic[96], T. Mlinarevic[96], M. Mlynarikova[36], S. Mobius[55], K. Mochizuki[108], P. Moder[48], P. Mogg[109], A.F. Mohammed[14a,14d], S. Mohapatra[41], G. Mokgatitswane[33g], B. Mondal[141], S. Mondal[132], K. Mönig[48], E. Monnier[102], L. Monsonis Romero[163], J. Montejo Berlingen[83], M. Montella[119], F. Monticelli[90], N. Morange[66], A.L. Moreira De Carvalho[130a], M. Moreno Llácer[163], C. Moreno Martinez[56], P. Morettini[57b], S. Morgenstern[167], M. Morii[61],

M. Morinaga[153], A.K. Morley[36], F. Morodei[75a,75b], L. Morvaj[36], P. Moschovakos[36], B. Moser[36], M. Mosidze[149b], T. Moskalets[54], P. Moskvitina[113], J. Moss[31,o], E.J.W. Moyse[103], O. Mtintsilana[33g], S. Muanza[102], J. Mueller[129], D. Muenstermann[91], R. Müller[19], G.A. Mullier[161], J.J. Mullin[128], D.P. Mungo[155], J.L. Munoz Martinez[13], D. Munoz Perez[163], F.J. Munoz Sanchez[101], M. Murin[101], W.J. Murray[167,134], A. Murrone[71a,71b], J.M. Muse[120], M. Muškinja[17a], C. Mwewa[29], A.G. Myagkov[37,a], A.J. Myers[8], A.A. Myers[129], G. Myers[68], M. Myska[132], B.P. Nachman[17a], O. Nackenhorst[49], A. Nag[50], K. Nagai[126], K. Nagano[83], J.L. Nagle[29,ag], E. Nagy[102], A.M. Nairz[36], Y. Nakahama[83], K. Nakamura[83], H. Nanjo[124], R. Narayan[44], E.A. Narayanan[112], I. Naryshkin[37], M. Naseri[34], C. Nass[24], G. Navarro[22a], J. Navarro-Gonzalez[163], R. Nayak[151], A. Nayaz[18], P.Y. Nechaeva[37], F. Nechansky[48], L. Nedic[126], T.J. Neep[20], A. Negri[73a,73b], M. Negrini[23b], C. Nellist[114], C. Nelson[104], K. Nelson[106], S. Nemecek[131], M. Nessi[36,i], M.S. Neubauer[162], F. Neuhaus[100], J. Neundorf[48], R. Newhouse[164], P.R. Newman[20], C.W. Ng[129], Y.W.Y. Ng[48], B. Ngair[35e], H.D.N. Nguyen[108], R.B. Nickerson[126], R. Nicolaidou[135], J. Nielsen[136], M. Niemeyer[55], N. Nikiforou[36], V. Nikolaenko[37,a], I. Nikolic-Audit[127], K. Nikolopoulos[20], P. Nilsson[29], I. Ninca[48], H.R. Nindhito[56], G. Ninio[151], A. Nisati[75a], N. Nishu[2], R. Nisius[110], J-E. Nitschke[50], E.K. Nkadimeng[33g], S.J. Noacco Rosende[90], T. Nobe[153], D.L. Noel[32], Y. Noguchi[87], T. Nommensen[147], M.A. Nomura[29], M.B. Norfolk[139], R.R.B. Norisam[96], B.J. Norman[34], J. Novak[93], T. Novak[48], L. Novotny[132], R. Novotny[112], L. Nozka[122], K. Ntekas[160], N.M.J. Nunes De Moura Junior[82b], E. Nurse[96], J. Ocariz[127], A. Ochi[84], I. Ochoa[130a], S. Oerdek[161], J.T. Offermann[39], A. Ogrodnik[85a], A. Oh[101], C.C. Ohm[144], H. Oide[83], R. Oishi[153], M.L. Ojeda[48], Y. Okazaki[87], M.W. O'Keefe[92], Y. Okumura[153], A. Olariu[27b], L.F. Oleiro Seabra[130a], S.A. Olivares Pino[137d], D. Oliveira Damazio[29], D. Oliveira Goncalves[82a], J.L. Oliver[160], M.J.R. Olsson[160], A. Olszewski[86], J. Olszowska[86,*], Ö.O. Öncel[54], D.C. O'Neil[142], A.P. O'Neill[19], A. Onofre[130a,130e], P.U.E. Onyisi[11], M.J. Oreglia[39], G.E. Orellana[90], D. Orestano[77a,77b], N. Orlando[13], R.S. Orr[155], V. O'Shea[59], R. Ospanov[62a], G. Otero y Garzon[30], H. Otono[89], P.S. Ott[63a], G.J. Ottino[17a], M. Ouchrif[35d], J. Ouellette[29], F. Ould-Saada[125], M. Owen[59], R.E. Owen[134], K.Y. Oyulmaz[21a], V.E. Ozcan[21a], N. Ozturk[8], S. Ozturk[21d], H.A. Pacey[32], K. Pachal[51], A. Pacheco Pages[13], C. Padilla Aranda[13], G. Padovano[75a,75b], S. Pagan Griso[17a], G. Palacino[68], A. Palazzo[70a,70b], S. Palestini[36], J. Pan[172], T. Pan[64a], D.K. Panchal[11], C.E. Pandini[114], J.G. Panduro Vazquez[95], H. Pang[14b], P. Pani[48], G. Panizzo[69a,69c], L. Paolozzi[56], C. Papadatos[108], S. Parajuli[44], A. Paramonov[6], C. Paraskevopoulos[10], D. Paredes Hernandez[64b], T.H. Park[155], M.A. Parker[32], F. Parodi[57b,57a], E.W. Parrish[115], V.A. Parrish[52], J.A. Parsons[41], U. Parzefall[54], B. Pascual Dias[108], L. Pascual Dominguez[151], F. Pasquali[114], E. Pasqualucci[75a], S. Passaggio[57b], F. Pastore[95], P. Pasuwan[47a,47b], P. Patel[86], U.M. Patel[51], J.R. Pater[101], T. Pauly[36], J. Pearkes[143], M. Pedersen[125], R. Pedro[130a], S.V. Peleganchuk[37], O. Penc[36], E.A. Pender[52], H. Peng[62a], K.E. Penski[109], M. Penzin[37], B.S. Peralva[82d,82d], A.P. Pereira Peixoto[60], L. Pereira Sanchez[47a,47b], D.V. Perepelitsa[29,ag], E. Perez Codina[156a], M. Perganti[10],

JHEP07(2023)086

L. Perini[71a,71b,*], H. Pernegger[36], S. Perrella[36], A. Perrevoort[113], O. Perrin[40], K. Peters[48], R.F.Y. Peters[101], B.A. Petersen[36], T.C. Petersen[42], E. Petit[102], V. Petousis[132], C. Petridou[152,f], A. Petrukhin[141], M. Pettee[17a], N.E. Pettersson[36], A. Petukhov[37], K. Petukhova[133], A. Peyaud[135], R. Pezoa[137f], L. Pezzotti[36], G. Pezzullo[172], T.M. Pham[170], T. Pham[105], P.W. Phillips[134], M.W. Phipps[162], G. Piacquadio[145], E. Pianori[17a], F. Piazza[71a,71b], R. Piegaia[30], D. Pietreanu[27b], A.D. Pilkington[101], M. Pinamonti[69a,69c], J.L. Pinfold[2], B.C. Pinheiro Pereira[130a], C. Pitman Donaldson[96], D.A. Pizzi[34], L. Pizzimento[76a,76b], A. Pizzini[114], M.-A. Pleier[29], V. Plesanovs[54], V. Pleskot[133], E. Plotnikova[38], G. Poddar[4], R. Poettgen[98], L. Poggioli[127], D. Pohl[24], I. Pokharel[55], S. Polacek[133], G. Polesello[73a], A. Poley[142,156a], R. Polifka[132], A. Polini[23b], C.S. Pollard[167], Z.B. Pollock[119], V. Polychronakos[29], E. Pompa Pacchi[75a,75b], D. Ponomarenko[113], L. Pontecorvo[36], S. Popa[27a], G.A. Popeneciu[27d], D.M. Portillo Quintero[156a], S. Pospisil[132], P. Postolache[27c], K. Potamianos[126], P.P. Potepa[85a], I.N. Potrap[38], C.J. Potter[32], H. Potti[1], T. Poulsen[48], J. Poveda[163], M.E. Pozo Astigarraga[36], A. Prades Ibanez[163], M.M. Prapa[46], J. Pretel[54], D. Price[101], M. Primavera[70a], M.A. Principe Martin[99], R. Privara[122], M.L. Proffitt[138], N. Proklova[128], K. Prokofiev[64c], G. Proto[76a,76b], S. Protopopescu[29], J. Proudfoot[6], M. Przybycien[85a], W.W. Przygoda[85b], J.E. Puddefoot[139], D. Pudzha[37], D. Pyatiizbyantseva[37], J. Qian[106], D. Qichen[101], Y. Qin[101], T. Qiu[94], A. Quadt[55], M. Queitsch-Maitland[101], G. Quetant[56], G. Rabanal Bolanos[61], D. Rafanoharana[54], F. Ragusa[71a,71b], J.L. Rainbolt[39], J.A. Raine[56], S. Rajagopalan[29], E. Ramakoti[37], K. Ran[48,14d], N.P. Rapheeha[33g], V. Raskina[127], D.F. Rassloff[63a], S. Rave[100], B. Ravina[55], I. Ravinovich[169], M. Raymond[36], A.L. Read[125], N.P. Readioff[139], D.M. Rebuzzi[73a,73b], G. Redlinger[29], K. Reeves[45], J.A. Reidelsturz[171], D. Reikher[151], A. Rej[141], C. Rembser[36], A. Renardi[48], M. Renda[27b], M.B. Rendel[110], F. Renner[48], A.G. Rennie[59], S. Resconi[71a], M. Ressegotti[57b,57a], E.D. Resseguie[17a], S. Rettie[36], J.G. Reyes Rivera[107], B. Reynolds[119], E. Reynolds[17a], M. Rezaei Estabragh[171], O.L. Rezanova[37], P. Reznicek[133], N. Ribaric[91], E. Ricci[78a,78b], R. Richter[110], S. Richter[47a,47b], E. Richter-Was[85b], M. Ridel[127], S. Ridouani[35d], P. Rieck[117], P. Riedler[36], M. Rijssenbeek[145], A. Rimoldi[73a,73b], M. Rimoldi[48], L. Rinaldi[23b,23a], T.T. Rinn[29], M.P. Rinnagel[109], G. Ripellino[161], I. Riu[13], P. Rivadeneira[48], J.C. Rivera Vergara[165], F. Rizatdinova[121], E. Rizvi[94], C. Rizzi[56], B.A. Roberts[167], B.R. Roberts[17a], S.H. Robertson[104,x], M. Robin[48], D. Robinson[32], C.M. Robles Gajardo[137f], M. Robles Manzano[100], A. Robson[59], A. Rocchi[76a,76b], C. Roda[74a,74b], S. Rodriguez Bosca[63a], Y. Rodriguez Garcia[22a], A. Rodriguez Rodriguez[54], A.M. Rodríguez Vera[156b], S. Roe[36], J.T. Roemer[160], A.R. Roepe-Gier[136], J. Roggel[171], O. Røhne[125], R.A. Rojas[103], B. Roland[54], C.P.A. Roland[68], J. Roloff[29], A. Romaniouk[37], E. Romano[73a,73b], M. Romano[23b], A.C. Romero Hernandez[162], N. Rompotis[92], L. Roos[127], S. Rosati[75a], B.J. Rosser[39], E. Rossi[4], E. Rossi[72a,72b], L.P. Rossi[57b], L. Rossini[48], R. Rosten[119], M. Rotaru[27b], B. Rottler[54], C. Rougier[102], D. Rousseau[66], D. Rousso[32], G. Rovelli[73a,73b], A. Roy[162], S. Roy-Garand[155], A. Rozanov[102], Y. Rozen[150], X. Ruan[33g],

JHEP07(2023)086

A. Rubio Jimenez[163], A.J. Ruby[92], V.H. Ruelas Rivera[18], T.A. Ruggeri[1], F. Rühr[54], A. Ruiz-Martinez[163], A. Rummler[36], Z. Rurikova[54], N.A. Rusakovich[38], H.L. Russell[165], J.P. Rutherfoord[7], K. Rybacki[91], M. Rybar[133], E.B. Rye[125], A. Ryzhov[37], J.A. Sabater Iglesias[56], P. Sabatini[163], L. Sabetta[75a,75b], H.F-W. Sadrozinski[136], F. Safai Tehrani[75a], B. Safarzadeh Samani[146], M. Safdari[143], S. Saha[104], M. Sahinsoy[110], M. Saimpert[135], M. Saito[153], T. Saito[153], D. Salamani[36], A. Salnikov[143], J. Salt[163], A. Salvador Salas[13], D. Salvatore[43b,43a], F. Salvatore[146], A. Salzburger[36], D. Sammel[54], D. Sampsonidis[152,f], D. Sampsonidou[62d,62c], J. Sánchez[163], A. Sanchez Pineda[4], V. Sanchez Sebastian[163], H. Sandaker[125], C.O. Sander[48], J.A. Sandesara[103], M. Sandhoff[171], C. Sandoval[22b], D.P.C. Sankey[134], T. Sano[87], A. Sansoni[53], L. Santi[75a,75b], C. Santoni[40], H. Santos[130a,130b], S.N. Santpur[17a], A. Santra[169], K.A. Saoucha[139], J.G. Saraiva[130a,130d], J. Sardain[7], O. Sasaki[83], K. Sato[157], C. Sauer[63b], F. Sauerburger[54], E. Sauvan[4], P. Savard[155,ad], R. Sawada[153], C. Sawyer[134], L. Sawyer[97], I. Sayago Galvan[163], C. Sbarra[23b], A. Sbrizzi[23b,23a], T. Scanlon[96], J. Schaarschmidt[138], P. Schacht[110], D. Schaefer[39], U. Schäfer[100], A.C. Schaffer[66,44], D. Schaile[109], R.D. Schamberger[145], E. Schanet[109], C. Scharf[18], M.M. Schefer[19], V.A. Schegelsky[37], D. Scheirich[133], F. Schenck[18], M. Schernau[160], C. Scheulen[55], C. Schiavi[57b,57a], Z.M. Schillaci[26], E.J. Schioppa[70a,70b], M. Schioppa[43b,43a], B. Schlag[100], K.E. Schleicher[54], S. Schlenker[36], J. Schmeing[171], M.A. Schmidt[171], K. Schmieden[100], C. Schmitt[100], S. Schmitt[48], L. Schoeffel[135], A. Schoening[63b], P.G. Scholer[54], E. Schopf[126], M. Schott[100], J. Schovancova[36], S. Schramm[56], F. Schroeder[171], H-C. Schultz-Coulon[63a], M. Schumacher[54], B.A. Schumm[136], Ph. Schune[135], H.R. Schwartz[136], A. Schwartzman[143], T.A. Schwarz[106], Ph. Schwemling[135], R. Schwienhorst[107], A. Sciandra[136], G. Sciolla[26], F. Scuri[74a], F. Scutti[105], C.D. Sebastiani[92], K. Sedlaczek[49], P. Seema[18], S.C. Seidel[112], A. Seiden[136], B.D. Seidlitz[41], C. Seitz[48], J.M. Seixas[82b], G. Sekhniaidze[72a], S.J. Sekula[44], L. Selem[4], N. Semprini-Cesari[23b,23a], S. Sen[51], D. Sengupta[56], V. Senthilkumar[163], L. Serin[66], L. Serkin[69a,69b], M. Sessa[77a,77b], H. Severini[120], F. Sforza[57b,57a], A. Sfyrla[56], E. Shabalina[55], R. Shaheen[144], J.D. Shahinian[128], D. Shaked Renous[169], L.Y. Shan[14a], M. Shapiro[17a], A. Sharma[36], A.S. Sharma[164], P. Sharma[80], S. Sharma[48], P.B. Shatalov[37], K. Shaw[146], S.M. Shaw[101], Q. Shen[62c,5], P. Sherwood[96], L. Shi[96], C.O. Shimmin[172], Y. Shimogama[168], J.D. Shinner[95], I.P.J. Shipsey[126], S. Shirabe[60], M. Shiyakova[38], J. Shlomi[169], M.J. Shochet[39], J. Shojaii[105], D.R. Shope[125], S. Shrestha[119,ah], E.M. Shrif[33g], M.J. Shroff[165], P. Sicho[131], A.M. Sickles[162], E. Sideras Haddad[33g], A. Sidoti[23b], F. Siegert[50], Dj. Sijacki[15], R. Sikora[85a], F. Sili[90], J.M. Silva[20], M.V. Silva Oliveira[36], S.B. Silverstein[47a], S. Simion[66], R. Simoniello[36], E.L. Simpson[59], H. Simpson[146], L.R. Simpson[106], N.D. Simpson[98], S. Simsek[21d], S. Sindhu[55], P. Sinervo[155], S. Singh[142], S. Singh[155], S. Sinha[48], S. Sinha[33g], M. Sioli[23b,23a], I. Siral[36], S.Yu. Sivoklokov[37,*], J. Sjölin[47a,47b], A. Skaf[55], E. Skorda[98], P. Skubic[120], M. Slawinska[86], V. Smakhtin[169], B.H. Smart[134], J. Smiesko[36], S.Yu. Smirnov[37], Y. Smirnov[37], L.N. Smirnova[37,a], O. Smirnova[98], A.C. Smith[41], E.A. Smith[39], H.A. Smith[126], J.L. Smith[92], R. Smith[143], M. Smizanska[91], K. Smolek[132], A. Smykiewicz[86], A.A. Snesarev[37], H.L. Snoek[114],

JHEP07(2023)086

S. Snyder[29], R. Sobie[165,x], A. Soffer[151], C.A. Solans Sanchez[36], E.Yu. Soldatov[37], U. Soldevila[163], A.A. Solodkov[37], S. Solomon[54], A. Soloshenko[38], K. Solovieva[54], O.V. Solovyanov[40], V. Solovyev[37], P. Sommer[36], A. Sonay[13], W.Y. Song[156b], J.M. Sonneveld[114], A. Sopczak[132], A.L. Sopio[96], F. Sopkova[28b], V. Sothilingam[63a], S. Sottocornola[68], R. Soualah[116b], Z. Soumaimi[35e], D. South[48], S. Spagnolo[70a,70b], M. Spalla[110], D. Sperlich[54], G. Spigo[36], M. Spina[146], S. Spinali[91], D.P. Spiteri[59], M. Spousta[133], E.J. Staats[34], A. Stabile[71a,71b], R. Stamen[63a], M. Stamenkovic[114], A. Stampekis[20], M. Standke[24], E. Stanecka[86], M.V. Stange[50], B. Stanislaus[17a], M.M. Stanitzki[48], M. Stankaityte[126], B. Stapf[48], E.A. Starchenko[37], G.H. Stark[136], J. Stark[102], D.M. Starko[156b], P. Staroba[131], P. Starovoitov[63a], S. Stärz[104], R. Staszewski[86], G. Stavropoulos[46], J. Steentoft[161], P. Steinberg[29], B. Stelzer[142,156a], H.J. Stelzer[129], O. Stelzer-Chilton[156a], H. Stenzel[58], T.J. Stevenson[146], G.A. Stewart[36], J.R. Stewart[121], M.C. Stockton[36], G. Stoicea[27b], M. Stolarski[130a], S. Stonjek[110], A. Straessner[50], J. Strandberg[144], S. Strandberg[47a,47b], M. Strauss[120], T. Strebler[102], P. Strizenec[28b], R. Ströhmer[166], D.M. Strom[123], L.R. Strom[48], R. Stroynowski[44], A. Strubig[47a,47b], S.A. Stucci[29], B. Stugu[16], J. Stupak[120], N.A. Styles[48], D. Su[143], S. Su[62a], W. Su[62d,138,62c], X. Su[62a,66], K. Sugizaki[153], V.V. Sulin[37], M.J. Sullivan[92], D.M.S. Sultan[78a,78b], L. Sultanaliyeva[37], S. Sultansoy[3b], T. Sumida[87], S. Sun[106], S. Sun[170], O. Sunneborn Gudnadottir[161], M.R. Sutton[146], M. Svatos[131], M. Swiatlowski[156a], T. Swirski[166], I. Sykora[28a], M. Sykora[133], T. Sykora[133], D. Ta[100], K. Tackmann[48,v], A. Taffard[160], R. Tafirout[156a], J.S. Tafoya Vargas[66], R.H.M. Taibah[127], R. Takashima[88], E.P. Takeva[52], Y. Takubo[83], M. Talby[102], A.A. Talyshev[37], K.C. Tam[64b], N.M. Tamir[151], A. Tanaka[153], J. Tanaka[153], R. Tanaka[66], M. Tanasini[57b,57a], J. Tang[62c], Z. Tao[164], S. Tapia Araya[137f], S. Tapprogge[100], A. Tarek Abouelfadl Mohamed[107], S. Tarem[150], K. Tariq[62b], G. Tarna[102,27b], G.F. Tartarelli[71a], P. Tas[133], M. Tasevsky[131], E. Tassi[43b,43a], A.C. Tate[162], G. Tateno[153], Y. Tayalati[35e,w], G.N. Taylor[105], W. Taylor[156b], H. Teagle[92], A.S. Tee[170], R. Teixeira De Lima[143], P. Teixeira-Dias[95], J.J. Teoh[155], K. Terashi[153], J. Terron[99], S. Terzo[13], M. Testa[53], R.J. Teuscher[155,x], A. Thaler[79], O. Theiner[56], N. Themistokleous[52], T. Theveneaux-Pelzer[102], O. Thielmann[171], D.W. Thomas[95], J.P. Thomas[20], E.A. Thompson[17a], P.D. Thompson[20], E. Thomson[128], E.J. Thorpe[94], Y. Tian[55], V. Tikhomirov[37,a], Yu.A. Tikhonov[37], S. Timoshenko[37], E.X.L. Ting[1], P. Tipton[172], S.H. Tlou[33g], A. Thourji[40], K. Todome[23b,23a], S. Todorova-Nova[133], S. Todt[50], M. Togawa[83], J. Tojo[89], S. Tokár[28a], K. Tokushuku[83], O. Toldaiev[68], R. Tombs[32], M. Tomoto[83,111], L. Tompkins[143], K.W. Topolnicki[85b], P. Tornambe[103], E. Torrence[123], H. Torres[50], E. Torró Pastor[163], M. Toscani[30], C. Tosciri[39], M. Tost[11], D.R. Tovey[139], A. Traeet[16], I.S. Trandafir[27b], T. Trefzger[166], A. Tricoli[29], I.M. Trigger[156a], S. Trincaz-Duvoid[127], D.A. Trischuk[26], B. Trocmé[60], C. Troncon[71a], L. Truong[33c], M. Trzebinski[86], A. Trzupek[86], F. Tsai[145], M. Tsai[106], A. Tsiamis[152,f], P.V. Tsiareshka[37], S. Tsigaridas[156a], A. Tsirigotis[152,t], V. Tsiskaridze[145], E.G. Tskhadadze[149a], M. Tsopoulou[152,f], Y. Tsujikawa[87], I.I. Tsukerman[37], V. Tsulaia[17a], S. Tsuno[83], O. Tsur[150], D. Tsybychev[145], Y. Tu[64b], A. Tudorache[27b], V. Tudorache[27b], A.N. Tuna[36], S. Turchikhin[38], I. Turk Cakir[3a], R. Turra[71a],

T. Turtuvshin[38,y], P.M. Tuts[41], S. Tzamarias[152,f], P. Tzanis[10], E. Tzovara[100], K. Uchida[153], F. Ukegawa[157], P.A. Ulloa Poblete[137c], E.N. Umaka[29], G. Unal[36], M. Unal[11], A. Undrus[29], G. Unel[160], J. Urban[28b], P. Urquijo[105], G. Usai[8], R. Ushioda[154], M. Usman[108], Z. Uysal[21b], L. Vacavant[102], V. Vacek[132], B. Vachon[104], K.O.H. Vadla[125], T. Vafeiadis[36], A. Vaitkus[96], C. Valderanis[109], E. Valdes Santurio[47a,47b], M. Valente[156a], S. Valentinetti[23b,23a], A. Valero[163], A. Vallier[102], J.A. Valls Ferrer[163], D.R. Van Arneman[114], T.R. Van Daalen[138], P. Van Gemmeren[6], M. Van Rijnbach[125,36], S. Van Stroud[96], I. Van Vulpen[114], M. Vanadia[76a,76b], W. Vandelli[36], M. Vandenbroucke[135], E.R. Vandewall[121], D. Vannicola[151], L. Vannoli[57b,57a], R. Vari[75a], E.W. Varnes[7], C. Varni[17a], T. Varol[148], D. Varouchas[66], L. Varriale[163], K.E. Varvell[147], M.E. Vasile[27b], L. Vaslin[40], G.A. Vasquez[165], F. Vazeille[40], T. Vazquez Schroeder[36], J. Veatch[31], V. Vecchio[101], M.J. Veen[103], I. Veliscek[126], L.M. Veloce[155], F. Veloso[130a,130c], S. Veneziano[75a], A. Ventura[70a,70b], A. Verbytskyi[110], M. Verducci[74a,74b], C. Vergis[24], M. Verissimo De Araujo[82b], W. Verkerke[114], J.C. Vermeulen[114], C. Vernieri[143], P.J. Verschuuren[95], M. Vessella[103], M.C. Vetterli[142,ad], A. Vgenopoulos[152,f], N. Viaux Maira[137f], T. Vickey[139], O.E. Vickey Boeriu[139], G.H.A. Viehhauser[126], L. Vigani[63b], M. Villa[23b,23a], M. Villaplana Perez[163], E.M. Villhauer[52], E. Vilucchi[53], M.G. Vincter[34], G.S. Virdee[20], A. Vishwakarma[52], C. Vittori[36], I. Vivarelli[146], V. Vladimirov[167], E. Voevodina[110], F. Vogel[109], P. Vokac[132], J. Von Ahnen[48], E. Von Toerne[24], B. Vormwald[36], V. Vorobel[133], K. Vorobev[37], M. Vos[163], K. Voss[141], J.H. Vossebeld[92], M. Vozak[114], L. Vozdecky[94], N. Vranjes[15], M. Vranjes Milosavljevic[15], M. Vreeswijk[114], R. Vuillermet[36], O. Vujinovic[100], I. Vukotic[39], S. Wada[157], C. Wagner[103], J.M. Wagner[17a], W. Wagner[171], S. Wahdan[171], H. Wahlberg[90], R. Wakasa[157], M. Wakida[111], J. Walder[134], R. Walker[109], W. Walkowiak[141], A.M. Wang[61], A.Z. Wang[170], C. Wang[100], C. Wang[62c], H. Wang[17a], J. Wang[64a], R.-J. Wang[100], R. Wang[61], R. Wang[6], S.M. Wang[148], S. Wang[62b], T. Wang[62a], W.T. Wang[80], X. Wang[14c], X. Wang[162], X. Wang[62c], Y. Wang[62d], Y. Wang[14c], Z. Wang[106], Z. Wang[62d,51,62c], Z. Wang[106], A. Warburton[104], R.J. Ward[20], N. Warrack[59], A.T. Watson[20], H. Watson[59], M.F. Watson[20], G. Watts[138], B.M. Waugh[96], A.F. Webb[11], C. Weber[29], H.A. Weber[18], M.S. Weber[19], S.M. Weber[63a], C. Wei[62a], Y. Wei[126], A.R. Weidberg[126], E.J. Weik[117], J. Weingarten[49], M. Weirich[100], C. Weiser[54], C.J. Wells[48], T. Wenaus[29], B. Wendland[49], T. Wengler[36], N.S. Wenke[110], N. Wermes[24], M. Wessels[63a], K. Whalen[123], A.M. Wharton[91], A.S. White[61], A. White[8], M.J. White[1], D. Whiteson[160], L. Wickremasinghe[124], W. Wiedenmann[170], C. Wiel[50], M. Wielers[134], C. Wiglesworth[42], L.A.M. Wiik-Fuchs[54], D.J. Wilbern[120], H.G. Wilkens[36], D.M. Williams[41], H.H. Williams[128], S. Williams[32], S. Willocq[103], B.J. Wilson[101], P.J. Windischhofer[39], F. Winklmeier[123], B.T. Winter[54], J.K. Winter[101], M. Wittgen[143], M. Wobisch[97], R. Wölker[126], J. Wollrath[160], M.W. Wolter[86], H. Wolters[130a,130c], V.W.S. Wong[164], A.F. Wongel[48], S.D. Worm[48], B.K. Wosiek[86], K.W. Woźniak[86], K. Wraight[59], J. Wu[14a,14d], M. Wu[64a], M. Wu[113], S.L. Wu[170], X. Wu[56], Y. Wu[62a], Z. Wu[135,62a], J. Wuerzinger[110], T.R. Wyatt[101], B.M. Wynne[52], S. Xella[42], L. Xia[14c],

JHEP07(2023)086

M. Xia[14b], J. Xiang[64c], X. Xiao[106], M. Xie[62a], X. Xie[62a], S. Xin[14a,14d], J. Xiong[17a], I. Xiotidis[146], D. Xu[14a], H. Xu[62a], H. Xu[62a], L. Xu[62a], R. Xu[128], T. Xu[106], Y. Xu[14b], Z. Xu[62b], Z. Xu[14a], B. Yabsley[147], S. Yacoob[33a], N. Yamaguchi[89], Y. Yamaguchi[154], H. Yamauchi[157], T. Yamazaki[17a], Y. Yamazaki[84], J. Yan[62c], S. Yan[126], Z. Yan[25], H.J. Yang[62c,62d], H.T. Yang[62a], S. Yang[62a], T. Yang[64c], X. Yang[62a], X. Yang[14a], Y. Yang[44], Y. Yang[62a], Z. Yang[62a,106], W-M. Yao[17a], Y.C. Yap[48], H. Ye[14c], H. Ye[55], J. Ye[44], S. Ye[29], X. Ye[62a], Y. Yeh[96], I. Yeletskikh[38], B.K. Yeo[17a], M.R. Yexley[91], P. Yin[41], K. Yorita[168], S. Younas[27b], C.J.S. Young[54], C. Young[143], Y. Yu[62a], M. Yuan[106], R. Yuan[62b,l], L. Yue[96], M. Zaazoua[35e], B. Zabinski[86], E. Zaid[52], T. Zakareishvili[149b], N. Zakharchuk[34], S. Zambito[56], J.A. Zamora Saa[137d,137b], J. Zang[153], D. Zanzi[54], O. Zaplatilek[132], C. Zeitnitz[171], J.C. Zeng[162], D.T. Zenger Jr[26], O. Zenin[37], T. Ženiš[28a], S. Zenz[94], S. Zerradi[35a], D. Zerwas[66], M. Zhai[14a,14d], B. Zhang[14c], D.F. Zhang[139], J. Zhang[62b], J. Zhang[6], K. Zhang[14a,14d], L. Zhang[14c], P. Zhang[14a,14d], R. Zhang[170], S. Zhang[106], T. Zhang[153], X. Zhang[62c], X. Zhang[62b], Y. Zhang[62c,5], Z. Zhang[17a], Z. Zhang[66], H. Zhao[138], P. Zhao[51], T. Zhao[62b], Y. Zhao[136], Z. Zhao[62a], A. Zhemchugov[38], X. Zheng[62a], Z. Zheng[143], D. Zhong[162], B. Zhou[106], C. Zhou[170], H. Zhou[7], N. Zhou[62c], Y. Zhou[7], C.G. Zhu[62b], H.L. Zhu[62a], J. Zhu[106], Y. Zhu[62c], Y. Zhu[62a], X. Zhuang[14a], K. Zhukov[37], V. Zhulanov[37], N.I. Zimine[38], J. Zinsser[63b], M. Ziolkowski[141], L. Živković[15], A. Zoccoli[23b,23a], K. Zoch[56], T.G. Zorbas[139], O. Zormpa[46], W. Zou[41], L. Zwalinski[36]

[1] *Department of Physics, University of Adelaide, Adelaide; Australia*
[2] *Department of Physics, University of Alberta, Edmonton AB; Canada*
[3] [(a)] *Department of Physics, Ankara University, Ankara;*[(b)] *Division of Physics, TOBB University of Economics and Technology, Ankara; Türkiye*
[4] *LAPP, Univ. Savoie Mont Blanc, CNRS/IN2P3, Annecy; France*
[5] *APC, Université Paris Cité, CNRS/IN2P3, Paris; France*
[6] *High Energy Physics Division, Argonne National Laboratory, Argonne IL; United States of America*
[7] *Department of Physics, University of Arizona, Tucson AZ; United States of America*
[8] *Department of Physics, University of Texas at Arlington, Arlington TX; United States of America*
[9] *Physics Department, National and Kapodistrian University of Athens, Athens; Greece*
[10] *Physics Department, National Technical University of Athens, Zografou; Greece*
[11] *Department of Physics, University of Texas at Austin, Austin TX; United States of America*
[12] *Institute of Physics, Azerbaijan Academy of Sciences, Baku; Azerbaijan*
[13] *Institut de Física d'Altes Energies (IFAE), Barcelona Institute of Science and Technology, Barcelona; Spain*
[14] [(a)] *Institute of High Energy Physics, Chinese Academy of Sciences, Beijing;*[(b)] *Physics Department, Tsinghua University, Beijing;*[(c)] *Department of Physics, Nanjing University, Nanjing;*[(d)] *University of Chinese Academy of Science (UCAS), Beijing; China*
[15] *Institute of Physics, University of Belgrade, Belgrade; Serbia*
[16] *Department for Physics and Technology, University of Bergen, Bergen; Norway*
[17] [(a)] *Physics Division, Lawrence Berkeley National Laboratory, Berkeley CA;*[(b)] *University of California, Berkeley CA; United States of America*
[18] *Institut für Physik, Humboldt Universität zu Berlin, Berlin; Germany*
[19] *Albert Einstein Center for Fundamental Physics and Laboratory for High Energy Physics, University of Bern, Bern; Switzerland*
[20] *School of Physics and Astronomy, University of Birmingham, Birmingham; United Kingdom*

JHEP07(2023)086

[21] [(a)] *Department of Physics, Bogazici University, Istanbul;* [(b)] *Department of Physics Engineering, Gaziantep University, Gaziantep;* [(c)] *Department of Physics, Istanbul University, Istanbul;* [(d)] *Istinye University, Sariyer, Istanbul; Türkiye*
[22] [(a)] *Facultad de Ciencias y Centro de Investigaciónes, Universidad Antonio Nariño, Bogotá;* [(b)] *Departamento de Física, Universidad Nacional de Colombia, Bogotá; Colombia*
[23] [(a)] *Dipartimento di Fisica e Astronomia A. Righi, Università di Bologna, Bologna;* [(b)] *INFN Sezione di Bologna; Italy*
[24] *Physikalisches Institut, Universität Bonn, Bonn; Germany*
[25] *Department of Physics, Boston University, Boston MA; United States of America*
[26] *Department of Physics, Brandeis University, Waltham MA; United States of America*
[27] [(a)] *Transilvania University of Brasov, Brasov;* [(b)] *Horia Hulubei National Institute of Physics and Nuclear Engineering, Bucharest;* [(c)] *Department of Physics, Alexandru Ioan Cuza University of Iasi, Iasi;* [(d)] *National Institute for Research and Development of Isotopic and Molecular Technologies, Physics Department, Cluj-Napoca;* [(e)] *University Politehnica Bucharest, Bucharest;* [(f)] *West University in Timisoara, Timisoara;* [(g)] *Faculty of Physics, University of Bucharest, Bucharest; Romania*
[28] [(a)] *Faculty of Mathematics, Physics and Informatics, Comenius University, Bratislava;* [(b)] *Department of Subnuclear Physics, Institute of Experimental Physics of the Slovak Academy of Sciences, Kosice; Slovak Republic*
[29] *Physics Department, Brookhaven National Laboratory, Upton NY; United States of America*
[30] *Universidad de Buenos Aires, Facultad de Ciencias Exactas y Naturales, Departamento de Física, y CONICET, Instituto de Física de Buenos Aires (IFIBA), Buenos Aires; Argentina*
[31] *California State University, CA; United States of America*
[32] *Cavendish Laboratory, University of Cambridge, Cambridge; United Kingdom*
[33] [(a)] *Department of Physics, University of Cape Town, Cape Town;* [(b)] *iThemba Labs, Western Cape;* [(c)] *Department of Mechanical Engineering Science, University of Johannesburg, Johannesburg;* [(d)] *National Institute of Physics, University of the Philippines Diliman (Philippines);* [(e)] *University of South Africa, Department of Physics, Pretoria;* [(f)] *University of Zululand, KwaDlangezwa;* [(g)] *School of Physics, University of the Witwatersrand, Johannesburg; South Africa*
[34] *Department of Physics, Carleton University, Ottawa ON; Canada*
[35] [(a)] *Faculté des Sciences Ain Chock, Réseau Universitaire de Physique des Hautes Energies — Université Hassan II, Casablanca;* [(b)] *Faculté des Sciences, Université Ibn-Tofail, Kénitra;* [(c)] *Faculté des Sciences Semlalia, Université Cadi Ayyad, LPHEA-Marrakech;* [(d)] *LPMR, Faculté des Sciences, Université Mohamed Premier, Oujda;* [(e)] *Faculté des sciences, Université Mohammed V, Rabat;* [(f)] *Institute of Applied Physics, Mohammed VI Polytechnic University, Ben Guerir; Morocco*
[36] *CERN, Geneva; Switzerland*
[37] *Affiliated with an institute covered by a cooperation agreement with CERN*
[38] *Affiliated with an international laboratory covered by a cooperation agreement with CERN*
[39] *Enrico Fermi Institute, University of Chicago, Chicago IL; United States of America*
[40] *LPC, Université Clermont Auvergne, CNRS/IN2P3, Clermont-Ferrand; France*
[41] *Nevis Laboratory, Columbia University, Irvington NY; United States of America*
[42] *Niels Bohr Institute, University of Copenhagen, Copenhagen; Denmark*
[43] [(a)] *Dipartimento di Fisica, Università della Calabria, Rende;* [(b)] *INFN Gruppo Collegato di Cosenza, Laboratori Nazionali di Frascati; Italy*
[44] *Physics Department, Southern Methodist University, Dallas TX; United States of America*
[45] *Physics Department, University of Texas at Dallas, Richardson TX; United States of America*
[46] *National Centre for Scientific Research "Demokritos", Agia Paraskevi; Greece*
[47] [(a)] *Department of Physics, Stockholm University;* [(b)] *Oskar Klein Centre, Stockholm; Sweden*
[48] *Deutsches Elektronen-Synchrotron DESY, Hamburg and Zeuthen; Germany*
[49] *Fakultät Physik, Technische Universität Dortmund, Dortmund; Germany*
[50] *Institut für Kern- und Teilchenphysik, Technische Universität Dresden, Dresden; Germany*
[51] *Department of Physics, Duke University, Durham NC; United States of America*
[52] *SUPA — School of Physics and Astronomy, University of Edinburgh, Edinburgh; United Kingdom*

JHEP07(2023)086

[53] *INFN e Laboratori Nazionali di Frascati, Frascati; Italy*
[54] *Physikalisches Institut, Albert-Ludwigs-Universität Freiburg, Freiburg; Germany*
[55] *II. Physikalisches Institut, Georg-August-Universität Göttingen, Göttingen; Germany*
[56] *Département de Physique Nucléaire et Corpusculaire, Université de Genève, Genève; Switzerland*
[57] [(a)] *Dipartimento di Fisica, Università di Genova, Genova;* [(b)] *INFN Sezione di Genova; Italy*
[58] *II. Physikalisches Institut, Justus-Liebig-Universität Giessen, Giessen; Germany*
[59] *SUPA — School of Physics and Astronomy, University of Glasgow, Glasgow; United Kingdom*
[60] *LPSC, Université Grenoble Alpes, CNRS/IN2P3, Grenoble INP, Grenoble; France*
[61] *Laboratory for Particle Physics and Cosmology, Harvard University, Cambridge MA; United States of America*
[62] [(a)] *Department of Modern Physics and State Key Laboratory of Particle Detection and Electronics, University of Science and Technology of China, Hefei;* [(b)] *Institute of Frontier and Interdisciplinary Science and Key Laboratory of Particle Physics and Particle Irradiation (MOE), Shandong University, Qingdao;* [(c)] *School of Physics and Astronomy, Shanghai Jiao Tong University, Key Laboratory for Particle Astrophysics and Cosmology (MOE), SKLPPC, Shanghai;* [(d)] *Tsung-Dao Lee Institute, Shanghai; China*
[63] [(a)] *Kirchhoff-Institut für Physik, Ruprecht-Karls-Universität Heidelberg, Heidelberg;* [(b)] *Physikalisches Institut, Ruprecht-Karls-Universität Heidelberg, Heidelberg; Germany*
[64] [(a)] *Department of Physics, Chinese University of Hong Kong, Shatin, N.T., Hong Kong;* [(b)] *Department of Physics, University of Hong Kong, Hong Kong;* [(c)] *Department of Physics and Institute for Advanced Study, Hong Kong University of Science and Technology, Clear Water Bay, Kowloon, Hong Kong; China*
[65] *Department of Physics, National Tsing Hua University, Hsinchu; Taiwan*
[66] *IJCLab, Université Paris-Saclay, CNRS/IN2P3, 91405, Orsay; France*
[67] *Centro Nacional de Microelectrónica (IMB-CNM-CSIC), Barcelona; Spain*
[68] *Department of Physics, Indiana University, Bloomington IN; United States of America*
[69] [(a)] *INFN Gruppo Collegato di Udine, Sezione di Trieste, Udine;* [(b)] *ICTP, Trieste;* [(c)] *Dipartimento Politecnico di Ingegneria e Architettura, Università di Udine, Udine; Italy*
[70] [(a)] *INFN Sezione di Lecce;* [(b)] *Dipartimento di Matematica e Fisica, Università del Salento, Lecce; Italy*
[71] [(a)] *INFN Sezione di Milano;* [(b)] *Dipartimento di Fisica, Università di Milano, Milano; Italy*
[72] [(a)] *INFN Sezione di Napoli;* [(b)] *Dipartimento di Fisica, Università di Napoli, Napoli; Italy*
[73] [(a)] *INFN Sezione di Pavia;* [(b)] *Dipartimento di Fisica, Università di Pavia, Pavia; Italy*
[74] [(a)] *INFN Sezione di Pisa;* [(b)] *Dipartimento di Fisica E. Fermi, Università di Pisa, Pisa; Italy*
[75] [(a)] *INFN Sezione di Roma;* [(b)] *Dipartimento di Fisica, Sapienza Università di Roma, Roma; Italy*
[76] [(a)] *INFN Sezione di Roma Tor Vergata;* [(b)] *Dipartimento di Fisica, Università di Roma Tor Vergata, Roma; Italy*
[77] [(a)] *INFN Sezione di Roma Tre;* [(b)] *Dipartimento di Matematica e Fisica, Università Roma Tre, Roma; Italy*
[78] [(a)] *INFN-TIFPA;* [(b)] *Università degli Studi di Trento, Trento; Italy*
[79] *Universität Innsbruck, Department of Astro and Particle Physics, Innsbruck; Austria*
[80] *University of Iowa, Iowa City IA; United States of America*
[81] *Department of Physics and Astronomy, Iowa State University, Ames IA; United States of America*
[82] [(a)] *Departamento de Engenharia Elétrica, Universidade Federal de Juiz de Fora (UFJF), Juiz de Fora;* [(b)] *Universidade Federal do Rio De Janeiro COPPE/EE/IF, Rio de Janeiro;* [(c)] *Instituto de Física, Universidade de São Paulo, São Paulo;* [(d)] *Rio de Janeiro State University, Rio de Janeiro; Brazil*
[83] *KEK, High Energy Accelerator Research Organization, Tsukuba; Japan*
[84] *Graduate School of Science, Kobe University, Kobe; Japan*
[85] [(a)] *AGH University of Science and Technology, Faculty of Physics and Applied Computer Science, Krakow;* [(b)] *Marian Smoluchowski Institute of Physics, Jagiellonian University, Krakow; Poland*
[86] *Institute of Nuclear Physics Polish Academy of Sciences, Krakow; Poland*
[87] *Faculty of Science, Kyoto University, Kyoto; Japan*
[88] *Kyoto University of Education, Kyoto; Japan*

JHEP07(2023)086

[89] *Research Center for Advanced Particle Physics and Department of Physics, Kyushu University, Fukuoka; Japan*
[90] *Instituto de Física La Plata, Universidad Nacional de La Plata and CONICET, La Plata; Argentina*
[91] *Physics Department, Lancaster University, Lancaster; United Kingdom*
[92] *Oliver Lodge Laboratory, University of Liverpool, Liverpool; United Kingdom*
[93] *Department of Experimental Particle Physics, Jožef Stefan Institute and Department of Physics, University of Ljubljana, Ljubljana; Slovenia*
[94] *School of Physics and Astronomy, Queen Mary University of London, London; United Kingdom*
[95] *Department of Physics, Royal Holloway University of London, Egham; United Kingdom*
[96] *Department of Physics and Astronomy, University College London, London; United Kingdom*
[97] *Louisiana Tech University, Ruston LA; United States of America*
[98] *Fysiska institutionen, Lunds universitet, Lund; Sweden*
[99] *Departamento de Física Teorica C-15 and CIAFF, Universidad Autónoma de Madrid, Madrid; Spain*
[100] *Institut für Physik, Universität Mainz, Mainz; Germany*
[101] *School of Physics and Astronomy, University of Manchester, Manchester; United Kingdom*
[102] *CPPM, Aix-Marseille Université, CNRS/IN2P3, Marseille; France*
[103] *Department of Physics, University of Massachusetts, Amherst MA; United States of America*
[104] *Department of Physics, McGill University, Montreal QC; Canada*
[105] *School of Physics, University of Melbourne, Victoria; Australia*
[106] *Department of Physics, University of Michigan, Ann Arbor MI; United States of America*
[107] *Department of Physics and Astronomy, Michigan State University, East Lansing MI; United States of America*
[108] *Group of Particle Physics, University of Montreal, Montreal QC; Canada*
[109] *Fakultät für Physik, Ludwig-Maximilians-Universität München, München; Germany*
[110] *Max-Planck-Institut für Physik (Werner-Heisenberg-Institut), München; Germany*
[111] *Graduate School of Science and Kobayashi-Maskawa Institute, Nagoya University, Nagoya; Japan*
[112] *Department of Physics and Astronomy, University of New Mexico, Albuquerque NM; United States of America*
[113] *Institute for Mathematics, Astrophysics and Particle Physics, Radboud University/Nikhef, Nijmegen; Netherlands*
[114] *Nikhef National Institute for Subatomic Physics and University of Amsterdam, Amsterdam; Netherlands*
[115] *Department of Physics, Northern Illinois University, DeKalb IL; United States of America*
[116] [(a)] *New York University Abu Dhabi, Abu Dhabi;* [(b)] *University of Sharjah, Sharjah; United Arab Emirates*
[117] *Department of Physics, New York University, New York NY; United States of America*
[118] *Ochanomizu University, Otsuka, Bunkyo-ku, Tokyo; Japan*
[119] *Ohio State University, Columbus OH; United States of America*
[120] *Homer L. Dodge Department of Physics and Astronomy, University of Oklahoma, Norman OK; United States of America*
[121] *Department of Physics, Oklahoma State University, Stillwater OK; United States of America*
[122] *Palacký University, Joint Laboratory of Optics, Olomouc; Czech Republic*
[123] *Institute for Fundamental Science, University of Oregon, Eugene, OR; United States of America*
[124] *Graduate School of Science, Osaka University, Osaka; Japan*
[125] *Department of Physics, University of Oslo, Oslo; Norway*
[126] *Department of Physics, Oxford University, Oxford; United Kingdom*
[127] *LPNHE, Sorbonne Université, Université Paris Cité, CNRS/IN2P3, Paris; France*
[128] *Department of Physics, University of Pennsylvania, Philadelphia PA; United States of America*
[129] *Department of Physics and Astronomy, University of Pittsburgh, Pittsburgh PA; United States of America*
[130] [(a)] *Laboratório de Instrumentação e Física Experimental de Partículas — LIP, Lisboa;* [(b)] *Departamento de Física, Faculdade de Ciências, Universidade de Lisboa, Lisboa;* [(c)] *Departamento de Física,*

Universidade de Coimbra, Coimbra;[d] Centro de Física Nuclear da Universidade de Lisboa, Lisboa;[e] Departamento de Física, Universidade do Minho, Braga;[f] Departamento de Física Teórica y del Cosmos, Universidad de Granada, Granada (Spain);[g] Departamento de Física, Instituto Superior Técnico, Universidade de Lisboa, Lisboa; Portugal
[131] *Institute of Physics of the Czech Academy of Sciences, Prague; Czech Republic*
[132] *Czech Technical University in Prague, Prague; Czech Republic*
[133] *Charles University, Faculty of Mathematics and Physics, Prague; Czech Republic*
[134] *Particle Physics Department, Rutherford Appleton Laboratory, Didcot; United Kingdom*
[135] *IRFU, CEA, Université Paris-Saclay, Gif-sur-Yvette; France*
[136] *Santa Cruz Institute for Particle Physics, University of California Santa Cruz, Santa Cruz CA; United States of America*
[137] [a] *Departamento de Física, Pontificia Universidad Católica de Chile, Santiago;[b] Millennium Institute for Subatomic physics at high energy frontier (SAPHIR), Santiago;[c] Instituto de Investigación Multidisciplinario en Ciencia y Tecnología, y Departamento de Física, Universidad de La Serena;[d] Universidad Andres Bello, Department of Physics, Santiago;[e] Instituto de Alta Investigación, Universidad de Tarapacá, Arica;[f] Departamento de Física, Universidad Técnica Federico Santa María, Valparaíso; Chile*
[138] *Department of Physics, University of Washington, Seattle WA; United States of America*
[139] *Department of Physics and Astronomy, University of Sheffield, Sheffield; United Kingdom*
[140] *Department of Physics, Shinshu University, Nagano; Japan*
[141] *Department Physik, Universität Siegen, Siegen; Germany*
[142] *Department of Physics, Simon Fraser University, Burnaby BC; Canada*
[143] *SLAC National Accelerator Laboratory, Stanford CA; United States of America*
[144] *Department of Physics, Royal Institute of Technology, Stockholm; Sweden*
[145] *Departments of Physics and Astronomy, Stony Brook University, Stony Brook NY; United States of America*
[146] *Department of Physics and Astronomy, University of Sussex, Brighton; United Kingdom*
[147] *School of Physics, University of Sydney, Sydney; Australia*
[148] *Institute of Physics, Academia Sinica, Taipei; Taiwan*
[149] [a] *E. Andronikashvili Institute of Physics, Iv. Javakhishvili Tbilisi State University, Tbilisi;[b] High Energy Physics Institute, Tbilisi State University, Tbilisi;[c] University of Georgia, Tbilisi; Georgia*
[150] *Department of Physics, Technion, Israel Institute of Technology, Haifa; Israel*
[151] *Raymond and Beverly Sackler School of Physics and Astronomy, Tel Aviv University, Tel Aviv; Israel*
[152] *Department of Physics, Aristotle University of Thessaloniki, Thessaloniki; Greece*
[153] *International Center for Elementary Particle Physics and Department of Physics, University of Tokyo, Tokyo; Japan*
[154] *Department of Physics, Tokyo Institute of Technology, Tokyo; Japan*
[155] *Department of Physics, University of Toronto, Toronto ON; Canada*
[156] [a] *TRIUMF, Vancouver BC;[b] Department of Physics and Astronomy, York University, Toronto ON; Canada*
[157] *Division of Physics and Tomonaga Center for the History of the Universe, Faculty of Pure and Applied Sciences, University of Tsukuba, Tsukuba; Japan*
[158] *Department of Physics and Astronomy, Tufts University, Medford MA; United States of America*
[159] *United Arab Emirates University, Al Ain; United Arab Emirates*
[160] *Department of Physics and Astronomy, University of California Irvine, Irvine CA; United States of America*
[161] *Department of Physics and Astronomy, University of Uppsala, Uppsala; Sweden*
[162] *Department of Physics, University of Illinois, Urbana IL; United States of America*
[163] *Instituto de Física Corpuscular (IFIC), Centro Mixto Universidad de Valencia — CSIC, Valencia; Spain*
[164] *Department of Physics, University of British Columbia, Vancouver BC; Canada*
[165] *Department of Physics and Astronomy, University of Victoria, Victoria BC; Canada*

JHEP07(2023)086

[166] Fakultät für Physik und Astronomie, Julius-Maximilians-Universität Würzburg, Würzburg; Germany
[167] Department of Physics, University of Warwick, Coventry; United Kingdom
[168] Waseda University, Tokyo; Japan
[169] Department of Particle Physics and Astrophysics, Weizmann Institute of Science, Rehovot; Israel
[170] Department of Physics, University of Wisconsin, Madison WI; United States of America
[171] Fakultät für Mathematik und Naturwissenschaften, Fachgruppe Physik, Bergische Universität Wuppertal, Wuppertal; Germany
[172] Department of Physics, Yale University, New Haven CT; United States of America

[a] Also Affiliated with an institute covered by a cooperation agreement with CERN
[b] Also at An-Najah National University, Nablus; Palestine
[c] Also at Borough of Manhattan Community College, City University of New York, New York NY; United States of America
[d] Also at Bruno Kessler Foundation, Trento; Italy
[e] Also at Center for High Energy Physics, Peking University; China
[f] Also at Center for Interdisciplinary Research and Innovation (CIRI-AUTH), Thessaloniki; Greece
[g] Also at Centro Studi e Ricerche Enrico Fermi; Italy
[h] Also at CERN, Geneva; Switzerland
[i] Also at Département de Physique Nucléaire et Corpusculaire, Université de Genève, Genève; Switzerland
[j] Also at Departament de Fisica de la Universitat Autonoma de Barcelona, Barcelona; Spain
[k] Also at Department of Financial and Management Engineering, University of the Aegean, Chios; Greece
[l] Also at Department of Physics and Astronomy, Michigan State University, East Lansing MI; United States of America
[m] Also at Department of Physics, Ben Gurion University of the Negev, Beer Sheva; Israel
[n] Also at Department of Physics, California State University, East Bay; United States of America
[o] Also at Department of Physics, California State University, Sacramento; United States of America
[p] Also at Department of Physics, King's College London, London; United Kingdom
[q] Also at Department of Physics, University of Fribourg, Fribourg; Switzerland
[r] Also at Department of Physics, University of Thessaly; Greece
[s] Also at Department of Physics, Westmont College, Santa Barbara; United States of America
[t] Also at Hellenic Open University, Patras; Greece
[u] Also at Institucio Catalana de Recerca i Estudis Avancats, ICREA, Barcelona; Spain
[v] Also at Institut für Experimentalphysik, Universität Hamburg, Hamburg; Germany
[w] Also at Institute of Applied Physics, Mohammed VI Polytechnic University, Ben Guerir; Morocco
[x] Also at Institute of Particle Physics (IPP); Canada
[y] Also at Institute of Physics and Technology, Ulaanbaatar; Mongolia
[z] Also at Institute of Physics, Azerbaijan Academy of Sciences, Baku; Azerbaijan
[aa] Also at Institute of Theoretical Physics, Ilia State University, Tbilisi; Georgia
[ab] Also at Lawrence Livermore National Laboratory, Livermore; United States of America
[ac] Also at The Collaborative Innovation Center of Quantum Matter (CICQM), Beijing; China
[ad] Also at TRIUMF, Vancouver BC; Canada
[ae] Also at Università di Napoli Parthenope, Napoli; Italy
[af] Also at University of Chinese Academy of Sciences (UCAS), Beijing; China
[ag] Also at University of Colorado Boulder, Department of Physics, Colorado; United States of America
[ah] Also at Washington College, Maryland; United States of America
[*] Deceased

JHEP07(2023)086